RESEARCH PROGRAM ON NEW PEROVSKITE LASER HOST MATERIALS OF THE $A[B'_{0.5}B''_{0.5}]O_3$-TYPE HAVING CUBIC CENTROSYMMETRIC LATTICE SITES

PREPARED BY

F. S. GALASSO
G. K. LAYDEN
D. E. FLINCHBAUGH

FINAL REPORT
JULY 1965

PREPARED UNDER CONTRACT Nonr-4606(00)
PROJECT CODE NO. 4730 ARPA ORDER NO. 306

United Aircraft Research Laboratories

UNITED AIRCRAFT CORPORATION

EAST HARTFORD, CONNECTICUT

COPY NO.

UNITED AIRCRAFT CORPORATION
RESEARCH LABORATORIES
East Hartford, Connecticut

D910269-5
Final Report Under
Contract Nonr-4606(00)
August 1, 1964
through
July 31, 1965

Project Title: Research Program on New Perovskite Laser Host Materials of the $A(B'_{0.5}B''_{0.5})O_3$-Type Having Cubic Centrosymmetric Lattice Sites

Name of Contractor: United Aircraft Corporation Research Laboratories
Project Code No. 4730
ARPA Order No. 306

This research is part of project DEFENDER under the joint sponsorship of the Advanced Research Projects Agency, the Office of Naval Research, and the Department of Defense.

Reported By: F. S. Galasso
F. S. Galasso, Supervisor
Materials Synthesis Group

G. K. Layden
G. K. Layden
Senior Research Scientist

D. E. Flinchbaugh
D. E. Flinchbaugh
Research Scientist

Approved By: R. Ruffini
R. Ruffini, Chief
Materials Sciences

Date: July 30, 1965

Report D910269-5

Final Report Under Contract Nonr-4606(00)
for the Period August 1, 1964, through July 31, 1965

Research Program on New Perovskite Laser Host Materials of the $A(B'_{0.5}B''_{0.5})O_3$-Type Having Cubic Centrosymmetric Lattice Sites

ARPA Order No. 306, Project No. 4730

TABLE OF CONTENTS

TABLE OF CONTENTS (Contd.)

LIST OF TABLES

LIST OF FIGURES

LIST OF FIGURES (Contd.)

FOREWORD

This report constitutes the Final Report prepared by Dr. F. S. Galasso, Dr. G. K. Layden, and Dr. D. E. Tlinchbaugh in the United Aircraft Corporation Research Laboratories working under Contract Nonr-4606(00) and covers the period from August 1, 1964 through July 31, 1965. This report was administered under the direction of Dr. Van O. Nicolai of the Physics Branch of the Office of Naval Research.

The materials preparation studies conducted by W. Darby and J. Pinto, the electron paramagnetic resonance studies by A. Shuskus, and the X-ray investigations by A. Paton are appreciated and gratefully acknowledged.

Report D910269-5

Final Report Under Contract Nonr-4606(00)
for the Period August 1, 1964, through July 31, 1965

Research Program on New Perovskite Laser Host Materials of the $A(B'_{0.5}B''_{0.5})O_3$-Type Having Cubic Centrosymmetric Lattice Sites

ARPA Order No. 306, Project Code No. 4730

SUMMARY

During this contract period, powders of perovskite-type compounds having the general formula $Ba(B'_{0.5}Ta_{0.5})O_3$, where B' is a trivalent rare earth cation, In^{3+}, Y^{3+}, or Sc^{3+}, were doped with trivalent laser activating ions and the fluorescent lifetimes were measured. The values obtained, i.e. 850 μsec for Nd^{3+} doped $Ba(Lu_{0.5}Ta_{0.5})O_3$, 800 μsec for Nd^{3+} doped $Ba(Gd_{0.5}Ta_{0.5})O_3$, and the long lifetimes obtained for other rare earth doped phases of this type indicate that some of them may make promising laser materials. In addition, the optical properties of a number of other complex perovskite phases and some non-perovskite phases were measured.

Studies involving flux growth crystals also have been made during this period. In the first investigations, small, discolored crystals of $Ba(La_{0.5}Ta_{0.5})O_3$, $Ba(Gd_{0.5}Ta_{0.5})O_3$, $Ba(Lu_{0.5}Ta_{0.5})O_3$, $Ba(Sc_{0.5}Ta_{0.5})O_3$ and $Ba(Y_{0.5}Ta_{0.5})O_3$ were grown from a BaF_2 flux. After detailed phase diagram studies of the BaO-$YTaO_4$-B_2O_3 and BaO-$LuTaO_4$-B_2O_3 systems, clear single crystals of doped $Ba(Y_{0.5}Ta_{0.5})O_3$ and $Ba(Lu_{0.5}Ta_{0.5})O_3$ were grown from a B_2O_3 flux by slow cooling. In addition, a larger single crystal of $Ba(Y_{0.5}Ta_{0.5})O_3$ was grown by a modified Czochralski technique.

INTRODUCTION

The recent emphasis on laser research has brought about a concentrated search for new and improved materials which can be used as hosts for transition and rare earth doping ions. An important part of this effort has been directed toward the production of laser materials having fluorescing energy states with long lifetimes so that they will emit high energy pulses and will require low threshold pumping energies. Theoreticians calculate that these long lifetimes should be obtained in materials whose crystal lattices have the doping ions as centers of symmetry in cubic crystallographic sites. This has been substantiated by experimental results which have shown that the decay time of Cr^{3+} fluorescence increased from 3 msec in an aluminum oxide structure to 46 msec in the nearly cubic $LaAlO_3$ perovskite structure (Ref. 1).

Under the present contract, a series of $A(B'_{0.5}Ta_{0.5})O_3$ ordered perovskite-type compounds were investigated as laser host materials since it was found from the Research Laboratories' previous studies that some of them had structures which contained cubic centrosymmetric lattice sites ideally suited for trivalent laser activating ions. The more promising compounds were doped so that the fluorescing lines could be recorded, identified, and the lifetimes of these fluorescing states could be measured. In addition, some experiments were directed toward preparing these compounds as doped single crystals.

SELECTION OF LASER HOST MATERIALS

A survey was made of the various oxides in search of host materials with structures which contain cubic centrosymmetric crystallographic sites. In the selection of host materials, consideration was given to the stability of the oxides and doping ions which would be most suitable for substitution into the oxide structure.

Of the simple oxides, those with the sodium chloride and calcium fluoride structures have cubic centrosymmetric cation sites which will accept divalent and tetravalent ions respectively (Figs. 1a and 1b). While several of these oxides, such as MgO with the sodium chloride structure and ThO_2 and CeO_2 with the calcium fluoride structure, are quite suitable as laser host lattices, the availability of only a few relatively unstable divalent and tetravalent laser activating ions make them less desirable for the purposes of this study than host materials which will accept trivalent ions without the addition of other compensating ions.

The more complex spinel and perovskite structures contain centrosymmetric sites which can accommodate trivalent cations of oxide materials. However, oxides with the spinel structure were not selected as the best candidates for this investigation because of the difficulty of introducing ions in the octahedrally coordinated cation positions without any substitution in the tetrahedrally coordinated cation sites as well (Fig. 1c). Substitution of doping ions in two different cation sites was felt to be less probable in ABO_3-type oxides with the perovskite structure because the A ion is usually much larger than the B ion (Fig. 1d). In $LaAlO_3$, for example, large rare earth ions have been substituted for the La^{3+} ions and the smaller Cr^{3+} ion has been substituted for Al^{3+} (Ref. 2). The long lifetimes of the prominent fluorescing states in the Cr^{3+} doped $LaAlO_3$ indicate that this material may be nearly the ideal host oxide for this study except that its structure is slightly distorted. Other possible host materials have become available as a result of the work reported in Refs. 3 and 4 which demonstrated that two ions which are different in size and charge could be placed in the B position of the perovskite structure. A recent compilation of these compounds with the general formula $A(B'_xB''_y)O_3$, where B′ and B″ are two different elements with different charges, reveal that over 200 of them have been prepared in various laboratories (Ref. 5, Appendix I).

When the ratio of the B″ ions to B′ ions is two, as indicated by the formula $A(B'_{0.33}B''_{0.67})O_3$, and the B′ and B″ ions are ordered, the structure obtained is one in which the cubic centrosymmetric B site is not preserved (Figs. 2a, Refs. 6 - 9). However, when the B′ and B″ ions are present in equal amounts, as indicated by the formula $A(B'_{0.5}B''_{0.5})O_3$, a common ordered structure may be adopted in which the B ions alternate (Refs. 10,11); thus the symmetry about the B site is retained (Fig 2b). In these ordered $A(B'_{0.5}B''_{0.5})O_3$-type compounds it is most desirable for laser applications to have barium as the A ion since compounds containing barium are least distorted, and tantalum V as the B″ ion because of its resistance to reduction. The B′ ion should be a trivalent ion and should not produce energy levels which would interfere with those of the doping ions. Therefore, B′ should be trivalent scandium, yttrium or lanthanum which have rare gas electronic configurations, trivalent gadolinium with half filled f shells, trivalent lutecium with completely filled f shells, or trivalent indium with completely filled d shells. On this basis, the compounds selected for initial studies under this contract were $Ba(La_{0.5}Ta_{0.5})O_3$, $Ba(Gd_{0.5}Ta_{0.5})O_3$, $Ba(Y_{0.5}Ta_{0.5})O_3$, $Ba(Lu_{0.5}Ta_{0.5})O_3$, $Ba(In_{0.5}Ta_{0.5})O_3$, and $Ba(Sc_{0.5}Ta_{0.5})O_3$.

In searching for other host materials, similar multiple substitutions were considered in the sodium chloride, calcium fluoride, and spinel structures as

methods of obtaining new ordered structures containing cubic centrosymmetric sites. However, a survey of the limited amount of literature on oxides reported to have ordered sodium chloride, calcium fluoride, and spinel structures showed that the cations were distributed in such a way that the cubic center of symmetry about the cation sites was not retained. Several of these structures are shown in Figs. 3 - 7 (Refs. 12 - 15).

In summary, the compounds selected for initial studies had the general formula $Ba(B'_{0.5}Ta_{0.5})O_3$ where B' is La^{3+}, Gd^{3+}, Y^{3+}, Sc^{3+}, In^{3+} and Lu^{3+}. After considering the ionic radii of the B' ions, these compounds were selected as being most suitable for rare earth doping ions. Other promising complex perovskite compounds were selected from the list given in Appendix I, for both rare earth and transition metal ion doping. The last group of compounds were selected specifically for Cr^{3+} doping only.

Preparation of $Ba(B'_{0.50}Ta_{0.50})O_3$ Perovskite-Type Phases

Powder samples of these perovskite-type compounds were prepared following the dry technique of reacting solids at high temperatures. In these preparations reagent grade $BaCO_3$, and Ta_2O_5, and high purity (99.9%) rare earth oxides, Sc_2O_3, Y_2O_3 and In_2O_3 were used. For each sample, $BaCO_3$ was mixed with the trivalent metal oxide and the Ta_2O_5 in a molar ratio of 4:1:1. The mixture was ground in an agate mortar and fired on alumina trays in a box furnace heated by Kanthal molybdenum disilicide elements. During the firing cycle the samples were taken from the furnace and reground to insure thorough mixing. It was found that the ordered perovskite phases could be obtained by firing the powders at 1100 - 1200°C, however, at these firing temperatures the samples also contained trivalent metal oxides or $Ba_{5+d}Ta_4O_{15}$ impurities. Single phases of $Ba(La_{0.5}Ta_{0.5})O_3$, $Ba(Lu_{0.5}Ta_{0.5})O_3$, $Ba(Y_{0.5}Ta_{0.5})O_3$ and $Ba(Sc_{0.5}Ta_{0.5})O_3$ have been prepared by firing at 1560°C. The compound containing indium is an exception, however, requiring a firing temperature of only 1400°C. All other compounds have been obtained sufficiently pure so that lattice parameters for the perovskite phases could be determined.

X-ray Analysis of $Ba(B'_{0.50}Ta_{0.50})O_3$ Perovskite-Type Phases

All samples were examined by powder X-ray diffraction methods using a Philips 114.6 mm diameter camera and copper $K\alpha$ radiation. The lattice parameters were determined and diffraction line intensities were visually estimated for each compound.

It was found that compounds containing the larger trivalent cations were distorted from cubic symmetry. The X-ray pattern of $Ba(La_{0.5}Ta_{0.5})O_3$ had an orthorhombic unit cell and the X-ray pattern of $Ba(Gd_{0.5}Ta_{0.5})O_3$ was indexed on a tetragonal cell. These data are given in Table I. The samples containing trivalent cations with sizes between those of La^{3+} and Gd^{3+} have not been obtained pure enough to identify their unit cell distortions. Perovskites containing ions smaller than gadolinium exhibit cubic symmetry (see Table II).

The d-spacings and line intensities were computed for the phases containing La^{3+}, Lu^{3+}, In^{3+}, Y^{3+} and Sc^{3+} using Smith's program (Ref. 16) for the IBM 7090 computer. For this program, the cubic space group Fm3m and complete ordering of the B′ and B″ cation positions were assumed. (Thus, the data obtained for the lanthanum compound could not be compared exactly with the observed data for the orthorhombic cell, but could be used to study qualitatively the completeness of B ion ordering). The data for each phase were computed using the lattice parameters determined from powder diffraction films. Results showed that the intensities of the diffraction lines caused by ordering of the B cations (those for which h, k, and ℓ are odd integers) decreased as the difference in scattering factor decreased. Also, those lines for which $(h + k + \ell) = 4n$ were of nearly constant intensity throughout the series while the intensities of the remaining lines varied. As can be seen in Table III, experimental results agree well with these findings. The calculated ordering line intensities are seen to decrease in the order $Sc^{3+} > Y^{3+} > In^{3+} > La^{3+} > Lu^{3+}$. Where the difference in scattering factor is zero or one (see Table IV) the ordering lines were not seen on the films at normal exposure times. It is felt, however, that ordering of the B ions does persist throughout the series. This conclusion is based on a number of studies at the Research Laboratories which showed that the difference in size of the B ions has to be very small before they will distribute themselves randomly in the B position of the perovskite structure.

Using a plot of $(\text{volume})^{1/3}$ for $Ba(B'_{0.5}Ta_{0.5})O_3$-type compounds vs ionic radii of the B′ ions as given by Ahrens and obtained from a study of $Ba(B'_{0.5}Nb_{0.5})O_3$-type compounds (Ref. 11), the effective radii of the trivalent ions used in this study were determined (see Fig. 8). Table V presents the radii as determined by Ahrens, the radii as determined from unit cell data for $Ba(B'_{0.5}Nb_{0.5})O_3$-type compounds and the radii found in this study for the B′ ions. Note that the agreement between these values is quite good except for that determined for Sc^{3+}. Scandium ions appear to have a much smaller effective ionic radii in these ordered perovskite-type compounds.

Preparation of Doped Phases

Powder samples, doped with various trivalent or divalent cations, were prepared for study of their optical properties. Stoichiometric mixtures of the reactants were fired at temperatures between 1580 - 1650°C, except in the cases of the samples containing indium where a firing temperature of 1400° was sufficient. In these mixtures reagent grade chemicals were used except for TeO_2 and WO_3 which were purified grade and the rare earth oxides, Sc_2O_3, Y_2O_3, In_2O_3 and MgO which were high purity oxides. Since many phases were prepared in this survey-type experiment not all samples were worked until they were obtained as the purest single phase possible. The complex perovskite-type phases, with the general formula $Ba(B'_{0.5}Ta_{0.5})O_3$, were studied most extensively and with a greater variety of dopants. These compounds are listed on Table VI. Not only were other complex perovskites studied but also spinel and other non-perovskite-type phases as well; these are also listed in Table VI.

CRYSTAL GROWTH EXPERIMENTS

Melting Behavior of $Ba(Y_{0.5}Ta_{0.5})O_3$

Before attempting to grow crystals of $Ba(B'_{0.5}Ta_{0.5})O_3$-type compounds from a liquid phase, it was necessary to obtain information on the melting behavior of these compounds in order to determine which of the several crystal growing techniques would be most applicable and which container materials could be used.

Initial melting studies were conducted on $Ba(Y_{0.5}Ta_{0.5})O_3$. This compound was prepared by reacting $BaCO_3$, Y_2O_3 and Ta_2O_5 for several hours at 1600°C. An X-ray powder diffraction pattern was obtained for the material, and no extraneous lines were present. Attempts were made to measure the melting point of this material by placing a small piece (average dimension, 1/16 in.) on an electrically heated platinum strip, and sighting on the sample with an optical pyrometer. No melting of the sample was observed at the temperature at which the platinum strip fused. An iridium strip (MP = 2454°C) was substituted for the platinum and again the strip failed before any melting of the sample was observed. The last temperature reading made on the sample before the strip failed was 2200°C.

A piece of sintered $Ba(Y_{0.5}Ta_{0.5})O_3$ was then broken so that a sharp corner was obtained. This corner was heated with a propane-oxygen torch and observed with an optical pyrometer. Some liquid formation was observed at a nominal temperature about 2200°C. When the material had cooled to room temperature, the fused corner

was broken off and X-rayed. The pattern of the recrystallized material indicated the presence of perovskite and a second phase which was recognized to be an isomorph of $BaTa_2O_6$ (see Appendix II). The presence of the second phase in the recrystallized material cannot be taken as an indication of incongruent melting of the perovskite, and later phase equilibrium studies in the system $BaO\text{-}YTaO_4\text{-}B_2O_3$ (Appendix II) indicate congruent melting behavior for $Ba(Y_{0.5}Ta_{0.5})O_3$. It may be assumed, however, that the stoichiometry of the melt is lost because of incongruent vaporization.

From the above observations and preliminary experiments on other compounds of this type it was concluded that laboratory techniques involving congruent crystallization from the melt were impractical for these materials. The standard Czochralski technique was eliminated because of the unavailability of a suitable container, and the Verneuil technique also was eliminated because of the difficulty of maintaining correct stoichiometry. For these reasons the flux-growth technique, using slow cooling or a modified Czochralski technique, was selected as the most practical method to pursue.

Preliminary Flux-Growth Experiments

Initial attempts to grow crystals of perovskite-type compounds of the general formula $Ba(B'_{0.5}Ta_{0.5})O_3$ were made by the slow cooling technique using a number of fused salt fluxes, since this was found by workers at the UAC Research Laboratories to be a satisfactory technique for producing crystals of similar compounds of this type (Refs. 17, 18).

Compositions were prepared from C.P. grade $BaCO_3$, Ta_2O_5, and the appropriate rare earth oxides. The batches were prefired to react the starting materials, and then mixed with various amounts of flux, placed in platinum crucibles, and subjected to a given temperature cycle in a resistance furnace controlled by a Thermovolt model AZR-2478 cam controller.

The batch composition, various heat treatments, and observations are given in Table VII. The best results were obtained using BaF_2 flux, from which small crystals of $Ba(La_{0.5}Ta_{0.5})O_3$, $Ba(Gd_{0.5}Ta_{0.5})O_3$, $Ba(Lu_{0.5}Ta_{0.5})O_3$, $Ba(Sc_{0.5}Ta_{0.5})O_3$, and $Ba(Y_{0.5}Ta_{0.5})O_3$ were grown. A photograph of $Ba(Y_{0.5}Ta_{0.5})O_3$ crystals is shown in Fig. 9. All of the crystals were strongly discolored, probably as the result of the incorporation of platinum, which is known to have an appreciable solubility in BaF_2. The crystals were generally found in the lower region of the crucible, primarily near the crucible walls, in a matrix of fine-grained polycrystalline perovskite phase and flux. Moreover, close examination of the crystals disclosed that the great majority of them were twinned. While some of these crystals were satisfactory for X-ray studies, they were not suitable for optical measurements.

Since it was suspected that platinum from the crucibles was the source of discoloration of the crystals precipitated from the BaF_2 flux, compatibility experiments were performed using boron nitride crucibles. It was found that BN was not visibly attacked by molten BaF_2, but that when $Ba(Y_{0.5}Ta_{0.5})O_3$ was added to the melt, a reaction took place that precipitated TaB crystals, thus making BN also unsuitable as a container.

Before searching further for a suitable container, it was felt that a thorough evaluation of the BaF_2 system for growing crystals of $Ba(Y_{0.5}Ta_{0.5})O_3$ should be made. The solubility of $Ba(Y_{0.5}Ta_{0.5})O_3$ was determined experimentally with the hope that crystal size and quality could be improved if proper attention were given to liquidus equilibria. These data are presented in Appendix II, and the solubility curve is shown in Fig. 10. Attempts were made to nucleate and grow $Ba(Y_{0.5}Ta_{0.5})O_3$ by slowly cooling batches in covered 100 ml platinum crucibles from temperatures above the liquidus curve, but in several attempts no crystals larger than fractions of a millimeter were obtained. There appeared to be a severe nucleation problem in this system, probably connented with the very steep solubility curve and low critical undercooling so that a great number of crystals, rather than a requisite few, precipitated on cooling.

Because of the nucleation and contamination problems encountered using BaF_2, it was necessary to find a more suitable flux for $Ba(Y_{0.5}Ta_{0.5})O_3$. Oxide fluxes were considered since it was assumed that the solubility would be higher and nucleation problems would be less severe.

Crystal Growth Experiments Using a B_2O_3 Flux

Of the low melting oxides, B_2O_3 was deemed to be the most suitable since it would have the least tendency to enter the perovskite structure because of the greater size disparity between the B^{3+} ion and the cations in the perovskites. Studies were undertaken to delineate phase equilibrium in the systems $BaO\text{-}YTaO_4\text{-}B_2O_3$, $BaO\text{-}LuTaO_4\text{-}B_2O_3$ and $BaO\text{-}LaTaO_4\text{-}B_2O_3$. These are reported fully in Appendix II. The perovskite fields in the first two of these systems were mapped in sufficient detail to permit the selection of proper crystal growth conditions. The perovskite field in the latter system was not found in the analogous area of the diagram. As time did not permit further investigation of the $BaO\text{-}LaTaO_4\text{-}B_2O_3$ system, crystal growth experiments were confined to $Ba(Y_{0.5}Ta_{0.5})O_3$ and $Ba(Lu_{0.5}Ta_{0.5})O_3$.

The phase diagrams (Figs. 11, 12) were used to select batch compositions and temperature cooling ranges. Since, as can be seen from the above figures, the slope of the liquidus surfaces, $ds/d\theta$, is approximately 0.08 weight percent perovskite

per ^{o}C in the region of interest, the empirical observation of Laudise (Ref. 19) that satisfactory nucleation and growth requires $0.02 < d^{s}/d\theta \; d\theta/dt < 0.2$ predicates cooling rates $d\theta/dt$ in the order of less than $2.5^{o}C$/hr. This in turn necessitates temperature control considerably better than $\pm 1^{o}C$. Because phases other than perovskite crystallize when the liquid composition reaches the boundaries of the perovskite field, extraction of perovskite crystals from a melt that had been permitted to cool to room temperature would be extremely difficult. For this reason it was desirable to decant the liquid from the growing crystals at elevated temperature before this condition was reached.

Since no furnaces that satisfied the above requirements of temperature control were on hand, two special decanting furnaces were built. The decanting arrangement for the 50 ml crucible furnace is shown in Fig. 13. This arrangement permits the crucible holder to be rotated and the liquid poured off into a sump at any desired temperature during the cooling cycle. In the case of the 50 ml crucible furnace, the sump consisted of a standard low form 100 ml platinum crucible placed below the growth crucible. The second furnace was similar in design, but was made to accommodate a 250 ml crucible. In this case a firebrick tray filled with ground firebrick grain served as the sump. A photograph of the 250 ml furnace, showing the crucible in the decanted position, is shown in Fig. 14. The furnaces were each heated by eight Morganite silicon carbide elements and were controlled by Leeds and Northrup Speedomax Type G program controllers Series 60 proportional control units and Fincor FDG 1 saturable reactors. The program controllers were fitted with 5 mm range cards, and adapted with thermocouple bucking circuits in order to adjust the zero of the scale. The thermocouple bucking circuits are shown in Fig. 15. The temperature sensing thermocouples were 20 mil platinum-platinum, 10% rhodium without protection tubes placed in the vicinity of the crucible. In addition, auxiliary read-out thermocouples were placed in contact with the crucibles at various positions. The degree of temperature control and smoothness of cooling rate attained in these furnaces is shown in Fig. 16, in which a section of a recorder strip chart from a typical run is reproduced.

The various compositions were prepared from the following reagents:

$BaCO_3$	- Fisher Certified Reagent	
Ta_2O_5	- A. D. Mackay, Inc.	99.9%
Y_2O_3	- A. D. Mackay, Inc.	99.9%
Lu_2O_3	- Allied Chemical	99.9%
Gd_2O_3	- A. D. Mackay, Inc.	99.9%
Yb_2O_3	- Research Chemical, Inc.	99.9%
Nd_2O_3	- Research Chemical, Inc.	99.9%
B_2O_3	- J. T. Baker Co., purified, anhydrous	

The major constituents of a batch (i.e. $BaCO_3$, Ta_2O_5, B_2O_3, Y_2O_3 or Lu_2O_3) were blended together and slowly fired to about 900°C. The loosely sintered products were then broken up and melted into platinum crucibles using induction heating, the crucibles serving as susceptors. In instances where crystals were to be doped with Gd_2O_3, Yb_2O_3, or Nd_2O_3, the desired amounts of the latter oxides were added to the crucibles prior to placing in the crystal growth furnaces.

During the process of melting the charges into the crucibles a signigicant effect was observed: when the charges were heated to temperature considerably above the liquidus, a clear melt was not obtained; rather, second phase particles could be observed at the surface. Liquids above the perovskite field cannot be cooled to glasses. Since it would be instructive to observe these second phase particles in glasses, compositions in the $BaTa_2O_6$ and the $Ba_5Ta_4O_{15}$ primary fields, closely adjacent to the perovskite field but which can be cooled to glasses, were prepared in 50 gram batches and similarly melted into platinum crucibles, and their melts observed. The surfaces of these melts also appeared two-phase well above the liquidus temperature. When the melt was rapidly cooled the particles would appear to be redissolved in the cooling liquid, while a few would settle to the bottom of the crucible and be retained in the resulting glass. Due to the very small volume fraction and small size of the particles it was not possible to obtain X-ray diffraction patterns to positively identify them. However, microscopic examination under polarized light indicated them to be cubic-- presumably perovskite, since this is the only cubic phase enountered in the phase diagram. When samples of these glasses were sealed in platinum tubes and quenched from high temperature, no trace of crystalline material could be found above the previously determined liquidus temperature, and electron microscopy of fragments of the quenched glass gave no indication of inhomogeneity.

It was concluded from these observations that the surface of the melt in an open crucible is in a labile (supersaturated) state although the bulk may be considerably above liquidus temperature, and that crystals are being continuously nucleated at or near the surface, which redissolve when convection carries them into the bulk of the melt. The reason for the labile condition of the surfs is assumed to be a depletion of B_2O_3 and local cooling caused by evaporation.

Although the desirability of performing the crystal growth runs in completely sealed crucibles in order to prevent B_2O_3 loss was recognized, this was not practical considering the necessity of decanting the liquid. After the crucibles had been charged, the perforated platinum lids crimped in place, and the crucibles wired into place on the rotating crucible holders, the furnace was taken rapidly to soak temperature, held for various times, and slowly cooled. When the desired temperature was re. the liquid was decanted, the furnace cooled to room temperature, and the crystals extracted. The doped crystals were spectrochemically analyzed to determine the dopant concentration.

Table VIII is a summary of the slow cooling runs. Crystals of $Ba(Y_{0.5}Ta_{0.5})O_3$, undoped, and doped with three different levels of Gd^{3+}, and one level of Nd^{3+}, and crystals of $Ba(Lu_{0.5}Ta_{0.5})O_3$ doped with one level each of Gd^{3+} and Yb^{3+} were obtained. Also, crystals of $BaTa_2O_6$ and $Ba_5Ta_4O_{15}$ were obtained when the melts were permitted to cool to their respective boundary curves, as explained below.

The first run composition, sample 65-059, was selected to lie directly between the perovskite composition and the low melting four-phase equilibrium composition. This run was inadvertently permitted to cool to 955°C before being decanted, and the resulting crystal yield consisted primarily of hexagonal plates of $Ba_5Ta_4O_{15}$*, some of which are shown in Fig. 17. The second run, sample 65-080, somewhat richer in $YTaO_4$, and decanted at 1040°C resulted in about 80% of the original charge having crystallized, and the crystals appeared to consist primarily of $Ba_5Ta_4O_{15}$.

This unexpected result suggested that loss of B_2O_3 from the melt by vaporization was sufficient to alter the melt composition considerably. Weight loss measurements were made (see Appendix III) which indicated a loss from the 50 ml melts of about one gram per day in the temperature region where the crystal growth runs were made. How such a B_2O_3 loss affected the crystallization path of sample 65-080 is indicated graphically in Fig. 18. The actual crystallization path (locus of liquid compositions) bends away from the B_2O_3 apex and interacts the $Ba(Y_{0.5}Ta_{0.5})O_3$-$Ba_5Ta_4O_{15}$ boundary curve somewhat above 1100°C, at which point the latter phase begins to grow. The crystallization path after the liquid composition reaches the aforementioned boundary curve has not been determined; since the system BaO-$YTaO_4$-B_2O_3 is not a true ternary, the phase compositions are not constrained to this join. However, the amount of $Ba_5Ta_4O_{15}$ that crystallized in run 65-080 suggests that the increase in concentration of the $Ba_5Ta_4O_{15}$ phase with decreasing temperature is great; and that if perovskite crystals are to be easily recovered, the liquid composition must not be permitted to reach the $Ba_5Ta_4O_{15}$-$Ba(Y_{0.5}Ta_{0.5})O_3$ boundary curve.

In all subsequent slow cooling runs the B_2O_3 loss was compensated by using starting compositions to the right of the line between $Ba(Y_{0.5}Ta_{0.5})O_3$ and the four-phase equilibrium point on Figs. 11 and 12, and/or by decanting at higher temperatures. These runs yielded crystals of the desired perovskite phase only, with one exception that will be mentioned later.

*Spectrochemical analyses of these crystals gave a composition about $Ba_5Ta_3B_{1.5}Y_{.17}O_{15}$, indicating that some boron and yttrium can go into solution at the expense of tantalum. The formula $Ba_5Ta_4O_{15}$ will be used for convenience.

The crystals that were recovered appeared to be of two types: 1) those that had nucleated and grown on the crucible walls and 2) those which had apparently nucleated at the surface or in the bulk and had grown to sufficient size to sink to the bottom where they continued to grow. Figure 19 is a photograph of sample 65-114 showing the two types of crystals obtained after the liquid had been decanted.

Figure 20 is a photograph of some of the extracted perovskite crystals from this run which show more clearly the size and habit of the crystals. Spectrochemical analyses of these crystals showed no lines for boron, indicating that the boron concentration is below that which can be detected by routine spectrochemical analyses, i.e. less than about 0.05 weight percent.

In some of the runs the weight of perovskite crystals recovered was less than that predicted by the phase diagram. From this it is inferred that many small crystals were suspended in the liquid and were poured off with it. In run 65-135 when the crucible was inverted, the holes in the crucible cover became clogged, presumably with such suspended crystals, preventing some of the liquid from being poured off.

There was relatively lower loss of B_2O_3 from the larger crucibles due to the lower surface to bulk ratio. In run 65-204, the furnace was cooled too far before decanting, so that the liquid composition reached the $BaTa_2O_6$-$Ba(Y_{0.5}Ta_{0.5})O_3$ boundary curves, and $BaTa_2O_6$* solid solution crystals as well as perovskite crystals were recovered. The habit of the $BaTa_2O_6$ crystals is seen in Fig. 21.

The largest crystals were obtained from the 250 ml runs at the slowest cooling rates in which crystals of $Ba(Y_{0.5}Ta_{0.5})O_3$ doped with Gd^{3+} (sample 65-245) and Nd^{3+} (sample 65-247) were grown up to one-half centimeter on edge. Some Nd^{3+} doped crystals, polished for optical absorption measurements, are shown in Fig. 22.

The difficulties in obtaining large single crystals of these compounds are inherent in the phase systems, namely the steep slope of the liquidus surface and the apparently very narrow range of undercooling above the perovskite field, and the tendency for loss of B_2O_3 from the melts which causes changes in melt composition and possibly permits the melt surface to become labile. These conditions make control of nucleation difficult with the result that in all the slow cooling runs many nuclei formed. These problems however do not appear insurmountable. It is probable

*Spectrochemical analyses of these crystals gave the approximate composition $BaTa_{1.86}Y_{0.20}B_{0.06}O_6$.

that in crucibles sealed to prevent B_2O_3 loss, using slower cooling rates and finer temperature control than were available in the present study, that larger high quality crystals could be grown by this technique.

Gradient Growth Experiments

Growth of oxide crystals from a flux in a temperature gradient have been demonstrated by Laudise, Linares, and Dearborn (Ref. 20) who grew $Y_3Fe_5O_{12}$ from a $BaO-B_2O_3$ flux on a seed crystal suspended below the melt surface, and by Linares (Ref. 21), who grew $Y_3Fe_5O_{12}$ from a similar flux system by slowly withdrawing a rotating seed placed in contact with the saturated melt surface. The latter technique offers the advantage that larger crystals can be obtained than in the case for other flux techniques.

On both of the above methods, an excess of nutrient material (i.e. material of the composition to be grown) is available in the bottom of the crucible, which is maintained at a higher temperature than the surface of the melt. When the seed crystal is placed in the cooler region of the crucible, some of the nutrient dissolves, is transported by diffusion through the flux, and deposits on the seed.

These techniques appear to be appropriate for the growth of perovskite crystals from a B_2O_3 flux. A crystal pulling mechanism, capable of pulling speeds continuously variable between 0.01 cm per hour and 10 cm per hour and rotation speeds between 0 and 600 rpm was built. A photograph of the crystal puller and gradient furnace is shown in Fig. 23. Furnace control units were similar to those described earlier for the decanting furnaces. Earlier failure to obtain suitable seed crystals delayed gradient growth experiments until the final months of work on the contract.

Strontium titanate seed crystals were used in the first experiments. A 50 ml crucible, previously charged with about 200 grams of composition $BaO:YTaO_4:B_2O_3$ = 52.2:35.3:12.5 weight percent, was positioned in the furnace so as to maintain the surface about 40°C cooler than the bottom of the crucible. (The temperature profile down the center of the crucible was obtained by probing the melt with a Pt-Pt, 10 Rh thermocouple.)

The strontium titanate seeds were introduced into the melt surface after the melt had been at temperature for progressively longer periods of time. It was found that even after a soak period of ninety-six hours the seed crystals dissolved in the melt. From this it was concluded that strontium titanate has a considerable solubility in the melt, even though the latter is saturated with $Ba(Y_{0.5}Ta_{0.5})O_3$, and was therefore unsuitable as a seed material.

An experiment was performed similar to the one described above, with the exception that $Ba(Y_{0.5}Ta_{0.5})O_3$ seed crystals were used. When the seed was introduced after a four-hour soak period, it promptly dissolved, indicating that the melt surface was not yet saturated. After an additional twenty hours of soak time, another seed was introduced. Although it was difficult to distinguish features of the melt surface, there appeared to be an initial dendritic growth from the seed when it contacted the melt surface. Once the seed came into thermal equilibrium with the melt it was not possible to observe the details of the melt-seed interface.

Since there was low evidence of supersaturation at the melt surface, the seed was withdrawn at a rate of 1 mm per day with a rotation rate of about 60 rpm. After five days, considerable growth on the seed was evident, but it appeared that the crystal was no longer in contact with the melt. Also, it was observed that crystals had nucleated on the crucible wall and grown out on the melt surface about one-half inch. The position of the melt surface within the crucible was two or three millimeters below its original position, indicating loss of material not accounted for by material withdrawn on the seed. This material loss is due to two factors: 1) vaporization of B_2O_3 from the melt as mentioned earlier, and 2) crawling of melt over the lip and down the outside of the crucible.

Figure 24 shows two enlarged views of the material withdrawn. The material is polycrystalline, the crystallites becoming larger and clearer toward the circumference. There was little growth downward into the melt, but mostly outward on the melt surface resulting, as the seed was withdrawn, in the lens-like cavity on the underside as shown in Fig. 24.

The above experiment demonstrated that $Ba(Y_{0.5}Ta_{0.5})O_3$ could be grown on a seed by transfer across a gradient, but that the gradient across the melt may have been too steep resulting in too high a supersaturation of the melt surface which resulted in spontaneous nucleation on the crucible walls and possibly initial dendritic or polycrystalline deposition on the seed crystal. A second experiment was performed using a different crucible arrangement. In this case a 100 ml platinum crucible, fitted with a lid to reflect heat back to the melt surface was used. A 400 gram charge of composition $BaO:YTaO_4:B_2O_3 = 52:35:13$ was equilibrated for 20 hours. The temperature difference across the melt was found to be 20°C. A $Ba(Y_{0.5}Ta_{0.5})O_3$ seed crystal was then suspended about one centimeter below the melt surface and rotated about 200 rpm, but not withdrawn from the melt. After three days, an examination disclosed that the seed had dissolved, while a polycrystalline deposit had grown on the platinum seed holder at the melt surface, indicating that again the melt surface was supersaturated to the extent that spontaneous nucleation could occur on a platinum surface.

The crucible was then repositioned in the furnace so as to give a very small gradient across the melt, and the temperature profile was probed; the resulting temperature profile is shown in Fig. 25, which shows that melt surface, on axis, was 8°C cooler than the bottom of the crucible. Another seed crystal was mounted on the puller and lowered into the melt surface. After one hour's time the seed was withdrawn and examined; no polycrystalline growth was evident on the seed or the platinum support wire. The seed was again lowered into the melt surface, rotated at about 100 rpm and withdrawn at a rate of 0.0025 in./hr. After 18 hr the seed was again withdrawn and examined. Single crystal growth had occurred on the seed resulting in the faceted crystal shown in Fig. 26a. The crystal was returned to the melt, and growth was continued under the same conditions for an additional four days. At the end of that period the crystal had the appearance shown in Fig. 26b. It was estimated on the basis of the increase in the size of the crystal during the four day growth period that the linear growth rate under these conditions was on the order of 0.025 mm/hr.

From these experiments it may be concluded that the technique of growth on a seed by temperature gradient transport is applicable to the growth of $Ba(Y_{0.5}Ta_{0.5})O_3$, and probably to the other perovskite phases studied in this investigation as well. A very small thermal gradient across the melt must be employed. A temperature gradient of 1.5°C/cm permits growth on the seed to proceed at about 0.025 mm/hr. A melt surface 8°C cooler than the nutrient is not critically supersaturated and spontaneous nucleation does not occur. However, a melt surface 20°C cooler than the nutrient will promote spontaneous nucleation and polycrystalline growth. A precise value of the critical undercooling has not been determined and probably varies with composition.

OPTICAL MEASUREMENTS

This section describes the apparatus, techniques, and some results of experimental observations of optical measurements taken on powders of doped $Ba(B'_{0.5}B''_{0.5})O_3$-type phases and a single crystal of Ni^{3+} doped $Ba(Y_{0.5}Ta_{0.5})O_3$. With the equipment presently available, optical absorption spectra and absorption coefficients can be obtained on clear single crystals. Fluorescence emission spectra, the line width of each prominent fluorescing line, and the lifetime of the prominent fluorescing state can be obtained on either single crystals or finely ground powders. All of these measurements may be carried out at both room temperature and liquid nitrogen temperature.

Apparatus and Procedure

The UAC Research Laboratories' Cary Model 14 spectrophotometer covers the 1860 Å to 2.65 μ spectral range with automatic range change for switching the high-intensity hydrogen lamp in the ultraviolet, a high-intensity tungsten lamp in the visible range, and a separate tungsten lamp for the infrared region. The resolving power of the Model 14 is better than 1.0 Å in the ultraviolet-visible region and better than 3.0 Å in much of the near infrared. The wavelength scale is accurate to better than 4.0 Å with a reproducibility better than 0.5 Å. The photometric circuit and signal identification system is phototube shot-noise limited to give optimum signal-to-noise ratio. This instrument employs a double monochromator consisting of a 30° fused silica prism in series with a 600 line/mm echelette grating, each with its own collimating mirrors and slit system. This combination of dispersing elements provides the high resolving power and low temperature coefficient which are available with the grating at long wavelengths and at the same time retains the high optical efficiency and low scattered light characteristic of the prism monochromator. Both halves of the monochromator operate with an aperture ratio of f/8, the focal lengths being 30 cm for the prism collimator and 40 cm for the grating collimator. The monochromator has 2-cm long slits, leading to high light gathering power.

The spectrophotometer is utilized for performing transmission, absorption, and reflectivity investigations of crystals and dielectric reflecting coatings. Its optical measurement capabilities have recently been greatly expanded. The Cary spectrophotometer has been fitted with additional apparatus to allow continuous recording of fluorescence emission spectra of crystal or powder samples. An RCA 7102 photomultiplier detector having an S-1 spectral response is used to provide the recorder signal for this mode of operation. This detector is cooled near liquid nitrogen temperature to reduce thermal noise when maximum gain is required. This allows observation of fluorescence emission from 2000 Å to 1.2 microns wavelength. A 200 watt mercury-xenon arc lamp is used as an excitation radiation source lamp. A set of multiple-dielectric interference filters, in addition to glass and liquid filters, is employed to control the band pass of the pump light.

An additional source for use in determining average lifetimes of excited states of impurity ion electrons has been constructed. It consists of a high-pressure xenon flash lamp and power supply designed to give it peak light output for 6 microseconds and decay to less than one-third that intensity in less than a microsecond. The intensity decay of the source lamp and of the sample fluorescence line are displayed on a dual-beam oscilloscope screen. Two special dewars to cool sample materials have been designed and fabricated so that optical absorption, fluorescence, and life-time measurements can be made at temperatures down to 77°K.

For optical absorption measurements the Cary can be used in its normal mode of operation as a double monochromator. Single crystal samples with a diameter of 5 mm or more and thickness from several millimeters to several centimeters (depending on the impurity ion concentration) can be readily investigated. The unit is calibrated to read directly in absorption units with four different scale ranges: 0-0.1, 0.1-0.2, 0-1, and 1-2. Absorption or density units are defined in terms of the transmission as the logarithm of the reciprocal transmission. The sample is ground with reasonably flat and parallel ends and is positioned so that one of the monochromator beams must pass entirely through it. An SP28 photomultiplier, a thermopile, and a lead sulfide cell serve as detectors over different portions of the spectrum. Thus the absorption bands and absorption coefficients of optical quality crystals may be easily found in the near ultraviolet, visible, and near infrared spectral regions.

Fluorescence emission spectra are obtained by front lighting the sample and detecting the selected emitted light with a cooled 7102 photomultiplier tube connected to the Cary amplifier chain. The detector is also electrostatically and magnetically shielded. The d-c excited Hanovia source arc is imaged upon the sample at angles several degrees off axis to the Cary optics and the normal of the sample face. This is accomplished by a front-surface spherical condensing mirror with a central window. Fluorescence emission which leaves essentially normal to the sample face is then collected and analyzed in the instrument.

This system is ideally suited for the use of powder samples because only the front surface is illuminated and little transmission of excitation or emitted radiation through the sample medium is required. These samples are prepared either as a compressed tablet or as an opaque coating on a glass microscope slide. A sample under observation is held in contact with an arm of a stainless steel dewar with silicon grease. Combinations of liquid, colored glass, and multiple dielectric interference filters are used to select the pump light band pass. An alternative method of selecting excitation wavelengths is to use a second monochromator system as Murphy et al do (Ref. 2). Such an arrangement was tried but the Baush and Lomb instrument used was not optically fast enough to be efficient in this application. Copper and nickel sulfate solutions have been found to be useful absorbers in the long wavelength visible and infrared.

It was found that the Cary instrument lacked sensitivity in recording fluorescence emission, and that large slit widths (up to 3 mm) were required to obtain some of the data. A separate study revealed that the emission lines were often severely broadened due to instrumental effects and that the resolution of fine structure was poor. In order to obtain additional information about some of the samples, a Jarrell-Ash 0.5 meter grating monochromator with variable curved slits was used. A selected

low-noise EMI 9558 photomultiplier tube with S-20 response served as the detector, and slit widths varied from 5 to 20 microns. More nearly "true" line profiles were recorded on an x-y recorder with this apparatus coupled optically to the fluorescence attachment off of the Cary. Since neither photomultiplier detector responded to radiation beyond 1.3 micron wavelength, a lead sulfide cell was substituted in the Cary to look for Er^{3+} and Ho^{3+} emission. The sensitivity of two such cells was found to be too low for this application even with the addition of several high gain signal amplifiers.

For lifetime measurements the sample is held the same way as above, but the arc lamp is removed and an E.G. and G. FX-12 xenon flash tube is substituted in its position. It is fired at 1000-2000 volts with 1.5-6 joules input. Its output spike is very sharp, but the afterglow has about a 35 μsec duration. However, even this can be neglected in view of the much greater excited state lifetimes. The 7102 signal is then fed directly to a Tektronix 551 oscilloscope and both the decay of the source light and the decay of the sample emission at a particular wavelength setting are recorded on a Polaroid Land print. The average lifetime is then measured as the sweep time required for an intensity fall of one logarithmic decrement.

Additional data were obtained with the fluorescence attachment removed from the Cary and the detector mounted in a light-tight enclosure at the exit window of the attachment. With a suitable combination of short-wavelength pass filters at the source and long-wavelength pass filters at the detector, only the pump light could reach the sample and only the emitted radiation was seen by the detector. This arrangement provided a much greater signal level and both the 7102 and PbS detectors could be used to observe fluorescent decay.

Optical Measurement Data on Powders of Perovskite-Type Phases

Preliminary data were obtained initially to check out the accuracy and reliability of the instrumentation and procedures. A set of measurements of absorption coefficient, spectral wavelength, line width, and lifetime for single crystal $Al_2O_3:Cr^{3+}$ was made and compared with published results. Additional measurements on a powder sample of the same composition which was prepared here were made to make a comparison of the fluorescing properties. Only small differences were noted between the single crystal and powder samples. Similar data were taken with Nd^{3+} doped barium crown glass and borate glass and were also found to agree with other work (Refs. 22, 23, 24, and 25).

Figure 27 shows the optical absorption spectrum of a crystal of $Ba(Y_{0.5}Ta_{0.5})O_3$ over the wavelength range 0.30 to 1.20 μ at both 77 and 300°K. This sample was several millimeters square by about one millimeter thick. The difference in the

bsorbance range between the two curves is due primarily to adjustment and alignment f the sample and reference apertures with the two sample holders used. The crystal as very lightly doped with Nd^{3+} and did not exhibit well-defined impurity ion bsorption properties or fluorescence emission. Its absorption trace was observed to ake on more structure at liquid nitrogen temperature than at room temperature.

The fluorescence emission data for Nd^{3+} in the first set of perovskite-type owders are summarized in Table IX. In most instances the fluorescence lines are road. When they overlap significantly no half-intensity point line widths are isted. A representative spectrophotometer tracing from which the numbers were aken is illustrated in Fig. 28. A powder sample of $Ba(Sc_{.48}Nd_{.02}Ta_{.50})O_3$ shows the ransitions $^4F_{3/2}$ to $^4I_{9/2}$ and to $^4I_{11/2}$ appearing at 0.877 and 1.060 μ, respectively, t room temperature. Other trivalent neodymium doped perovskites exhibited slight hifts in the position of the dominant line and changes in fine structure and intensity. lso, the temperature dependence of these properties varied from one sample to another s noted in Table IX.

An example of another rare earth dopant is found in Fig. 29. Here Yb^{3+} produced relatively intense line near its characteristic 1.01 μ output and a second well-efined shorter wavelength line when the $Ba(Y_{0.48}Yb_{0.02}Ta_{0.50})O_3$ sample was cooled o 77°K. At room temperature, however, the total intensity decreased considerably nd the distinct lines merged together. Other rare earth ions (eg. Pr^{3+}, Er^{3+}, Ho^{3+}, m^{3+}, and Tm^{3+}) in perovskite hosts were studied briefly with varying success.

A powder sample which fluoresces well with a Cr^{3+} impurity ion concentration s illustrated in Fig. 30. It is readily noticed that the emitted lines vary in elative intensity with temperature, and the data compiled in Table IX for K $(Al_{0.98}Cr_{0.02})O_2$ lso show a shifting of line position and line width with decreasing temperature. igure 31 illustrates the fluorescence emission lines of a $Zn(Al_{1.98}Cr_{0.02})O_4$ powder ample at two different temperatures. The relative intensities and line widths hanged slightly as a function of temperature. The overall intensity of the fluorescence ncreased with a drop in temperature and appeared to be quite strong, about one-third f the peak output intensity of a ruby rod sample. The complex structure of the pectral output is summarized in Table IX but it has not been fully analyzed in erms of crystal field splittings of the trivalent chromium R-lines. Samples doped ith other transition metal ions, such as nickel and iron, did not show any well-efined fluorescence.

The excited state lifetimes of the impurity ion electrons are summarized in Table . These represent approximately average spontaneous emission values as determined rom the decay rates of the dominant fluorescent lines. Some of these rate curves were est fit by a sum of exponential terms in place of a single, simple exponential function.

Discussion of Results

Although the fluorescence lines from many of these samples are relatively broad, this fact alone does not detract from their potential use as laser hosts. A very important consideration in this study is the energy storage capability of a a given system, which is proportional to several factors:

$$\text{Energy storage} \propto \nu^3 \, \Delta\nu \, \tau$$

The frequency of the emitted radiation ν, the line width $\Delta\nu$, and the lifetime τ, must be considered together for system optimization. The latter two factors have been of primary interest in this study of new materials.

While the lifetimes measured on powders of some of the Nd^{3+} doped $Ba(B'_{0.5}Ta_{0.5})O_3$-type phases are longer than those reported for most other Nd^{3+} doped phases, the lifetimes were not as long as was expected for Nd^{3+} situated in a cubic centrosymmetric crystallographic site. (See Table X). This may be due to the difficulty in obtaining complete ordering of the B ions which is necessary for the B sites to remain centrosymmetric. While there is no X-ray evidence of disorder in the other phases of this series, electron paramagnetic resonance, which is a much more sensitive measurement, did indicate some disorder in Gd^{3+} doped crystals of $Ba(Y_{0.5}Ta_{0.5})O_3$. Therefore, it is felt that if increased ordering can be obtained by careful control of crystal growth conditions the lifetimes also can be increased. Since most of the crystals were grown in the latter part of the contract, this hypothesis could not be tested.

Fluorescence was not detected in Cr^{3+}, Ni^{2+} and Fe^{3+} doped samples of perovskite-type phases. However, only preliminary studies were conducted. Since the ionic radii of Cr^{3+} was not particularly suitable for substituting for the large trivalent ions required in these phases to cause ordering, it is not surprising that its fluorescence was not observed.

Initial studies on non-perovskite phases indicate that compounds with the spinel structure may be much more suitable for Cr^{3+} doping. The lifetime of Cr^{3+} in $ZnAl_2O_4$ for example, was found to be 5200 μ sec. The optical data obtained using powder samples and the techniques described permit a relatively rapid survey of crystalline host and impurity properties which are useful in selecting potential laser materials.

REFERENCES

1. Ohlmann, R. C.: Bull. Am. Phys. Soc., 9, 281 (1964).
2. Murphy, J., R. C. Ohlmann and R. Mazelsky: Phys. Rev. Letters, 13, 131 (1964).
3. Roy, R.: J. Am. Ceram. Soc., 37, 581 (1954).
4. Galasso, F., L. Katz and R. Ward: J. Am. Chem. Soc., 81, 820 (1959).
5. Galasso, F.: UAC Research Laboratories Report UAR-B10, January 1963.
6. Galasso, F., J. Barrante and L. Katz: J. Am. Chem. Soc., 83, 2830 (1961).
7. Galasso, F. and J. Pyle: J. Phys. Chem., 67, 553 (1963).
8. Galasso, F. and J. Pyle: Inorg. Chem., 2, 482 (1963).
9. Galasso, F. and J. Pyle: J. Phys. Chem., 67, 1561 (1963).
10. Steward, E. G. and H. P. Rooksby: Acta Cryst., 4, 503 (1951).
11. Galasso, F. and W. Darby: J. Phys. Chem., 66, 131 (1963).
12. Blasse, G.: Z. anorg. allg. Chem., 326, 44 (1963).
13. Blasse, G.: Z. anorg. allg. Chem., 331, 44 (1964).
14. Blasse, G.: J. Inorg. Nucl. Chem., 25, 136 (1963).
15. Braun, P. B.: Nature, 170, 1123 (1952).
16. Smith, F. K.: University of California, Lawrence Radiation Laboratory Report UCRL-7196, April 8, 1963.
17. Galasso, F. and W. Darby: Inorg. Chem., 4, 71 (1965).
18. Galasso, F. and J. Pinto: Nature, 207, 70 (1965).
19. Laudise, R. A.: "Molten Salt Solvents" p. 259 in J. J. Gilman, ed., The Art and Science of Growing Crystals, John Wiley and Sons, Inc., New York, 1963.

REFERENCES (Contd.)

20. Laudise, R. A., R. C. Linares and E. F. Dearborn: J. Appl. Phys., 33S, 1362 (1962).

21. Linares, R. C.: J. Appl. Phys., 35, 433 (1964).

22. Maiman, T. H., R. H. Hoskins, I. J. D'Haenens, C. K. Asawa and V. Evtuhov: Phys. Rev., 123, 1151 (1961).

23. Brown, Jr., G. C.: J. Appl. Phys., 35, 3062 (1964).

24. Snitzer, E.: Phys. Rev. Letters, 7, 444 (1961).

25. Eastman Kodak Company Laser Glass Data Sheet, Type ND-102, September, 1964.

TABLE I

X-ray Data for Distorted, Ordered Perovskite-Type Compounds

$Ba(La_{0.5}Ta_{0.5})O_3$ a_o=8.611, b_o=8.639, c_o=8.764 Å			$Ba(Gd_{0.5}Ta_{0.5})O_3$ a_o= 8.487, c_o= 8.513 Å		
hkl (obs.)	d obs., Å	I/I_o	hkl (obs.)	d obs., Å	I/I_o
111	5.00	40	111	4.90	30
200,020	4.32	40	200	4.25	30
220	3.05	100	220	3.00	100
311	2.60	30	311	2.555	20
222	2.50	10	222	2.450	10
400	2.159	70	400	2.122	70
420	1.925	20	420	1.894	10
422	1.761	80	422	1.732	90
333	1.668	20	440	1.501	60
404	1.535	30	620	1.341	70
440	1.525	60	444	1.225	50
260	1.365	60	642	1.134	70
444	1.253	20	800	1.060	20
326	1.247	30	822,660	0.999	40
264	1.159	40	408	0.950	20
462	1.154	70	840	0.948	40
080	1.080	30	646	0.906	30
800	1.076	30	448	0.868	30
308	1.024	60	844	0.866	40
822	1.016	60	2,0,10	0.834	30
840	0.964	40	10,2,0	0.832	80
508	0.924	30	4,2,10	0.777	50
805	0.918	40	10,2,4	0.775	80
409	0.887	20			
484	0.883	20			
844	0.882	30			
10,1,1	0.852	20			
0,10,2	0.847	40			
10,0,2	0.845	70			
1,0,11	0.793	20			
1,1,11	0.790	20			
4,10,2	0.789	30			
10,4,2	0.787	30			
0,11,0	0.785	40			
11,0,0	0.783	20			

TABLE II

X-ray Data for Cubic, Ordered Perovskite-Type Compounds

	$Ba(Dy_{0.5}Ta_{0.5})O_3$ a_o = 8.454 Å		$Ba(Ho_{0.5}Ta_{0.5})O_3$ a_o = 8.442 Å		$Ba(Y_{0.5}Ta_{0.5})O_3$ a_o = 8.433 Å	
hkl	d_{obs} Å	I/I_o	d_{obs} Å	I/I_o	d_{obs} Å	I/I_o
111	4.88	30	4.88	40	4.88	40
200	4.22	30	4.22	30	4.24	10
220	2.98	100	2.98	100	2.98	100
311	2.544	10	2.544	20	2.543	30
222	2.445	10	2.438	10	2.430	20
400	2.113	80	2.109	80	2.108	70
331			1.934	10	1.930	10
420	1.887	20	1.875	10	1.88	<10
422	1.725	90	1.721	90	1.722	80
511,333			1.622	10	1.624	20
440	1.495	60	1.491	70	1.491	60
531			1.426	40	1.424	20
600,442			1.409	30		
620	1.337	70	1.335	70	1.335	60
533					1.29	≪10
622						
444	1.220	50	1.219	30	1.217	40
711,551			1.183	10	1.18	≪10
640						
642	1.130	80	1.127	80	1.127	70
731,553					1.10	≪10
800	1.057	30	1.054	30	1.053	20
733					1.03	≪10
820,644						
822,660	0.998	50	0.994	70	0.994	50
751,555					0.974	≪10
662						
840	0.945	40	0.944	60	0.942	50
911,753					0.926	≪10
842						
664	0.901	40	0.900	60	0.899	40
931					0.885	≪10
844	0.863	50	0.861	70	0.860	50
933,755,771					0.848	≪10
10,0,0						
10,2,0;862	0.829	80	0.828	90	0.827	70
951,773					0.815	≪10
10,2,2						
953			0.787	10	0.787	≪10
10,4,0;864						

TABLE II (Contd.)

hkl	$Ba(Er_{0.5}Ta_{0.5})O_3$ a_o = 8.423 Å		$Ba(Tm_{0.5}Ta_{0.5})O_3$ a_o = 8.406 Å		$Ba(Yb_{0.5}Ta_{0.5})O_3$ a_o = 8.390 Å	
	d_{obs} Å	I/I_o	d_{obs} Å	I/I_o	d_{obs} Å	I/I_o
111	4.86	20	4.82	<10		
200	4.21	40	4.18	50	4.20	50
220	2.97	100	2.97	100	2.96	100
311						
222						
400	2.103	70	2.099	70	2.099	80
331						
420	1.881	20	1.879	30	1.879	30
422	1.720	90	1.711	90	1.714	90
511,333						
440	1.491	70	1.485	60	1.485	60
531			1.425	20		
600,442	1.404	10	1.399	20	1.398	20
620	1.332	70	1.329	60	1.329	60
533						
622						
444	1.215	60	1.212	40	1.212	40
711,551						
640						
642	1.125	80	1.123	70	1.121	70
731,553						
800	1.052	30	1.050	30	1.048	30
733						
820,644						
822,660	0.992	70	0.991	50	0.988	50
751,555						
662						
840	0.941	70	0.940	50	0.938	50
911,753						
842						
664	0.898	60	0.897	40	0.894	40
931						
844	0.860	70	0.858	50	0.856	50
933,755,771						
10,0,0						
10,2,0;862	0.826	90	0.825	80	0.823	90
951,773						
10,2,2						
953						
10,4,0;864	0.782	20	0.782	20	0.779	20

TABLE II (Contd.)

hkl	$Ba(Lu_{0.5}Ta_{0.5})O_3$ a_o = 8.372 Å d_{obs} Å	I/I_o	$Ba(In_{0.5}Ta_{0.5})O_3$ a_o = 8.280 Å d_{obs} Å	I/I_o	$Ba(Sc_{0.5}Ta_{0.5})O_3$ a_o = 8.222 Å d_{obs} Å	I/I_o
111			4.76	30	4.75	60
200	4.20	50	4.14	30	4.12	<10
220	2.96	100	2.93	100	2.91	100
311			2.501	10	2.478	50
222			2.388	10	2.373	40
400	2.095	70	2.071	80	2.058	80
331			1.90	<10	1.884	30
420	1.869	30	1.850	10		
422	1.710	90	1.690	90	1.680	90
511,333			1.591	<10	1.582	30
440	1.480	60	1.464	70	1.455	70
531			1.399	<10	1.389	30
600,442	1.396	20	1.378	<10		
620	1.324	60	1.308	70	1.302	70
533						<<10
622						
444	1.209	40	1.195	50	1.188	40
711,551					1.153	10
640						
642	1.120	70	1.105	80	1.099	80
731,553					1.070	10
800	1.046	30	1.035	40	1.029	20
733						
820,644						
822,660	0.986	50	0.976	60	0.969	60
751,555						<<10
662						
840	0.936	50	0.926	60	0.919	50
911,753						<<10
842						
664	0.892	40	0.882	50	0.877	40
931						<< 10
844	0.854	50	0.845	60	0.839	60
933,755,771						<< 10
10,0,0						
10,2,0;862	0.821	80	0.812	90	0.806	90
951,773					0.795	10
10,2,2						
953						
10,4,0;864	0.777	10				

TABLE II (Contd.)

	$Ba(Lu_{0.5}Ta_{0.5})O_3$ $a_o = 8.372$ Å		$Ba(In_{0.5}Ta_{0.5})O_3$ $a_o = 8.280$ Å		$Ba(Sc_{0.5}Ta_{0.5})O_3$ $a_o = 8.222$ Å	
hkl	d_{obs} Å	I/I_o	d_{obs} Å	I/I_o	d_{obs} Å	I/I_o
111			4.76	30	4.75	60
200	4.20	50	4.14	30	4.12	<10
220	2.96	100	2.93	100	2.91	100
311			2.501	10	2.478	50
222			2.388	10	2.373	40
400	2.095	70	2.071	80	2.058	80
331			1.90	<10	1.884	30
420	1.869	30	1.850	10		
422	1.710	90	1.690	90	1.680	90
511,333			1.591	<10	1.582	30
440	1.480	60	1.464	70	1.455	70
531			1.399	<10	1.389	30
600,442	1.396	20	1.378	<10		
620	1.324	60	1.308	70	1.302	70
533						<<10
622						
444	1.209	40	1.195	50	1.188	40
711,551					1.153	10
640						
642	1.120	70	1.105	80	1.099	80
731,553					1.070	10
800	1.046	30	1.035	40	1.029	20
733						
820,644						
822,660	0.986	50	0.976	60	0.969	60
751,555						<<10
662						
840	0.936	50	0.926	60	0.919	50
911,753						<<10
842						
664	0.892	40	0.882	50	0.877	40
931						<< 10
844	0.854	50	0.845	60	0.839	60
33,755,771						<< 10
10,0,0						
10,2,0;862	0.821	80	0.812	90	0.806	90
951,773					0.795	10
10,2,2						
953						
10,4,0;864	0.777	10				

TABLE III

Observed and Calculated Intensities for $Ba(B'_{0.5}Ta_{0.5})O_3$ Compounds

	B′ = Sc		Y		In		La		Lu	
hkl	obs.	calc.	obs.	calc.	obs.	calc.	obs.	calc.	obs.	calc.
111	60	17.7	40	6.2	30	2.3		1.1	50	0.0
200	<10	0.0	10	0.6	30	1.6		2.6	50	4.7
220	100	100.0	100	100.0	100	100.0		100.0	100	100.0
311	50	11.0	30	4.0	10	0.8		0.7		0.0
222	40	3.6	20	1.4	10	0.7		0.3		0.0
400	80	30.3	70	29.6	80	28.7		29.2	70	28.0
331	30	5.0	10	1.9	<10	0.8		0.4		0.0
420		0.1	<10	0.2	10	0.6		1.1	30	2.0
422	90	41.0	80	41.5	90	41.0		42.4	90	41.5
511,333	30	3.8	20	1.4	<10	0.7		0.3		0.0
440	70	18.4	60	18.2	70	17.7		18.3	60	17.4
531	30	3.8	20	1.4	<10	0.7		0.3		0.0
600,442		0.0		0.1	<10	0.2		0.4	20	0.9
620	70	17.7	60	17.9	70	17.8		18.4	60	18.0
533	≪10	1.4	≪10	0.5		0.2		0.1		0.0
622		0.8		0.2		0.1		0.0		0.0
444	40	6.2	40	6.1	50	5.9		6.1	40	5.9
711,551	10	2.2	≪10	0.8		0.4		0.2		0.0
640		0.0		0.0		0.1		0.2		0.4
642	80	22.2	70	21.9	80	22.0		22.1	70	22.3

TABLE IV

Structure Data for $Ba(B'_{0.5}Ta_{0.5})O_3$-Type Compounds

Perovskite	Lattice Parameters, Å	Diff. in Ionic Radii of B Ions, Å *	Diff. in Atomic Scattering Factor of B Ions
$Ba(La_{0.5}Ta_{0.5})O_3$	$a_o = 8.611$ $b_o = 8.639$ $c_o = 8.764$	.46	14
$Ba(Nd_{0.5}Ta_{0.5})O_3$	$a_o = 8.556$**	.35	11
$Ba(Sm_{0.5}Ta_{0.5})O_3$	$a_o = 8.519$**	.32	9
$Ba(Eu_{0.5}Ta_{0.5})O_3$	$a_o = 8.506$**	.31	8
$Ba(Gd_{0.5}Ta_{0.5})O_3$	$a_o = 8.487$ $c_o = 8.513$	.30	7
$Ba(Dy_{0.5}Ta_{0.5})O_3$	$a_c = 8.454$	.26	5
$Ba(Ho_{0.5}Ta_{0.5})O_3$	$a_o = 8.442$	.25	4
$Ba(Y_{0.5}Ta_{0.5})O_3$	$a_o = 8.433$	.25	32
$Ba(Er_{0.5}Ta_{0.5})O_3$	$a_o = 8.423$	.23	3
$Ba(Tm_{0.5}Ta_{0.5})O_3$	$a_o = 8.406$	.22	2
$Ba(Yb_{0.5}Ta_{0.5})O_3$	$a_o = 8.390$	.20	1
$Ba(Lu_{0.5}Ta_{0.5})O_3$	$a_o = 8.372$	.18	0
$Ba(In_{0.5}Ta_{0.5})O_3$	$a_o = 8.280$	.10	22
$Ba(Sc_{0.5}Ta_{0.5})O_3$	$a_o = 8.236$	.06	50

* Values for the B^{3+} ion radii as obtained in the present study. The radius used for Ta^{5+} as determined by Ahrens.

** Sample not sufficiently pure to identify cell distortion.

TABLE V

Radii for Trivalent Cations

B^{3+} Ion	Radius, Å - Ahrens	From Previous UAC Study	This Study
La	1.14		1.14
Nd	1.04	1.04	1.04
Sm	1.00	1.00	1.00
Eu	.98	.99	.99
Gd	.97	.98	.98
Dy	.92	.92	.94
Y	.92		.92
Ho	.91	.91	.93
Er	.89	.91	.91
Tm	.87	.90	.90
Yb	.86	.86	.88
Lu	.85	.85	.86
In	.81	.78	.78
Sc	.81	.74	.74

TABLE VI

Doped Compounds

Doped $Ba(B'_{0.50}Ta_{0.50})O_3$ Perovskite-Type Phases

Nd^{3+} Doped Compounds

$Ba(La_{0.48}Nd_{0.02}Ta_{0.50})O_3$
$Ba(Gd_{0.48}Nd_{0.02}Ta_{0.50})O_3$
$Ba(Y_{0.495}Nd_{0.005}Ta_{0.50})O_3$
$Ba(Y_{0.48}Nd_{0.02}Ta_{0.50})O_3$
$Ba(Y_{0.40}Nd_{0.10}Ta_{0.50})O_3$
$Ba(Lu_{0.495}Nd_{0.005}Ta_{0.50})O_3$
$Ba(Lu_{0.48}Nd_{0.02}Ta_{0.50})O_3$
$Ba(Lu_{0.45}Nd_{0.05}Ta_{0.50})O_3$
$Ba(Lu_{0.40}Nd_{0.10}Ta_{0.50})O_3$
$Ba(In_{0.48}Nd_{0.02}Ta_{0.50})O_3$
$Ba(In_{0.40}Nd_{0.10}Ta_{0.50})O_3$
$Ba(Sc_{0.495}Nd_{0.005}Ta_{0.50})O_3$
$Ba(Sc_{0.48}Nd_{0.02}Ta_{0.50})O_3$
$Ba(Sc_{0.45}Nd_{0.05}Ta_{0.50})O_3$

Other B^{3+} Doped Compounds

$Ba(Sc_{0.48}Fe_{0.02}Ta_{0.50})O_3$
$Ba(Y_{0.48}Pr_{0.02}Ta_{0.50})O_3$
$Ba(Y_{0.48}Sm_{0.02}Ta_{0.50})O_3$
$Ba(Y_{0.48}Eu_{0.02}Ta_{0.50})O_3$
$Ba(Y_{0.48}Ho_{0.02}Ta_{0.50})O_3$
$Ba(Y_{0.48}Er_{0.02}Ta_{0.50})O_3$
$Ba(Tb_{0.40}Er_{0.10}Ta_{0.50})O_3$
$Ba(Lu_{0.48}Er_{0.02}Ta_{0.50})O_3$
$Ba(Y_{0.48}Tm_{0.02}Ta_{0.50})O_3$
$Ba(Y_{0.48}Yb_{0.02}Ta_{0.50})O_3$
$Ba(Y_{0.48}Bi_{0.02}Ta_{0.50})O_3$

Cr^{3+} Doped Compounds

$Ba(Y_{0.495}Cr_{0.005}Ta_{0.50})O_3$
$Ba(Y_{0.49}Cr_{0.01}Ta_{0.50})O_3$
$Ba(Y_{0.48}Cr_{0.02}Ta_{0.50})O_3$
$Ba(Y_{0.40}Cr_{0.10}Ta_{0.50})O_3$

TABLE VI (Contd.)

Cr^{3+} Doped Compounds (contd.)

$Ba(Y_{0.30}Cr_{0.20}Ta_{0.50})O_3$
$Ba(Lu_{0.48}Cr_{0.02}Ta_{0.50})O_3$
$Ba(Lu_{0.30}Cr_{0.20}Ta_{0.50})O_3$
$Ba(In_{0.48}Cr_{0.02}Ta_{0.50})O_3$
$Ba(In_{0.40}Cr_{0.10}Ta_{0.50})O_3$
$Ba(Sc_{0.495}Cr_{0.005}Ta_{0.50})O_3$
$Ba(Sc_{0.48}Cr_{0.02}Ta_{0.50})O_3$
$Ba(Sc_{0.45}Cr_{0.05}Ta_{0.50})O_3$

Other Doped Complex Perovskite-Type Phases

$Ba(Y_{0.48}Nd_{0.02}Nb_{0.50})O_3$
$Ba(Sc_{0.48}Cr_{0.02}Nb_{0.50})O_3$
$Ba(Sc_{0.495}Nd_{0.005}Sb_{0.50})O_3$
$Ba(Mg_{0.48}Ni_{0.02}Te_{0.50})O_3$
$Ba(Mg_{0.48}Ni_{0.02}W_{0.50})O_3$
$(Ba_{0.98}Na_{0.02})(Ca_{0.48}Nd_{0.02}W_{0.50})O_3$
$(Ba_{0.98}Na_{0.02})(Zn_{0.48}Cr_{0.02}W_{0.50})O_3$

Doped Non-Perovskite-Type Phases

$K(Al_{0.98}Cr_{0.02})O_2$ - cubic
$Ca(Al_{1.98}Cr_{0.02})O_4$ - orthorhombic or monoclinic
$Sr_3(Al_{1.98}Cr_{0.02})O_6$ - cubic
$Zn(Al_{1.98}Cr_{0.02})O_4$ - cubic spinel structure

TABLE VII

Preliminary Crystal Growth Runs

Composition in Weight %			Soak		Cooling Rate	Observations
	Perovskite	Flux	T °C	Hour	°C/hour	
25	$Ba(Y_{0.5}Ta_{0.5})O_3$	BaF_2	1400	1.5	9	no crystals
25	$Ba(Y_{0.5}Ta_{0.5})O_3$	$KF \cdot 2H_2O$	900	2.5	6	no crystals
16.5	$Ba(Y_{0.5}Ta_{0.5})O_3$	BaF_2	1400	7	12	yellow to orange cubic crystals < $\frac{1}{2}$ mm - x-ray, ordered perovskite
13.1	$Ba(Gd_{0.5}Ta_{0.5})O_3$	BaF_2	1400	5	7	few very small crystals
4	$Ba(Gd_{0.5}Ta_{0.5})O_3$	BaF_2	1415	15	3.5	black crystals < $\frac{1}{2}$ mm - x-ray, ordered perovskite (distorted)
8	$Ba(Lu_{0.5}Ta_{0.5})O_3$	BaF_2	1460	18	4.5	thin blue plates < $\frac{1}{2}$ mm on edge
13	$Ba(La_{0.5}Ta_{0.5})O_3$	BaF_2	1432	15	4	black, irregular shaped crystals up to 1 mm
15	$Ba(Sc_{0.5}Ta_{0.5})O_3$	BaF_2	1385	20	7	yellow crystals < $\frac{1}{2}$ mm
93	$Ba(Lu_{0.5}Ta_{0.5})O_3$	BaF_2	1385	3.5	4	no crystals
13	$Ba(In_{0.5}Ta_{0.5})O_3$	BaF_2	1385	5	4.5	no crystals
7	$Ba(In_{0.5}Ta_{0.5})O_3$	BaF_2-$BaCl_2$	1230	4	4.5	no crystals
5	$Ba(Y_{0.5}Ta_{0.5})O_3$	BaF_2	1385	20	4	no crystals
9.5	$Ba(In_{0.5}Ta_{0.5})O_3$	BaF_2	1452	15	4	no crystals
50	$Ba(Y_{0.5}Ta_{0.5})O_3$	PbO-PbF_2	1020	13	4.4	no crystals-perovskite powder has smaller cell size due to Pb substitution
8	$Ba(Gd_{0.5}Ta_{0.5})O_3$	GdF_3	1335	13	4	no crystals

TABLE VIII

Summary of Slow Cooling Runs Using B_2O_3 Flux

Laboratory Number	Basic Composition, w/o				Batch Composition, Grams				Crucible Size, mm	Time Hrs.	Temp °C	Cooling Rate °C/hr	Decanting Temp °C	Yield
	BaO	$YTaO_4$	B_2O_3	$BaCO_3$	Ta_2O_5	Y_2O_3	B_2O_3	Dopant						
65-059	58	25	17	149.3	33.1	16.9	34		50	4	1393	3.3	955	Mostly $Ba_5Ta_4O_{15}$ hexagonal plates
65-080	56	28	16	143	37.1	18.9	32		50	6	1442	3.3	1040	Mostly $Ba_5Ta_4O_{15}$ hexagonal plates
65-114	53	32	15	136.3	42.4	21.6	30		50	2	1470	2.8	1150	1-2 mm $Ba(Y_{0.5}Ta_{0.5})O_3$ crystals predominately octahedral habit, much twinning
65-135	52	35	13	114.4	39.4	20.1	22.1	.04 Gd_2O_3	50	14	1455	3.75	1155	1-3 mm $Ba(Y_{0.5}Ta_{0.5})O_3$, irregular habit, some twinning. $(Gd_2O_3:Y_2O_3) = 3.9 \times 10^{-4}$
65-164	53	32	15	136.3	42.4	21.6	30	.216 Gd_2O_3	50	2	1454	1.63	1170	1-4 mm $Ba(Y_{0.5}Ta_{0.5})O_3$ mixed, irregular habit, much twinning. $(Gd_2O_3:Y_2O_3) = 2.6 \times 10^{-3}$
65-245	54	33	13	556	168	86	104	0.5 Gd_2O_3	250	4	1457	1.3	1136	$Ba(Y_{0.5}Ta_{0.5})O_3$ mixed habit; some imperfect cubes up to 4 mm. $(Gd_2O_3:Y_2O_3) = 2 \times 10^{-3}$
65-204	53	32	15	545.2	169.6	86.4	120	0.65 Nd_2O_3	250	4	1473	1.3	1190	1 mm $Ba(Y_{0.5}Ta_{0.5})O_3$ octahedra + $BaTa_2O_6$ laths. note: faulty temperature control
65-247	55	31	14	566.3	164.1	83.9	112	0.67 Nd_2O_3	250	12	1470	1.3	1110	$Ba(Y_{0.5}Ta_{0.5})O_3$. mixed habit; some imperfect cubes up to 6 mm, suitable for seed crystals. $(Nd_2O_3:Y_2O_3) = 6 \times 10^{-4}$
	BaO	$LuTaO_4$	B_2O_3	$BaCO_3$	Ta_2O_5	Lu_2O_3	B_2O_3							
65-246	51.5	34	14.5	112.8	30.4	24.65	27.4	0.1 Gd_2O_3	50	4	1440	1.8	1163	1-2 mm $Ba(Lu_{0.5}Ta_{0.5})O_3$ cubic crystals. $(Gd_2O_3:Lu_2O_3) = 3 \times 10^{-4}$
65-248	51.5	34	14.5	112.8	30.4	24.65	27.4	0.15 Yb_2O_3	50	5	1450	1.3	35	1-2 mm $Ba(Lu_{0.5}Ta_{0.5})O_3$ cubic crystals. $(Yb_2O_3:Lu_2O_3) = 3.3 \times 10^{-3}$

TABLE IX

Fluorescent Emission Data for Selected Samples

Compound	Prominent Line Peaks	Half Power Width	Relative Intensity	Temperature
$Ba(Sc_{0.48}Nd_{0.02}Ta_{0.50})O_3$	0.877	500 Å	3.6%	300°K
	1.060	350	2.7	
	0.877	480	8.2	77°
	1.060		7.6	
	0.985		9.6	
$Ba(Y_{0.495}Nd_{0.005}Ta_{0.500})O_3$	0.896	375	1.8	300°
	0.935		.8	
	0.952		.7	
	1.060	375	1.6	
	0.896		2.4	77°
	1.066		2.2	
	0.980		3.4	
$Ba(Lu_{0.48}Nd_{0.02}Ta_{0.50})O_3$	0.893	510	3.4	300°
	1.066	430	3.0	
	0.984		8.5	77°
	1.072		2.6	
$Ba(Y_{0.48}Yb_{0.02}Ta_{0.50})O_3$	[illegible]			300°
	1.0			
	0.972		2.0	77°
	1.007	150	3.7	
$K(Al_{0.98}Cr_{0.02})O_2$	0.695	50	4.5	300°
	0.707	150	4.4	
	0.721		2.0	
	0.730		1.6	
	0.694	30	4.8	77°
	0.705	90	7.8	
	0.719		2.0	
	0.735		1.6	
	0.676	20	2.7	300°

TABLE IX (Contd.)

Compound	Prominent Line Peaks	Half Power Width	Relative Intensity	Temperature
$Zn(Al_{1.98}Cr_{0.02})O_4$	0.688 μ	20 Å	4.0%	300°K
	0.699	60	3.8	
	0.710		3.3	
	0.666		1.2	77°
	0.677		1.1	
	0.688	15	5.2	
	0.699	45	4.5	
	0.710		4.2	
	0.719		2.9	
	0.730		1.3	
	0.738		1.2	

TABLE X

Fluorescent Lifetime Data

Doped $Ba(B'_{0.5}Ta_{0.5})O_3$ Phases	Emission Line (μ)	Lifetime at 300°K (μs)	Lifetime at 77°K (μs)
Nd^{3+} Doped			
$Ba(La_{0.48}Nd_{0.02}Ta_{0.50})O_3$	1.06	500	650
$Ba(Gd_{0.48}Nd_{0.02}Ta_{0.50})O_3$		700	800
$Ba(Y_{0.48}Nd_{0.02}Ta_{0.50})O_3$		200	250
$Ba(Y_{0.495}Nd_{0.005}Ta_{0.500})O_3$		375	375
$Ba(Lu_{0.48}Nd_{0.02}Ta_{0.50})O_3$		400	850
$Ba(Lu_{0.495}Nd_{0.005}Ta_{0.500})O_3$		650	700
$Ba(In_{0.48}Nd_{0.02}Ta_{0.50})O_3$		150	250
$Ba(In_{0.4}Nd_{0.1}Ta_{0.5})O_3$		20	22
$Ba(Sc_{0.48}Nd_{0.02}Ta_{0.50})O_3$		200	220
Pr^{3+} Doped			
$Ba(Y_{0.48}Pr_{0.02}Ta_{0.50})O_3$	1.00	No fluorescence detected	
Tm^{3+} Doped			
$Ba(Y_{0.48}Tm_{0.02}Ta_{0.50})O_3$	1.10	No fluorescence detected	
Sm^{3+} Doped			
$Ba(Y_{0.48}Sm_{0.02}Ta_{0.50})O_3$	0.70	1450	
Yb^{3+} Doped			
$Ba(Y_{0.48}Yb_{0.02}Ta_{0.50})O_3$	1.01	1800	
Cr^{3+} Doped			
$Ba(Y_{0.48}Cr_{0.02}Ta_{0.50})O_3$		No fluorescence detected	
$Ba(Lu_{0.48}Cr_{0.02}Ta_{0.50})O_3$		No fluorescence detected	
$Ba(In_{0.48}Cr_{0.02}Ta_{0.50})O_3$		No fluorescence detected	
$Ba(Sc_{0.48}Cr_{0.02}Ta_{0.50})O_3$		No fluorescence detected	

TABLE X (Contd.)

Other Doped Complex Perovskite Phases Nd^{3+} Doped	Emission Line (Å)	Lifetime at 300°K (μs)	Lifetime at 77°K (μs)
$Ba(Y_{0.48}Nd_{0.02}Nb_{0.50})O_3$	1.06	300	380
$Ba_{0.98}Na_{0.02}(Ca_{0.48}Nd_{0.02}W_{0.50})O_3$		275	250
Doped Non-Perovskite-Type Phases Cr^{3+} Doped			
$K(Al_{0.98}Cr_{0.02})O_2$	0.70	2100	2700
$Zn(Al_{1.98}Cr_{0.02})O_4$		5200	5800

STRUCTURE DIAGRAMS

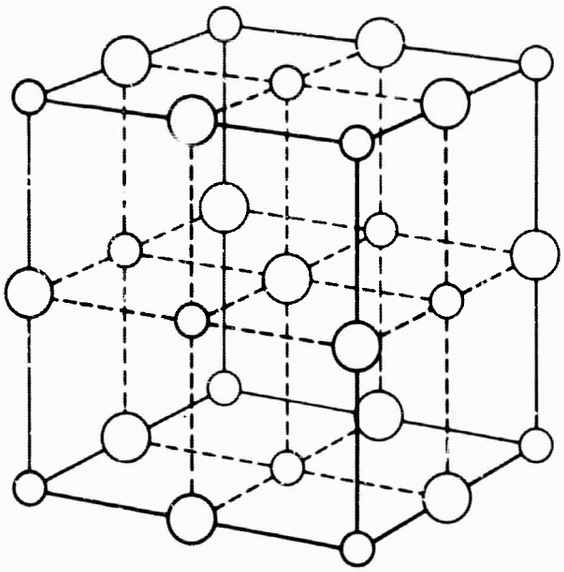

a) NaCl STRUCTURE

○ = Na ◯ = Cl

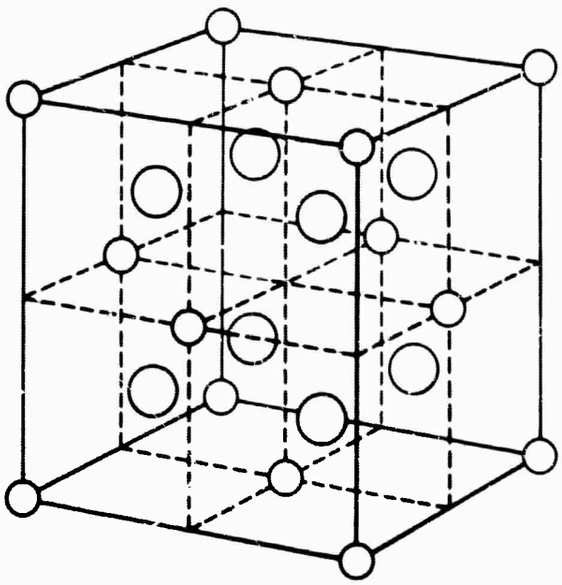

b) CaF_2 STRUCTURE

○ = Ca ◯ = F

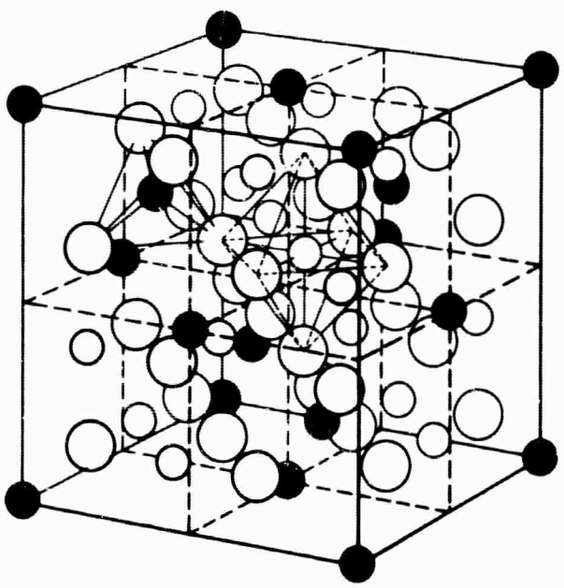

c) SPINEL STRUCTURE

AB_2O_4

● = A ○ = B ◯ = O

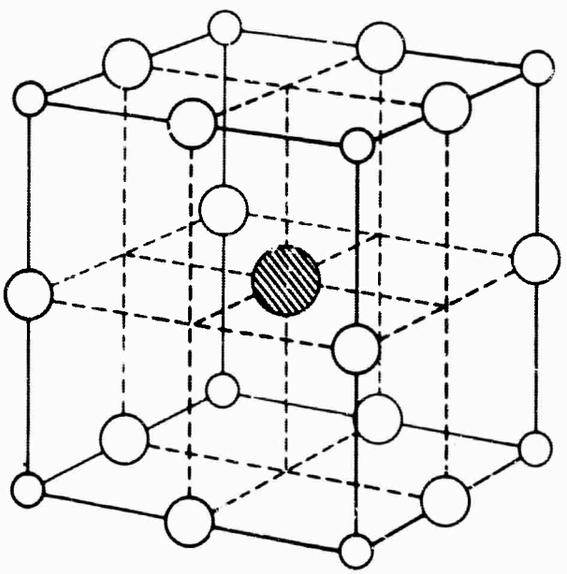

d) PEROVSKITE STRUCTURE

ABO_3

▨ = A ○ = B ◯ = O

ORDERED PEROVSKITE STRUCTURES

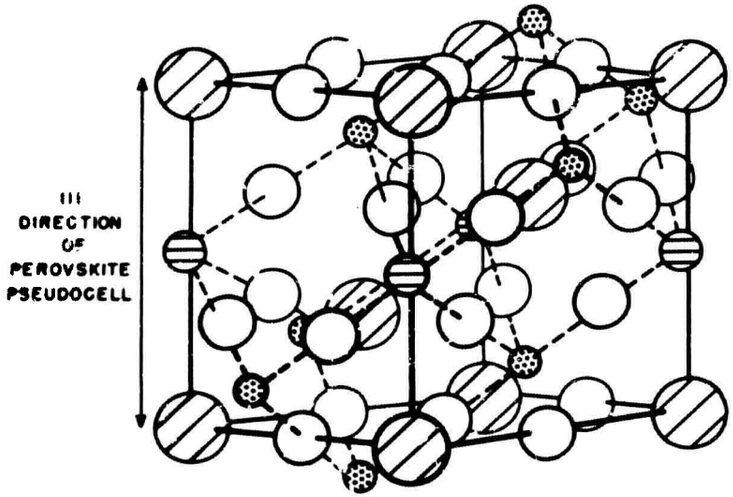

a) HEXAGONAL ORDERED PEROVSKITE-TYPE
$Ba(B'_{0.33}B''_{0.67})O_3$

= A, = B', = B'', = O

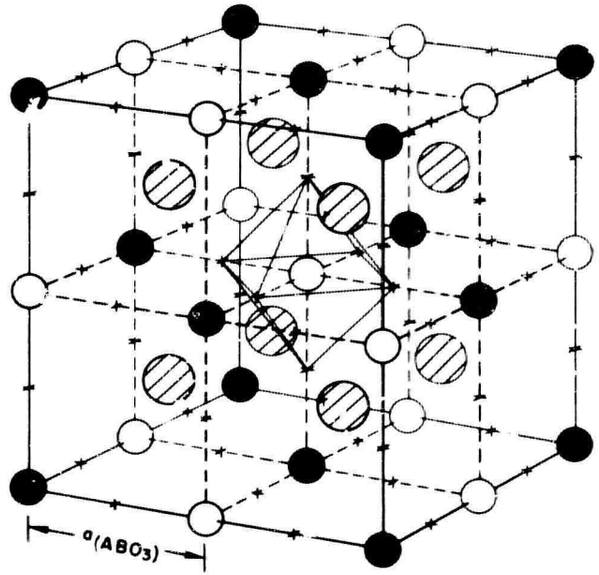

b) CUBIC ORDERED PEROVSKITE-TYPE
$Ba(B'_{0.5}B''_{0.5})O_3$

= A = B' = B'' x = O

D910269-5

FIG. 2

ORDERED NaCl STRUCTURES

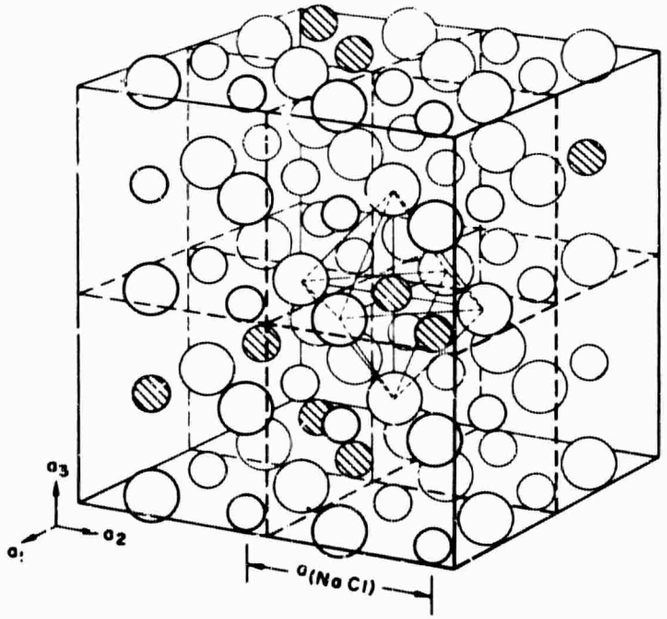

a) CUBIC, Li_3NbO_4

○ = Li ◍ = Nb ◯ = O

CATION POSITIONS AT ONE-QUARTER LEVELS IN UNIT CELL

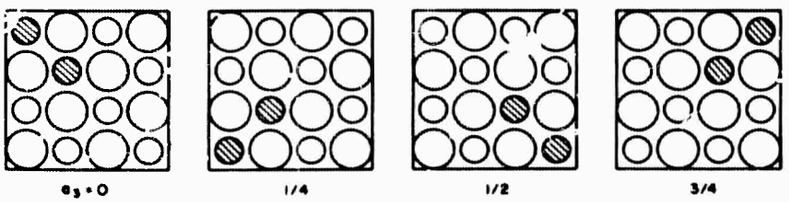

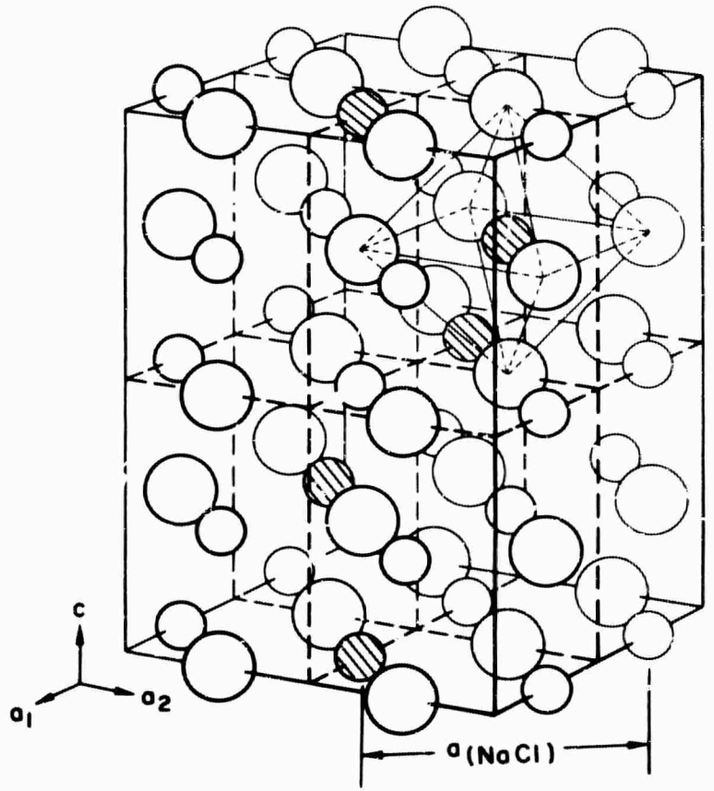

b) TETRAGONAL DISTORTION, Li_3SbO_4

○ = Li ◍ = Sb ◯ = O

CATION POSITIONS AT ONE-QUARTER LEVELS IN UNIT CELL

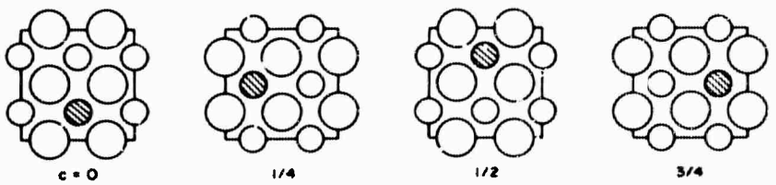

ORDERED SODIUM CHLORIDE STRUCTURES

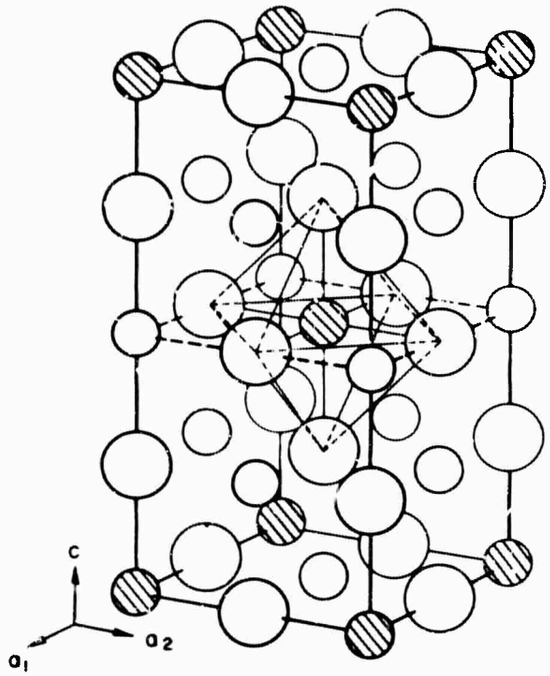

a) TETRAGONAL DISTORTION, Li_3UO_4

○ = Li ⊘ = U ◯ = O

CATION POSITIONS AT ONE-QUARTER LEVELS IN UNIT CELL

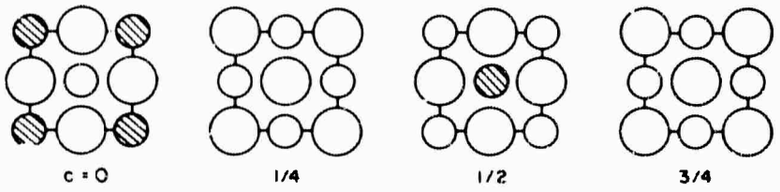

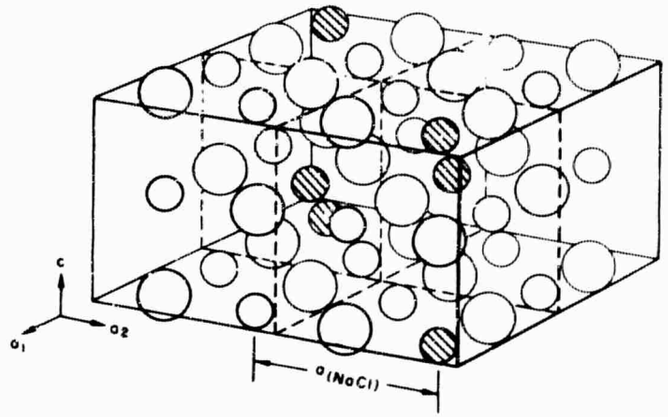

b) TETRAGONAL DISTORTION, Li_3BiO_4

○ = Li ⊘ = Bi ◯ = O

CATION POSITIONS AT ONE-HALF LEVELS IN UNIT CELL

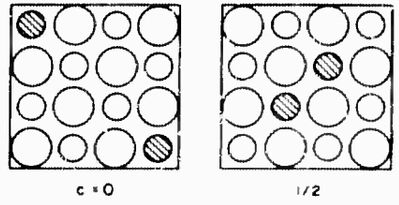

0910269-5

FIG. 4

ORDERED SODIUM CHLORIDE STRUCTURE

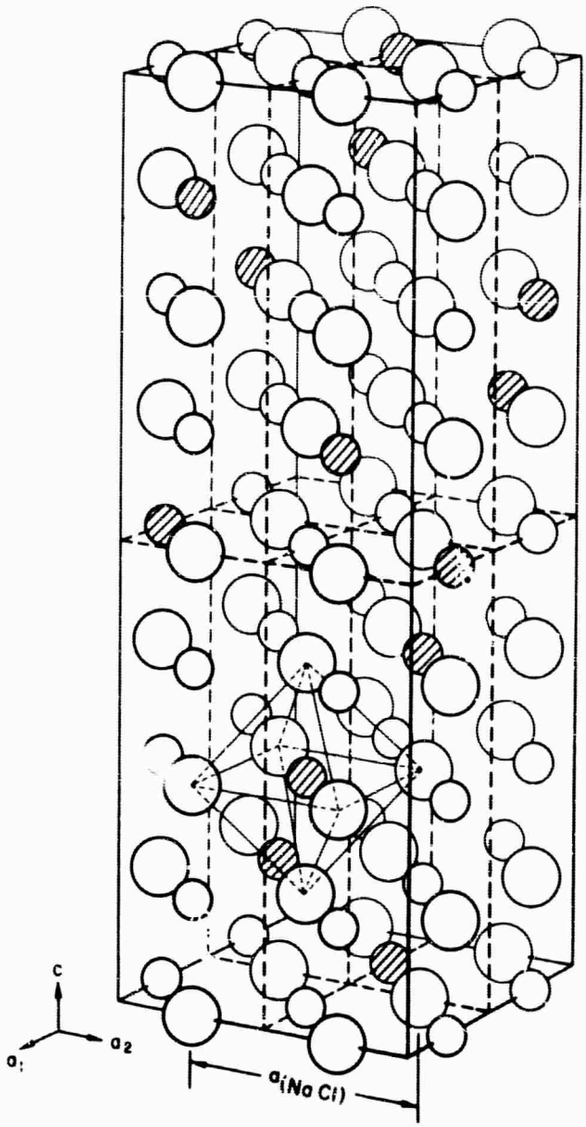

PSEUDO-TETRAGONAL DISTORTION, Li_3TaO_4

○ = Li ◍ = Ta ◯ = O

CATION POSITIONS AT ONE-EIGHTH LEVELS IN UNIT CELL

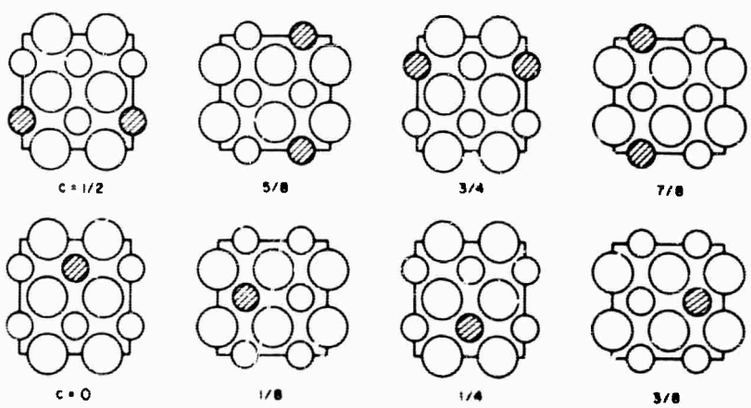

FIG. 6

ORDERED ANTIFLUORITE STRUCTURE

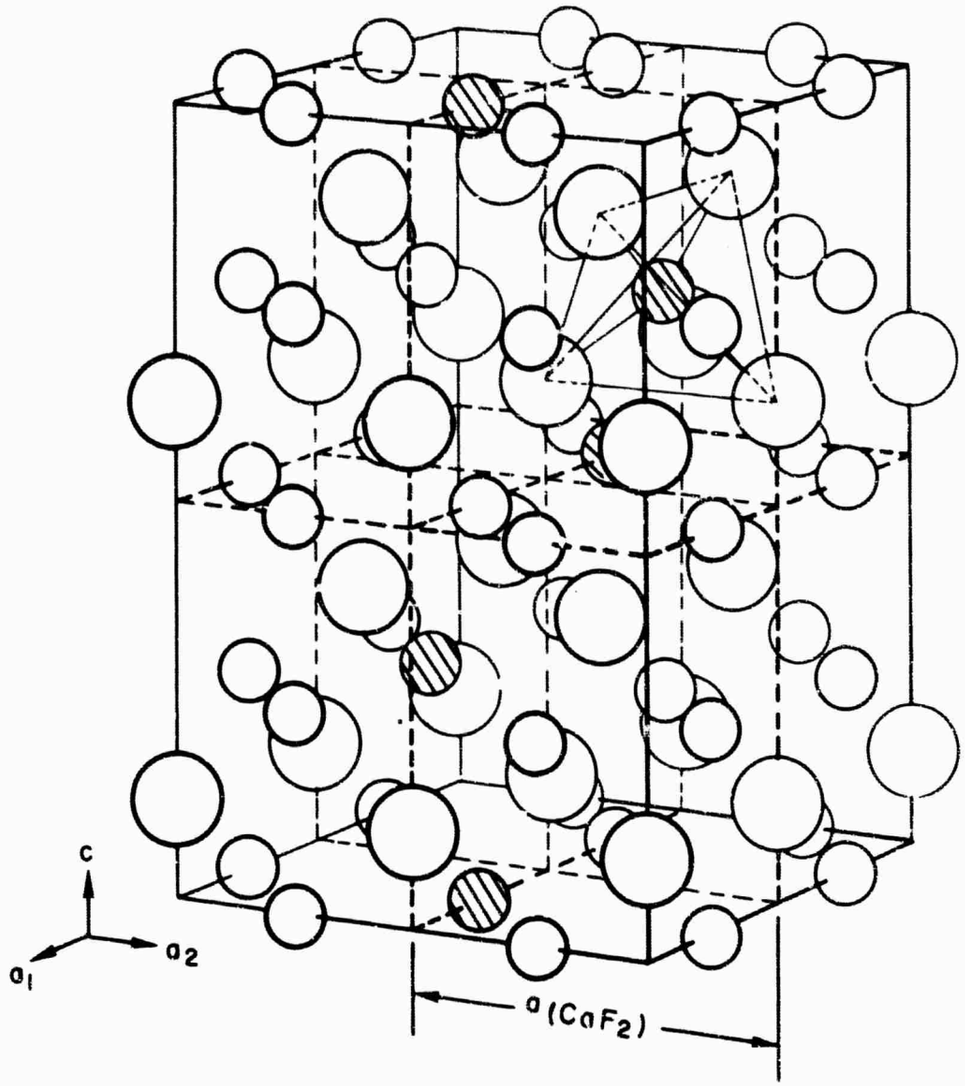

TETRAGONAL DISTORTION, Li_5GaO_4 AND Li_5AlO_4

○ = Li ▨ = Ga, Al ○ = O

CATION POSITIONS AT ONE-EIGHTH LEVELS IN UNIT CELL

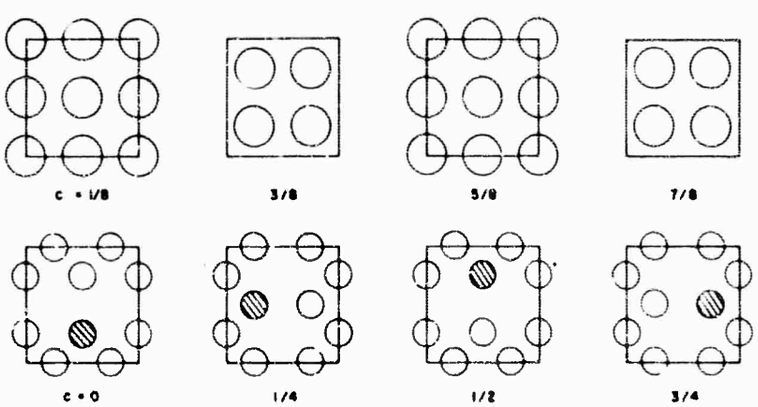

ORDERED SPINEL STRUCTURES

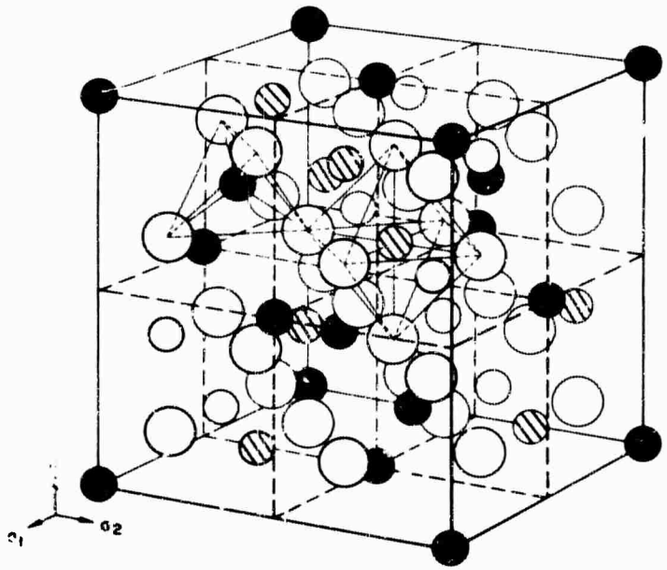

a) TETRAGONAL DISTORTION, $ZnLiNb_3O_4$

● = Zn ○ = Li ▨ = Nb ◯ = O

CATION POSITIONS AT ONE-EIGHTH LEVELS IN UNIT CELL

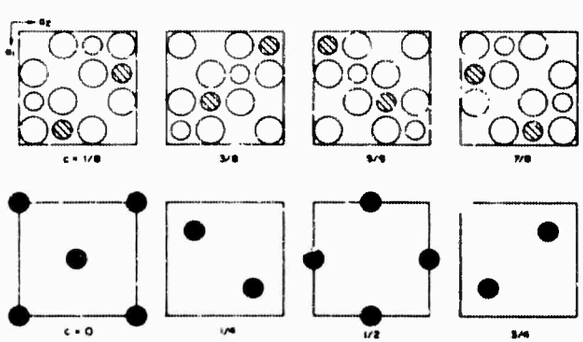

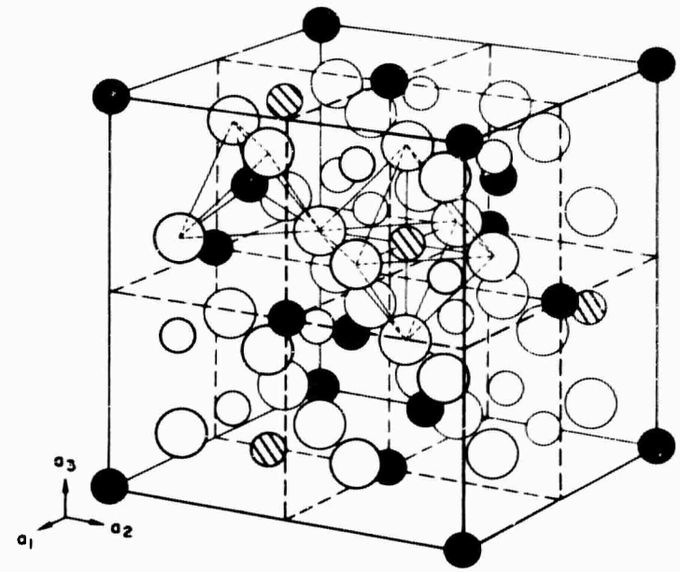

b) CUBIC; $Al_2(Al_3Li)O_8$ AND $Fe_2(Fe_3Li)O_8$

● = Fe, Al ○ = Fe, Al ▨ = Li ◯ = O

CATION POSITIONS AT ONE-EIGHTH LEVELS IN UNIT CELL

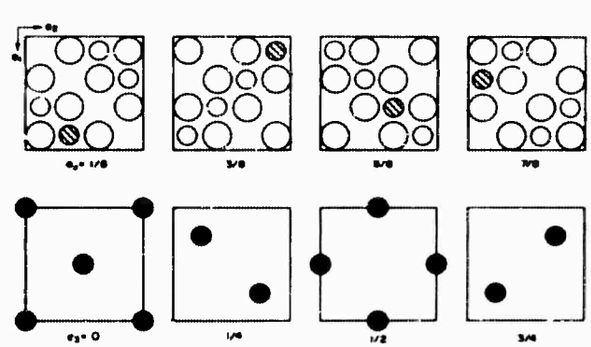

D910269-5

FIG. 7

(CELL VOLUME)$^{1/3}$ VS. IONIC RADII FOR $Ba(B'_{0.5}Ta_{0.5})O_3$ COMPOUNDS

□ AHRENS' RADII USED

○ B' RADII AS DETERMINED FROM STUDIES ON $Ba(B'_{0.5}Nb_{0.5})O_3$ COMPOUNDS

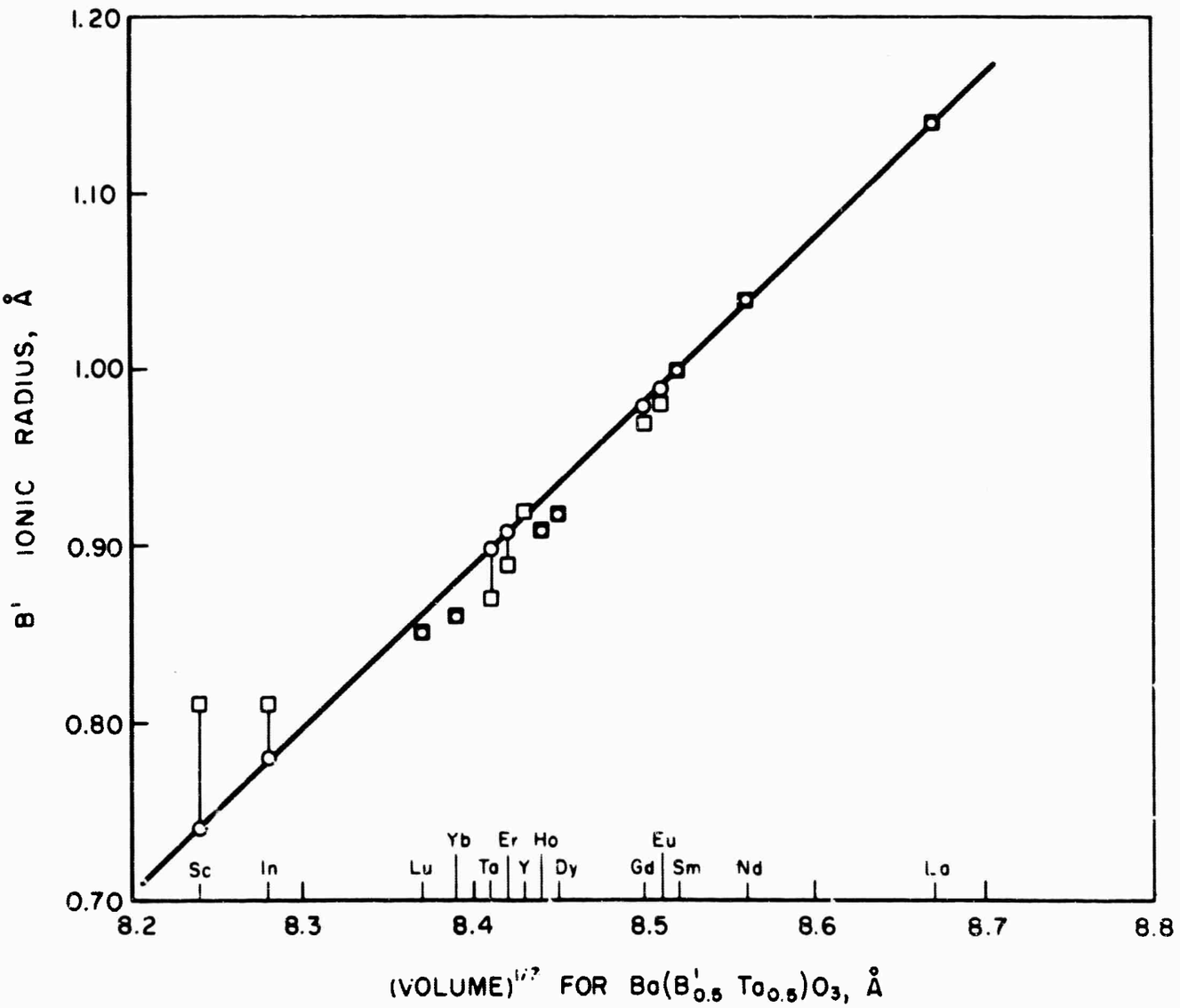

FIG. 9

$BaY_{0.5}Ta_{0.5}O_3$ CRYSTALS

GROWN FROM BaF_2 FLUX (85 w%)
BY COOLING FROM 1400°C AT 12°C/hr.
MAGNIFICATION: 10 X

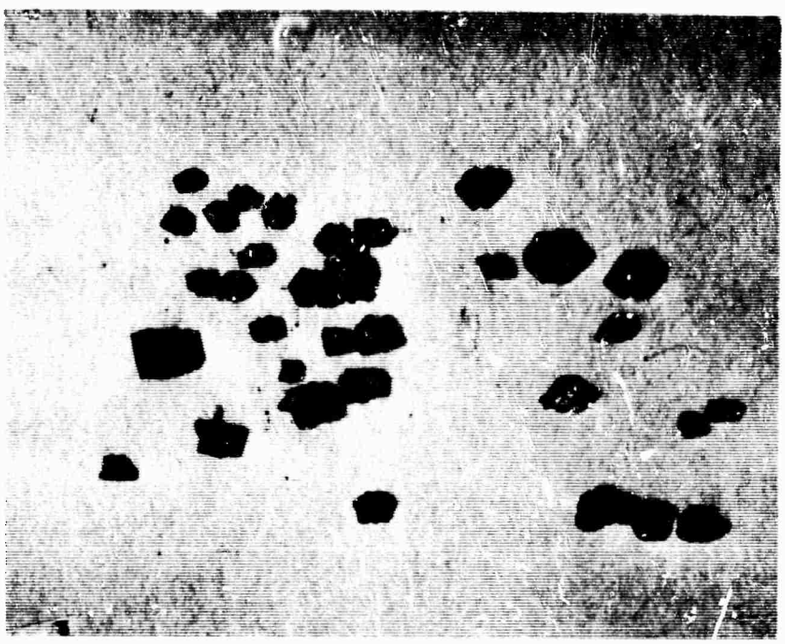

FIG. 10

SOLUBILITY OF $Ba(Y_{0.5}Ta_{0.5})O_3$ IN BaF_2

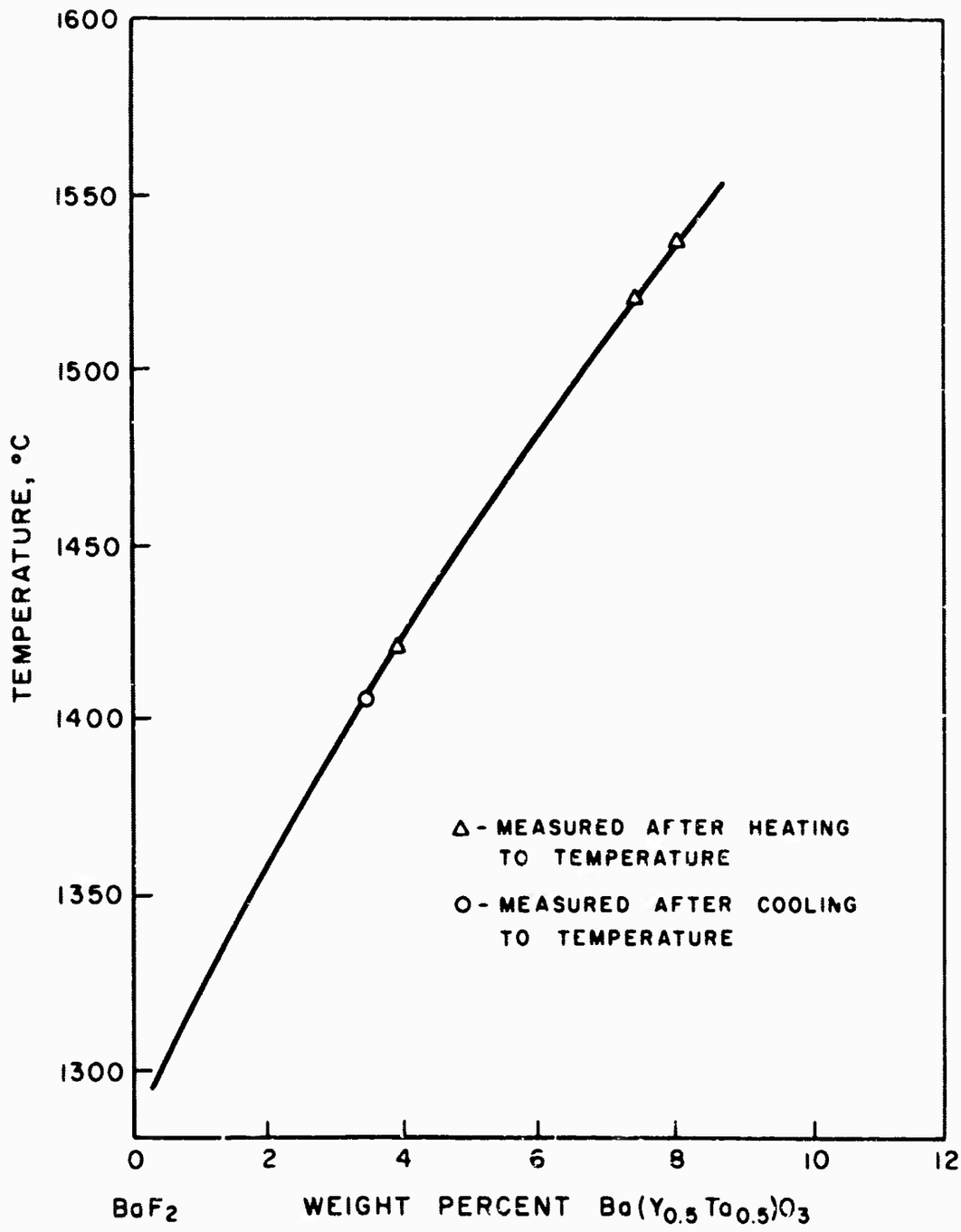

D910269-5

FIG. 11

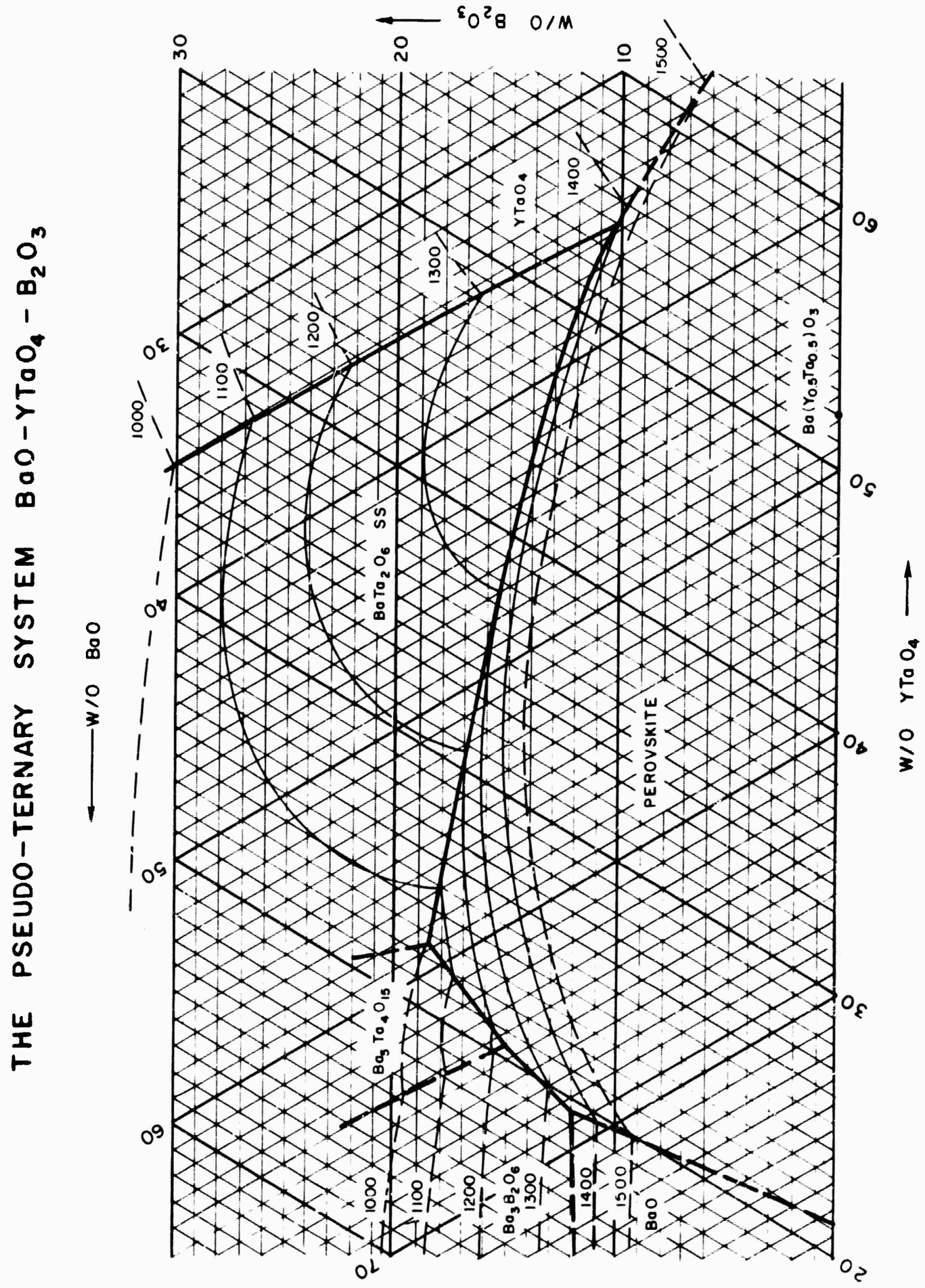

FIG. 12

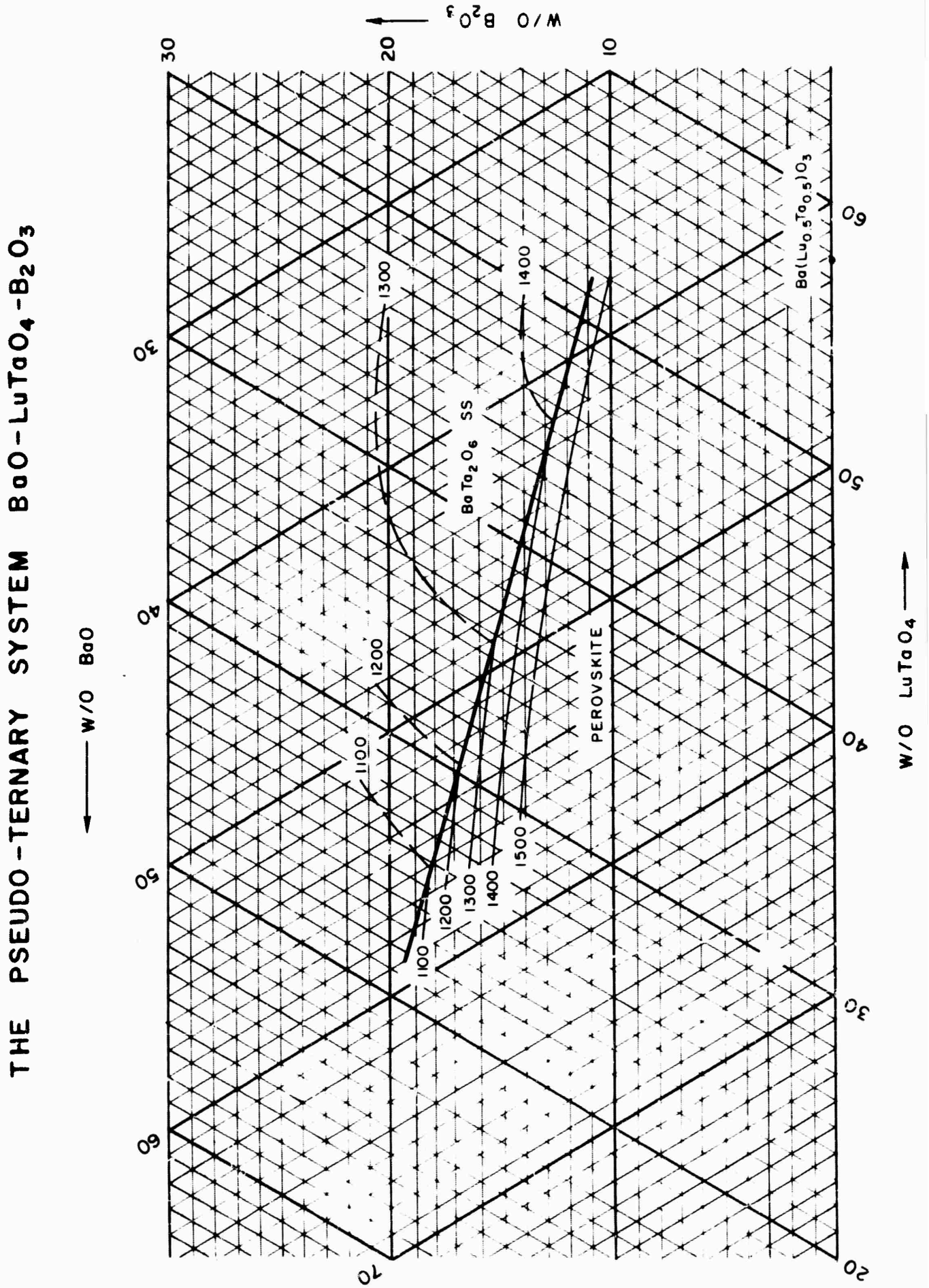
THE PSEUDO-TERNARY SYSTEM BaO-LuTaO4-B2O3
W/O BaO
W/O B2O3
W/O LuTaO4
Ba(Lu0.5Ta0.5)O3
Ba Ta2 O6 SS
PEROVSKITE
1100
1200
1300
1400
1500

DECANTING ARRANGEMENT FOR 50 ml. CRUCIBLE

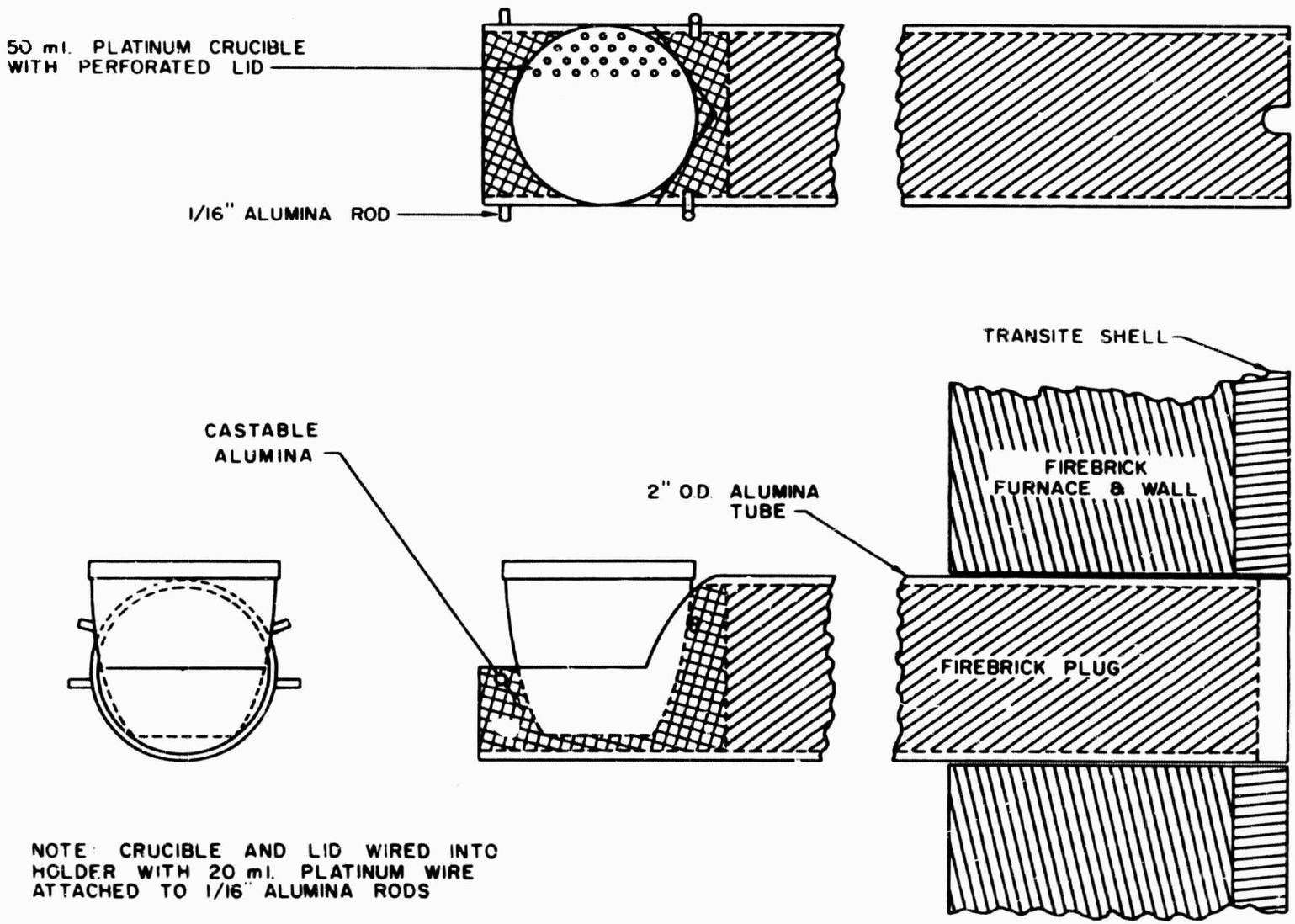

NOTE: CRUCIBLE AND LID WIRED INTO HOLDER WITH 20 ml. PLATINUM WIRE ATTACHED TO 1/16" ALUMINA RODS

250 mm DECANTING FURNACE

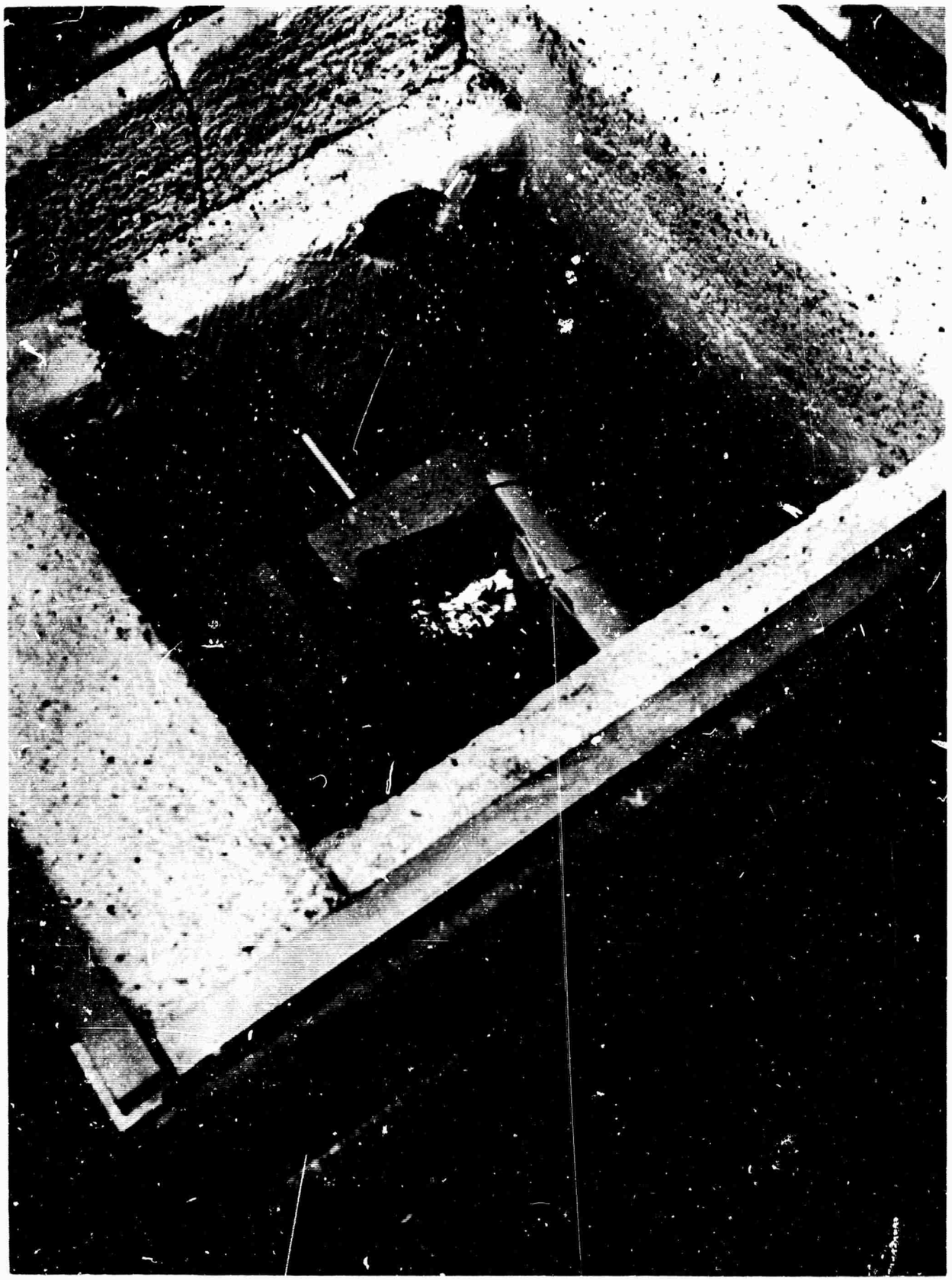

FIG. 15

THERMOCOUPLE BUCKING CIRCUIT

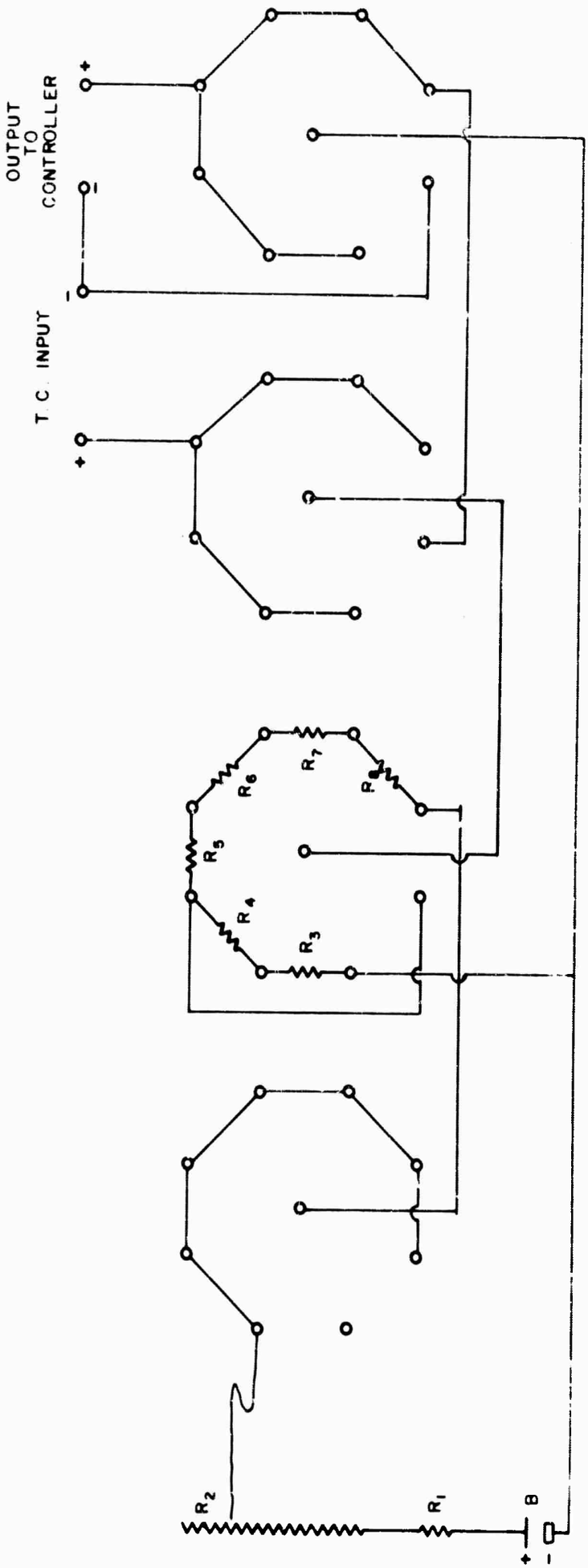

B - 1.35 VOLT Hg BATTERY
R_1 - 51 KΩ RESISTOR
R_2 - 25 KΩ HELIPOT
R_3 - R_8 - 100Ω 1% RESISTORS

TYPICAL STRIP CHART RECORD OF SLOW COOLING RUN

THERMOCOUPLE, pt - pt, 10% rh

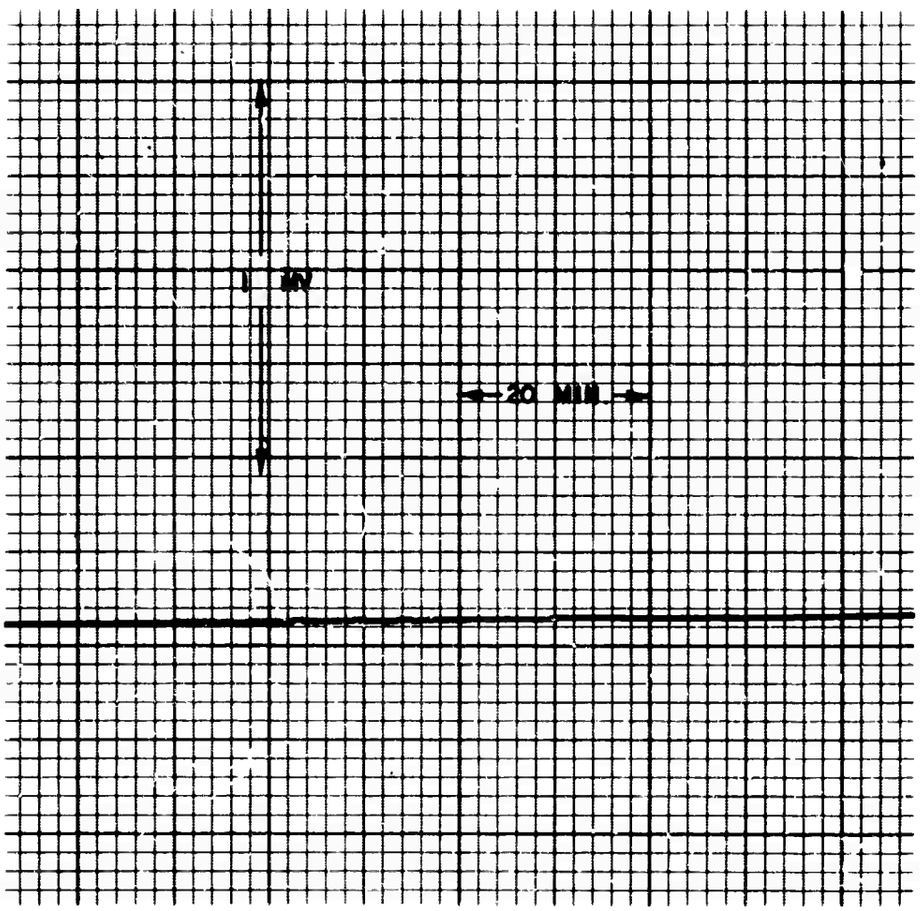

FIG. 17

$Ba_5Ta_4O_{15}$ CRYSTALS, SAMPLE 65-059

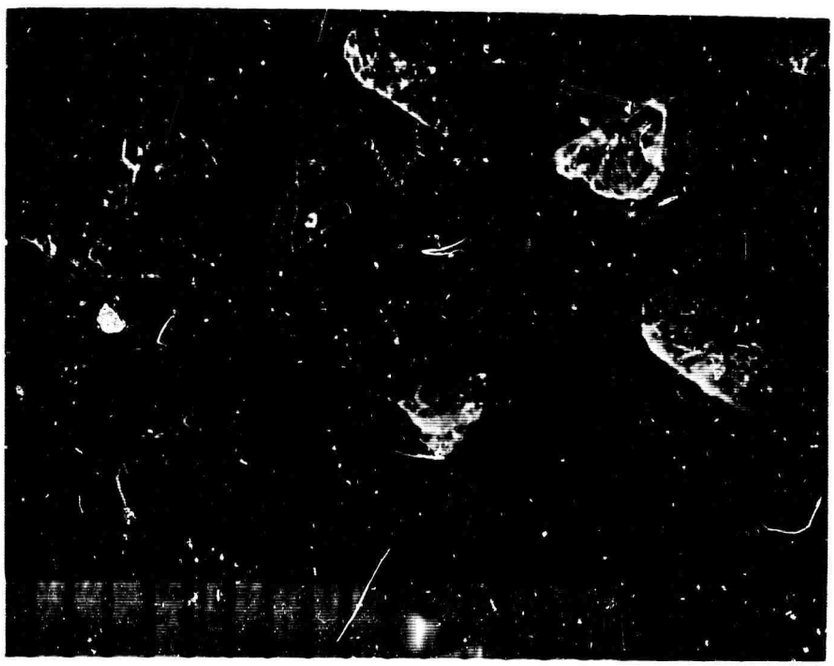

SCALE DISPLAYS 1 mm DIVISIONS

CRYSTALLIZATION PATH OF SAMPLE 65-080

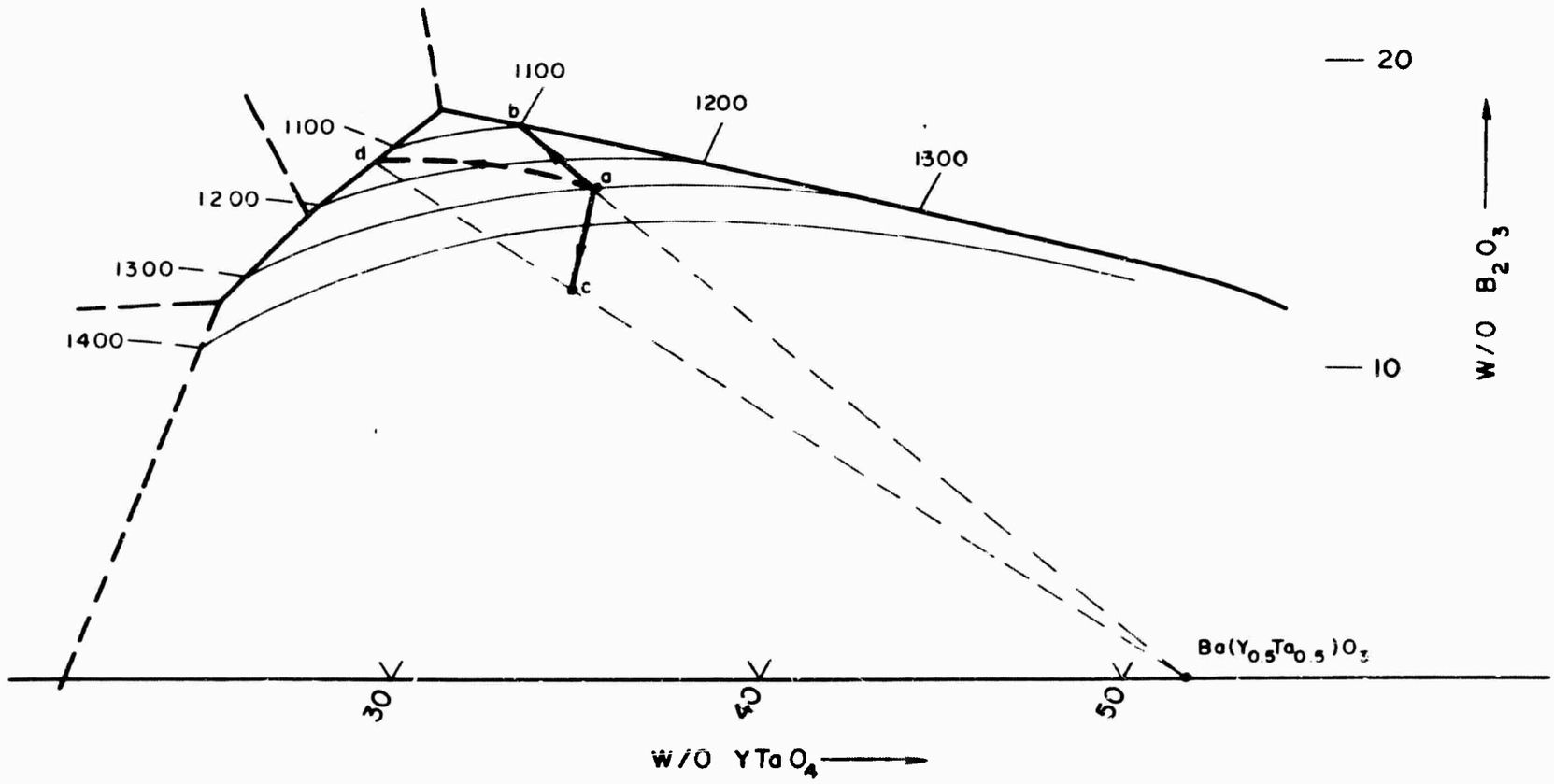

POINT a = ORIGINAL BATCH COMPOSITION
LINE a-c = DIRECTION OF CHANGE OF BATCH COMPOSITION DUE TO B_2O_3 VAPORIZATION
POINT C = BATCH COMPOSITION AT END OF COOLING PERIOD
LINE a-b = CRYSTALLIZATION PATH ASSUMING NO B_2O_3 LOSS
LINE C-d = ACTUAL CRYSTALLIZATION PATH

D910269-5

FIG. 18

CRUCIBLE AFTER DECANTING, RUN 65-114

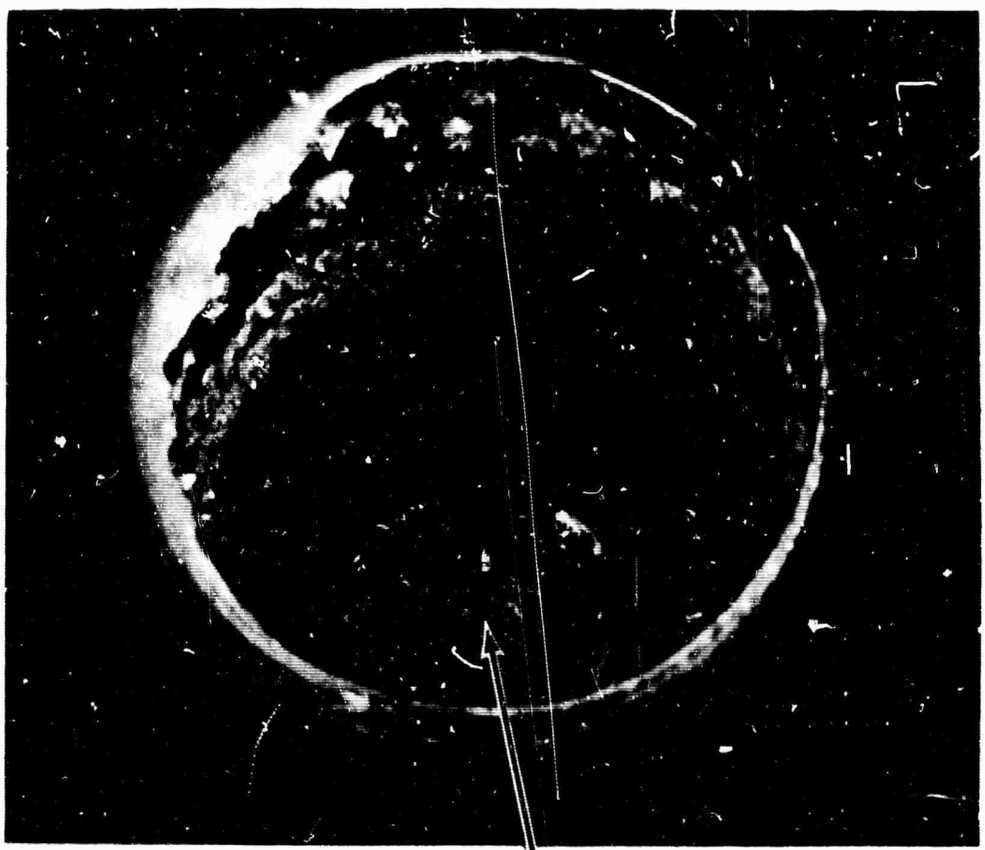

$Ba(Y_{0.5}Ta_{0.5})O_3$ CRYSTALS, SAMPLE 65-114

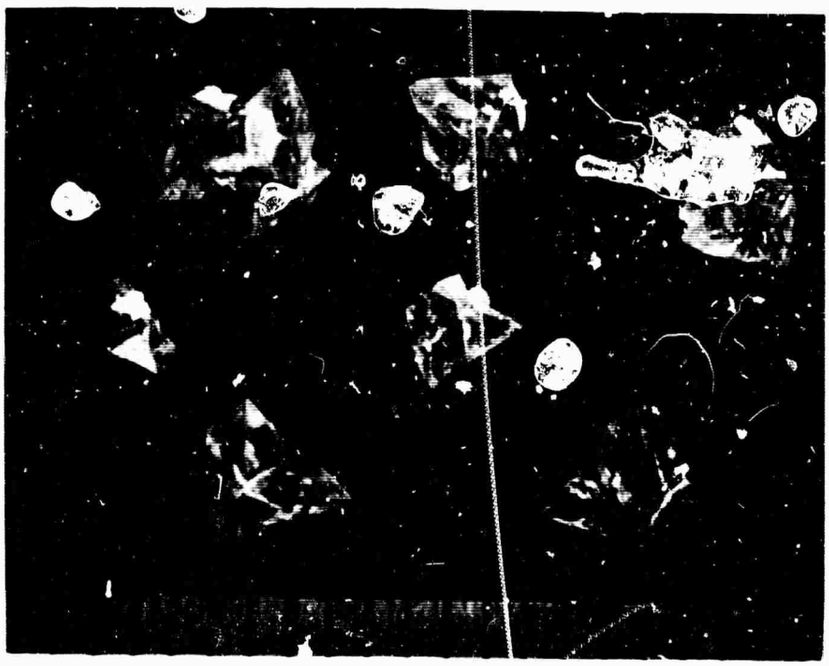

SCALE DISPLAYS 1 mm DIVISIONS

$BaTa_2O_6$ CRYSTALS, SAMPLE 65-204

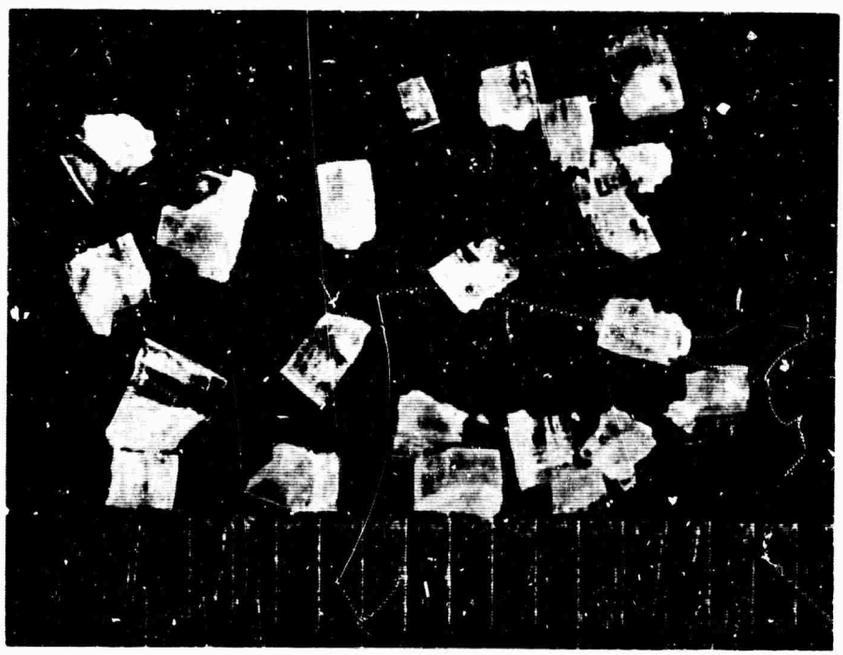

SCALE DISPLAYS 1 mm. DIVISIONS

Nd DOPED $Ba(Y_{0.5}Ta_{0.5})O_3$ CRYSTALS, SAMPLE 65—247

FLAT POLISHED FOR OPTICAL ABSORPTION MEASUREMENT

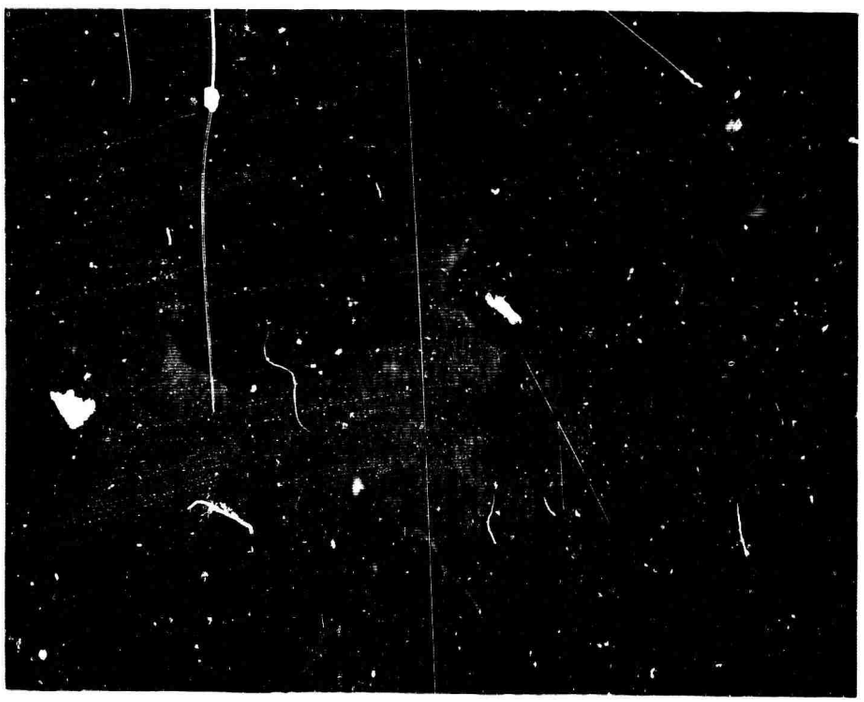

TOP SCALE DISPLAY, 1 mm DIVISIONS

CRYSTAL PULLER AND GRADIENT FURNACE

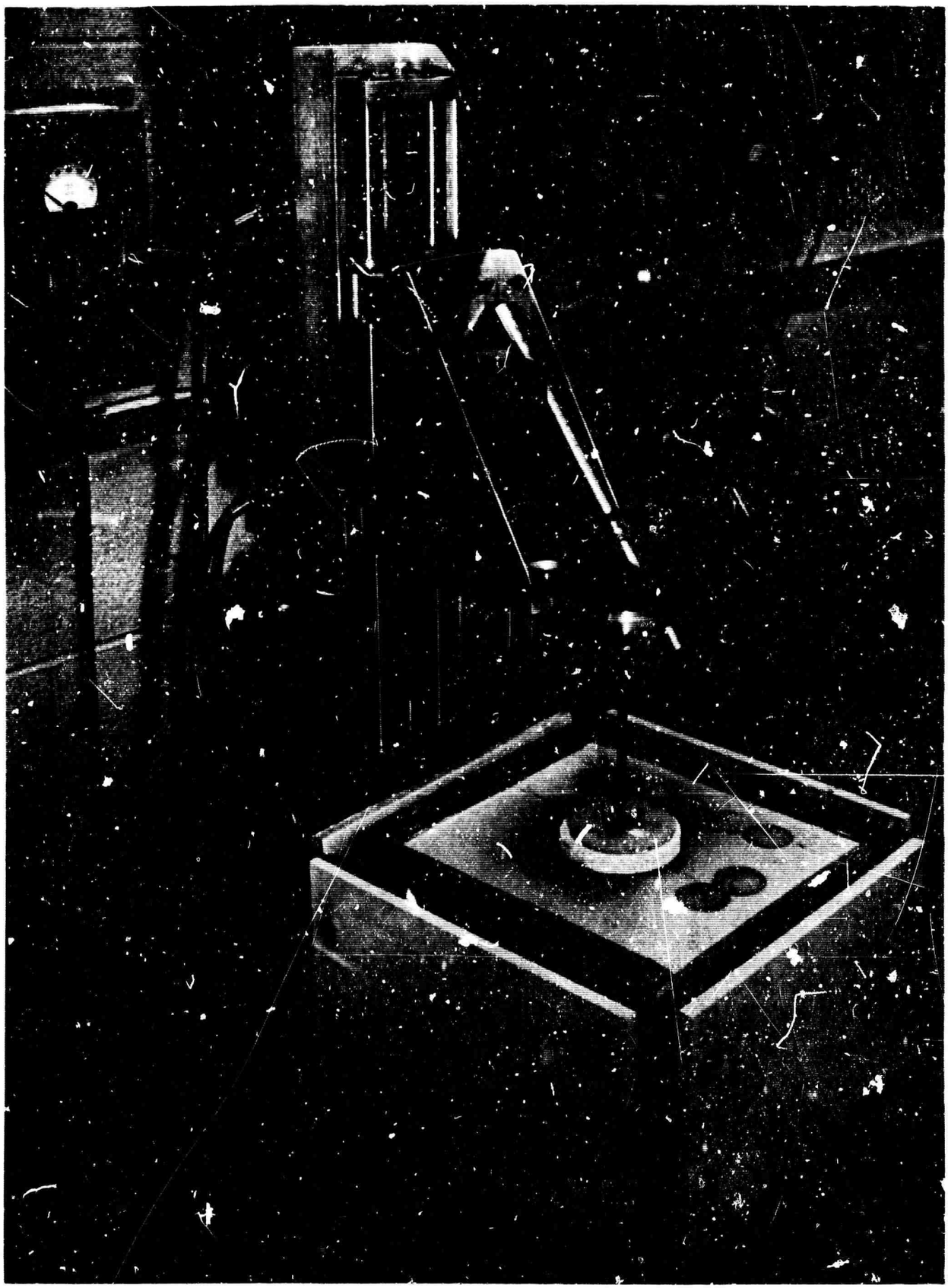

POLYCRYSTALLINE DEPOSIT ON SEED CRYSTAL

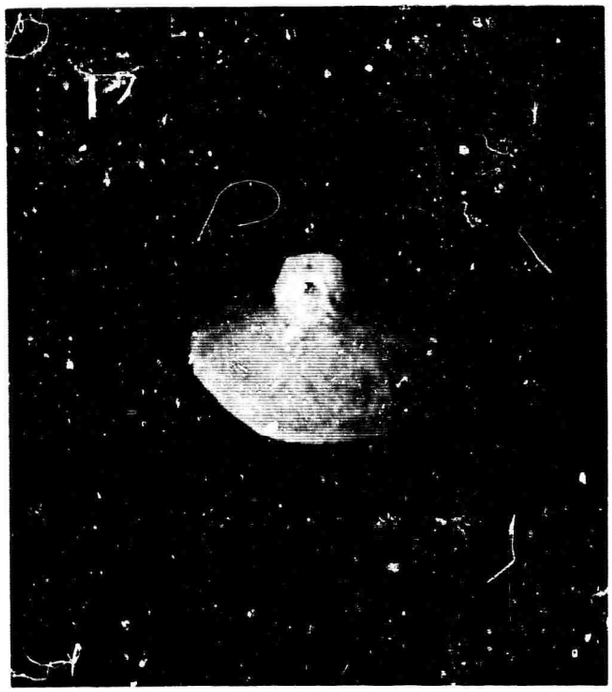

a) TOP VIEW

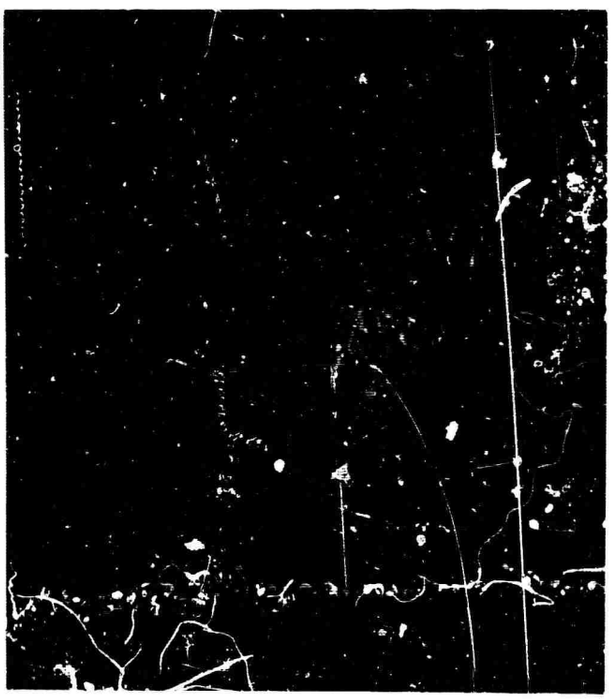

b) BOTTOM VIEW

TEMPERATURE PROFILE OF MELT FOR SINGLE CRYSTAL GROWTH AT SURFACE

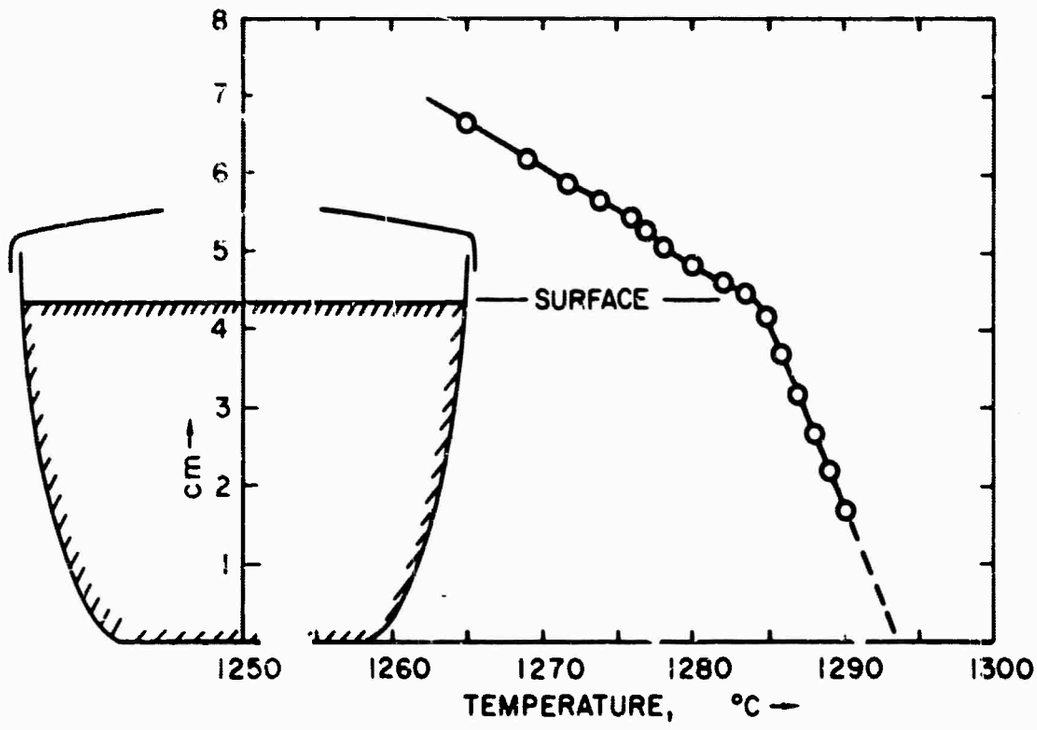

$Ba(Y_{0.5}Ta_{0.5})O_3$ CRYSTAL GROWN BY GRADIENT TRANSPORT

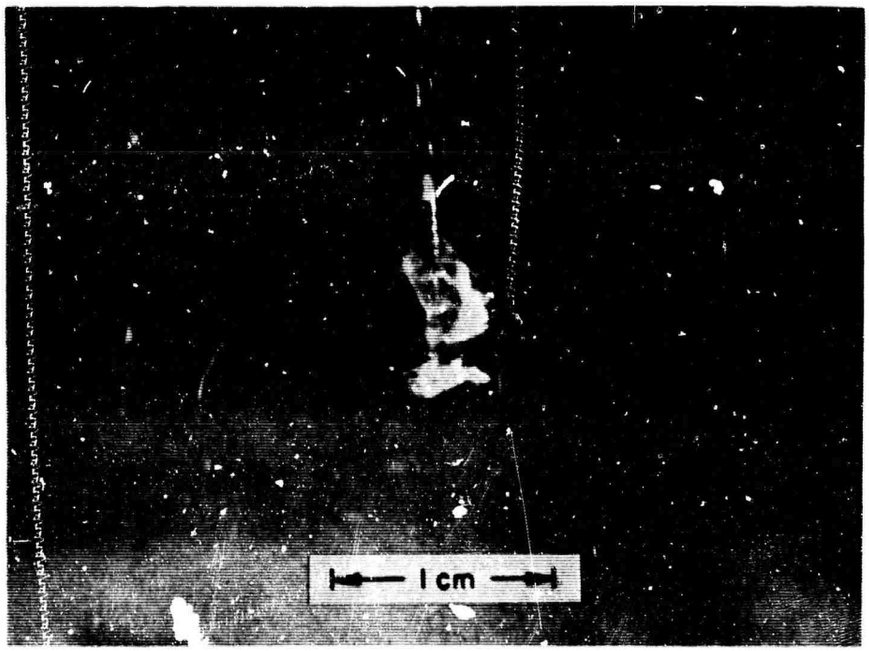

a) AFTER 24 HOURS OF GROWTH

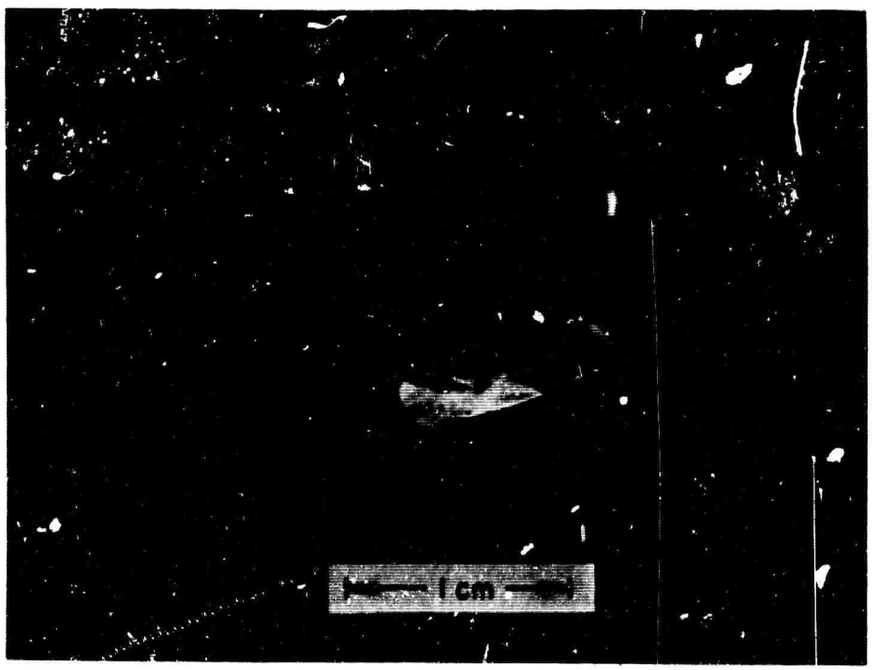

b) AFTER 120 HOURS OF GROWTH

FIG. 27

OPTICAL ABSORPTION SPECTRUM OF Nd^{3+} DOPED $Ba(Y_{0.5}Ta_{0.5})O_3$ CRYSTAL

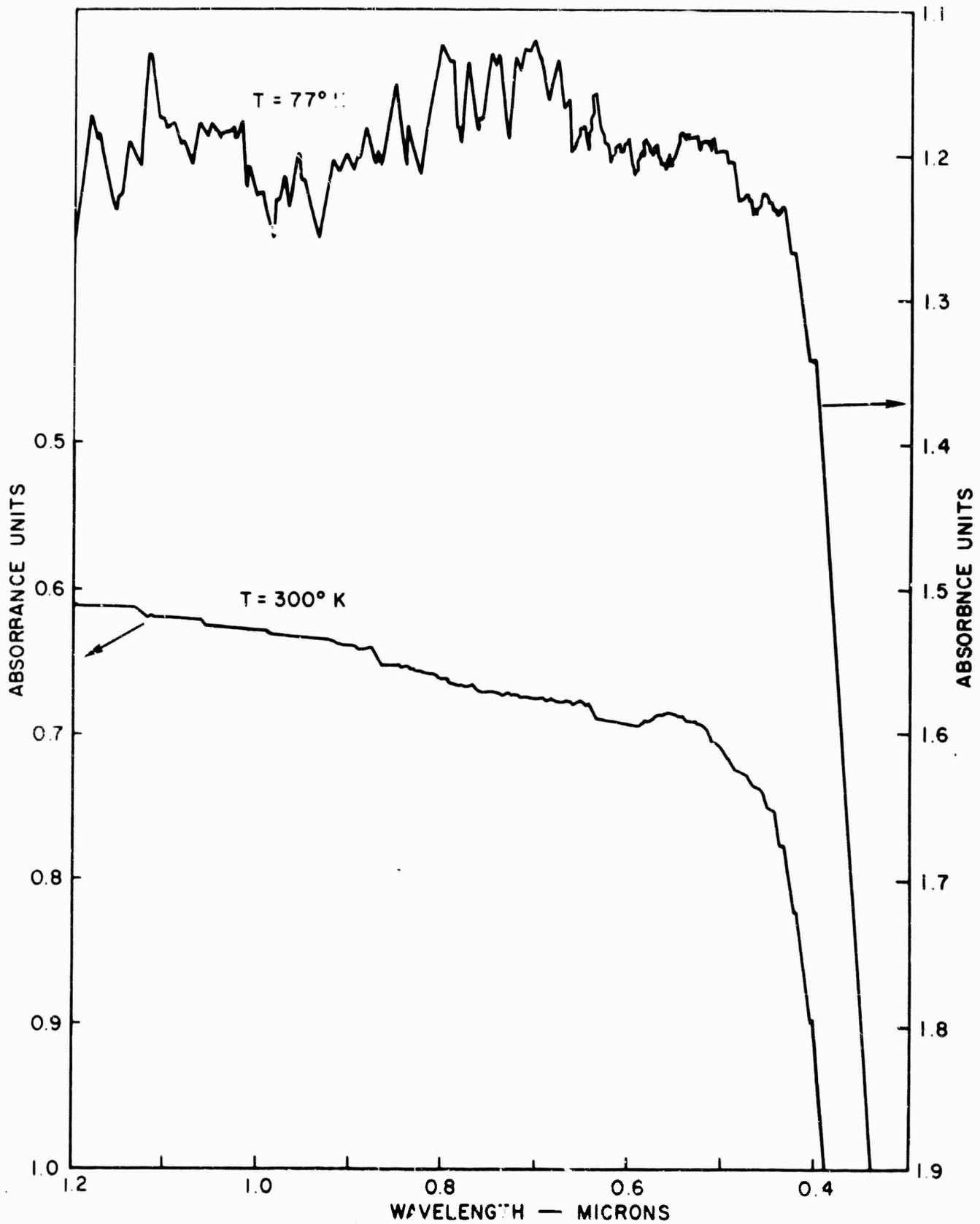

FLUORESCENCE EMISSION OF $Ba(Y_{0.495}Nd_{0.005}Ta_{0.500})O_3$ POWDER

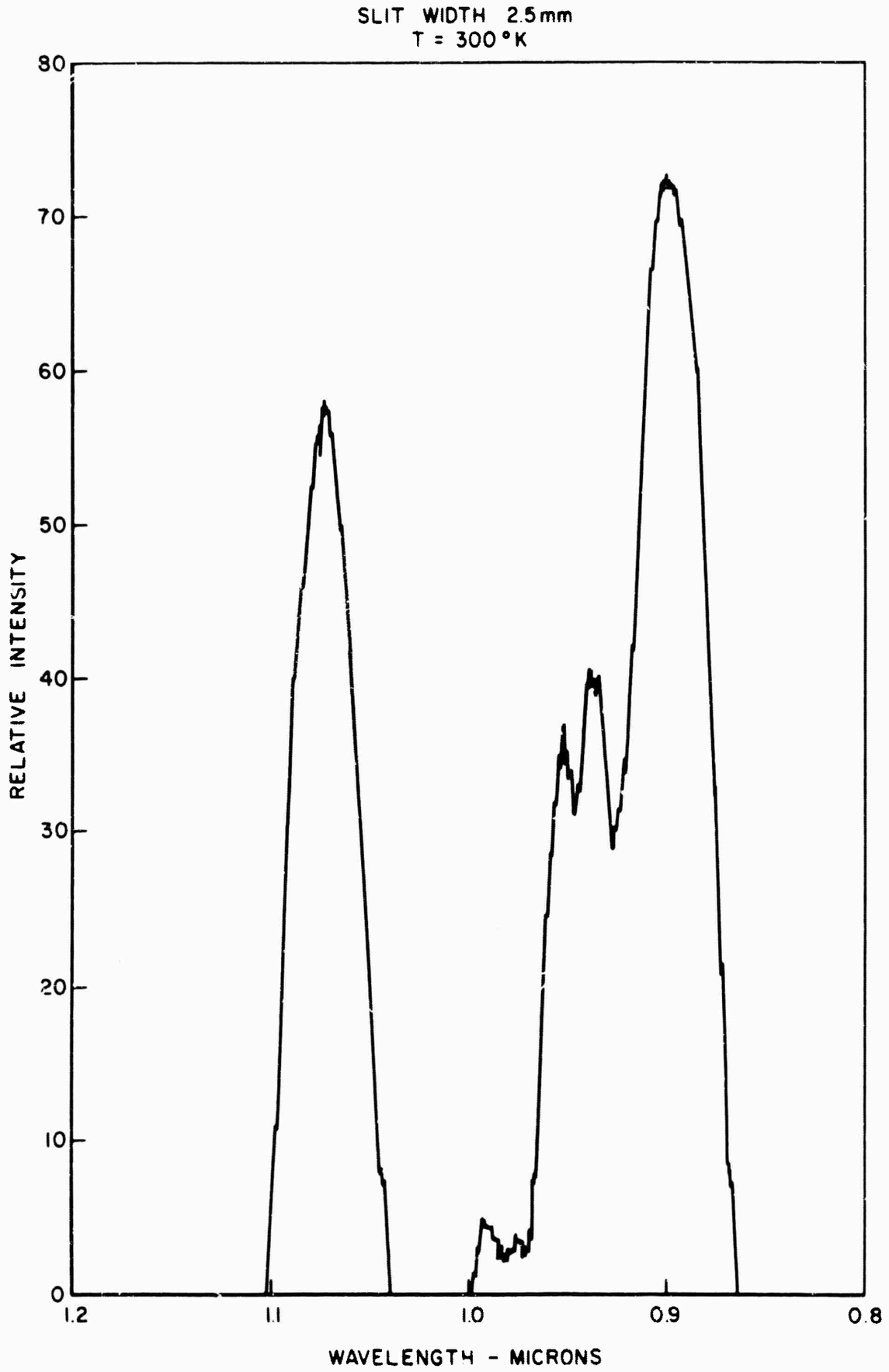

FLUORESCENCE EMISSION OF $Ba(Y_{0.48}Yb_{0.02}Ta_{0.50})O_3$ POWDER

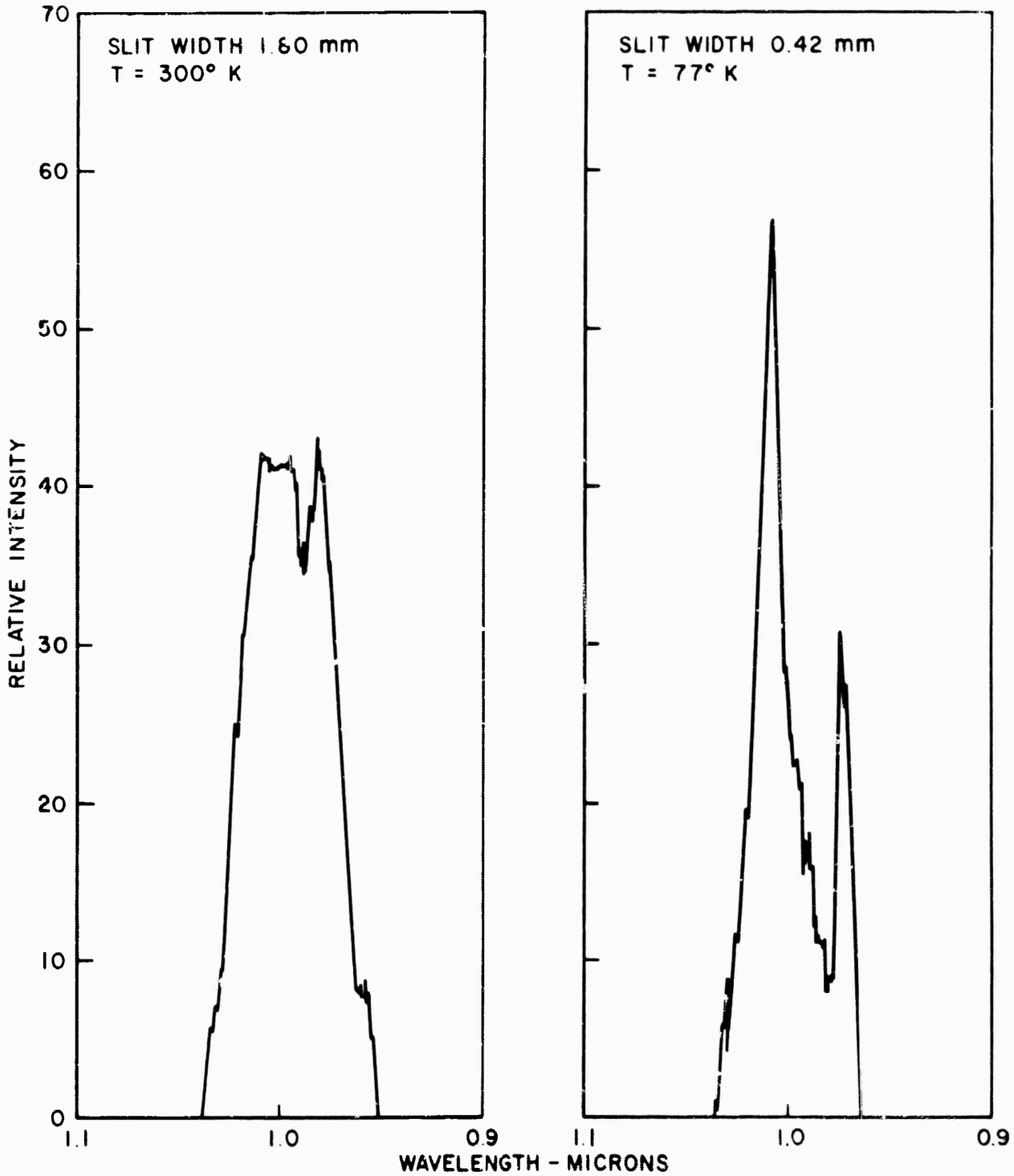

FIG. 30

FLUORESCENCE EMISSION OF $K(Al_{0.98}Cr_{0.02})O_2$ POWDER

SLIT WIDTH 0.6mm

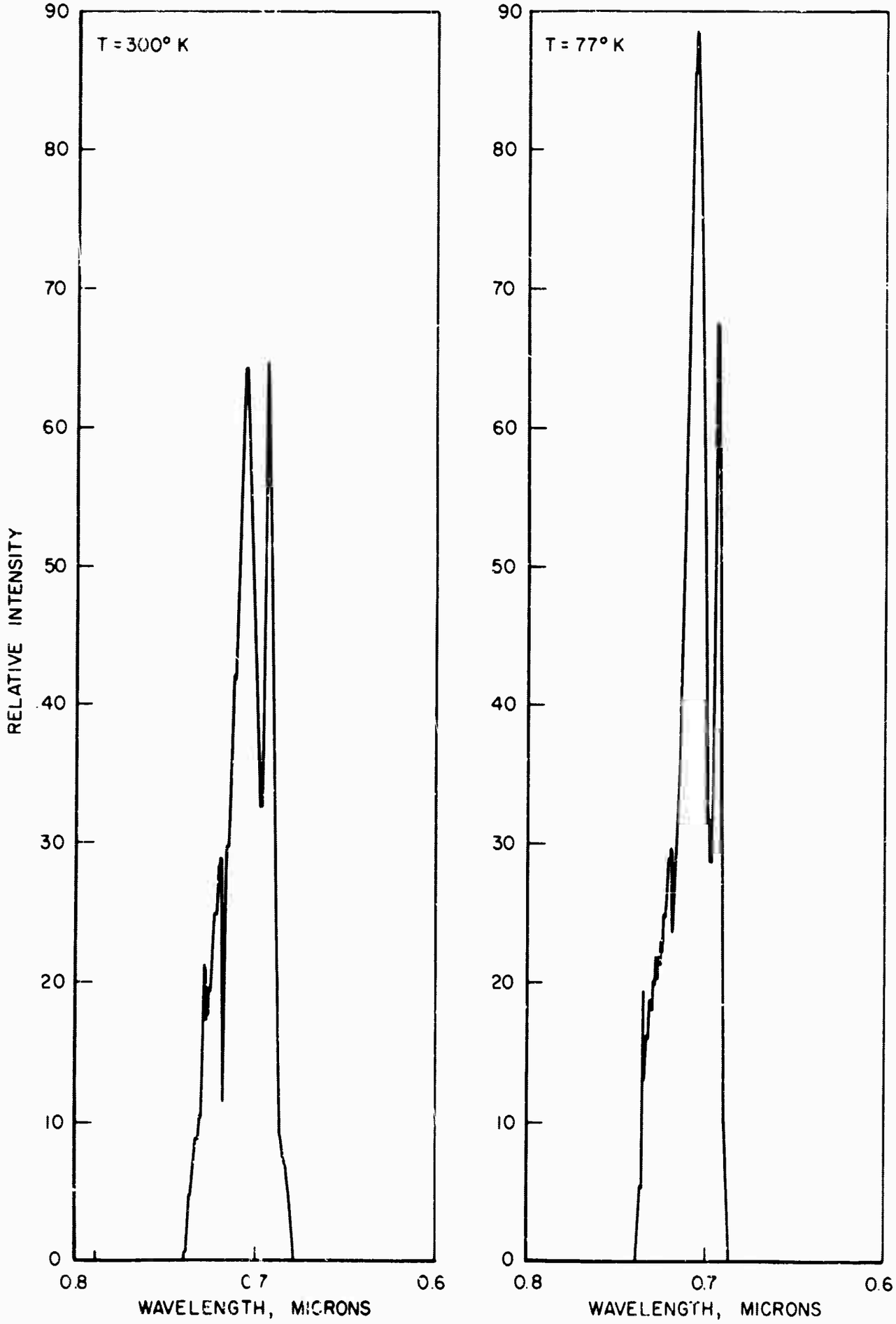

FLUORESCENCE EMISSION OF $Zn(Al_{1.98}Cr_{0.02})O_4$ POWDER

SLIT WIDTH 0.15mm

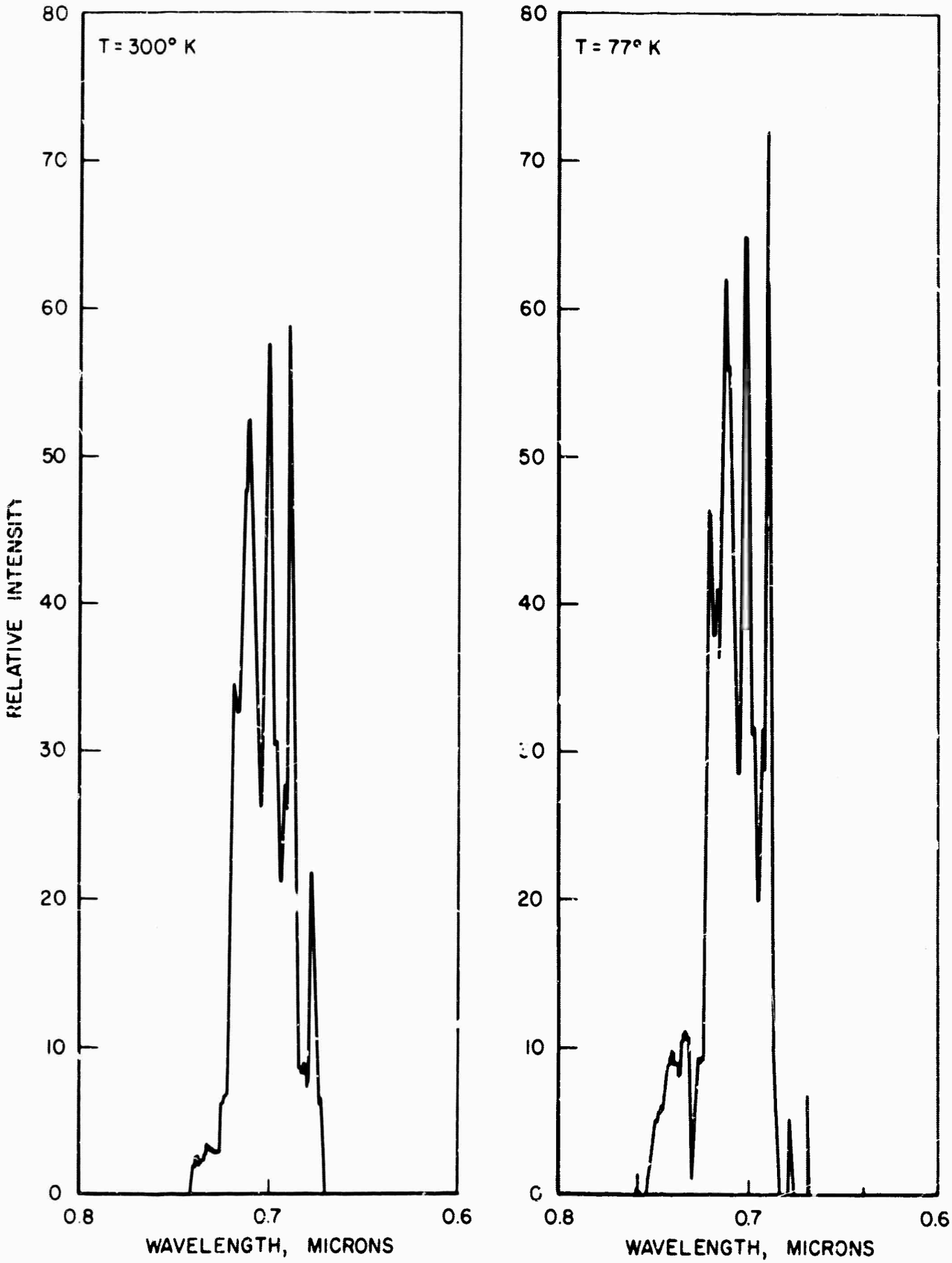

APPENDIX I

Tabulation of $A(B^V_xB^W_y)O_3$*-Type Compounds

The perovskite structure can be described by a cubic unit cell with an A ion in the center, small B ions at the corners, and oxygen ions at the edges. Work in Refs. 1 and 2 demonstrated that it is possible to place two ions which are different in size and charge in the B position of the perovskite structure. Since these papers were published, over two hundred of these compounds with the general formula, $A(B^V_xB^W_y)O_3$, where B^V and B^W are the two different elements with different charges in the perovskite B position, have been prepared in various laboratories throughout the world (Refs. 1-36). The purpose of this report is to tabulate these compounds and their X-ray data in a systematic manner in order to provide a reference for future work in this field.

This report presents the cell sizes and the references for $A(B^V_xB^W_y)O_3$-type compounds. Data for a few oxygen-deficient compounds are also given. It should be noted that compounds with large differences in the charges of the B ions appear to have ordered structures. When the B ions are ordered, the compounds with $x = 0.5$, $y = 0.5$ often have the $(NH_4)_3FeF_6$-type structure (Ref. 21), while those with $x = 0.33$, $y = 0.67$ can either have the $(NH_4)_3FeF_6$ or the $Ba(Sr_{0.33}Ta_{0.67})O_3$-type structure (Ref. 6). The compounds with $x = 0.33$, $y = 0.67$, which form the hexagonal barium-titanate structure, are also included for the purposes of this tabulation even though it cannot be considered that the hexagonal barium-titanate structure is an ordered perovskite type.

A few compounds have been reported to be ferromagnetics, some ferroelectrics and some semiconductors. These are listed in this report together with pertinent data. Preliminary dielectric measurements also have been made at the Research Laboratories on a number of them, but the properties of the majority of these compounds have not been studied.

$$A^{II}(B^{III}_{0.67}B^{VI}_{0.33})O_3$$

A^{II}	$B^{III}_{0.67}$	$B^{VI}_{0.33}$ W	Re	U	Mo
Ba	Al	(20)			
	Cr	5.75 H (22)** 14.35		H (17)†	5.72 H (22) 14.02
	Fe	5.75 (20) H (35) 14.07		8.232 (17)	5.74 H (35) 14.08
	Co	5.74 H (35) 14.10			
	Rh	5.74 H (35) 14.15			
	In	8.321 (20)		8.512 (17)	
	Sc	8.24 (15)(20)		8.49 (17)	
	Lu	(20)			
	Yb	(20)			
	Er	8.386 (20)			
	Y	8.374 (20)		8.70 (17)	
	Dy	8.386 (20)			
	Gd	8.411 (20)(35)			
	Eu	8.605 (20)			
	Nd	8.513 (20)			
	La	8.58 (35)			

ata.
s

$A^{II}(B^{III}_{0.67}B^{VI}_{0.33})O_3$

A^{II}	$B^{III}_{0.67}$	$B^{VI}_{0.33}$ W	Re	U	Mo
Sr	Fe	3.945 (20t)(35) 3.951	7.89 (12)		
	Cr		8.01 (12)	8.00 (17)	
	In		8.297 (12)		
Pb	Fe	(23)(27)			

$A^{II}(B^{II}_{0.33}B^{V}_{0.67})O_3$

A^{II}	$B^{II}_{0.33}$	Ta	Nb	Sb
Ba	Mg	5.782 Å 7.067 (3)	5.77 7.08 (5)(2c)(35)	5.83 H (35) 14.26
	Ni	5.758 7.052 (3)(1c)	4.074 (5)(1)(27)	5.82 H (35) 14.25
	Cu		8.04 (35t) 8.40	5.82 H (35) 14.22
	Co	5.776 7.082 (3)(1c)	4.09 (2)	5.84 H (35) 14.35
	Fe	4.10 (2)	4.085 (5)	
	Zn	5.782 7.097 (3)(2c)	4.094 (5)(2)(27)	
	Mn	5.819 7.127 (3)	(20)	
	Cd	4.167 (3)	4.168 (5)	
	Ca	5.895 7.284 (4)(6c)	5.92 7.25 (5)	5.99 H (35) 14.84

$A^{II}(B^{II}_{0.33}B^{V}_{0.67})O_3$

A^{II}	$B^{II}_{0.33}$	$B^{V}_{0.67}$					
		Ta		Nb		Sb	
Ba	Sr	5.95 7.47	(6)(2c)				
	Pb	4.25	(3)	4.26	(5)		
Sr	Mg	5.652 6.951	(3)(1c)	5.66 6.9?	(5)	7.96	(35)
	Ni	5.607 6.923	(3)(2c)	5.64 6.90	(5)(27)		
	Cu					7.84 8.19	(35t)
	Co	5.630 6.937	(3)(2c)	8.01	(35)	7.99	(35)
	Fe			3.997 4.018	(5t)		
	Zn	5.664 6.951	(3)(2c)	5.66 6.95	(5)(2c)		
	Mn		(20)		(20)		
	Cd			4.089	(5)		
	Ca	5.764 7.096	(3)	5.76 7.16	(5)	8.17	(35)
	Pb		(20)		(20)		
Pb	Mg	4.02	(8)(27)	4.041	(7)(27)		
	Ni	4.01	(8)(27)	4.025	(7)(27)		
	Co	4.01	(8)	4.04	(8)(27)		
	Zn			4.04	(8)		
	Mn				(27)		
Ca	Ni	3.93	(1)	3.88	(27)		

$A^{II}(B^{III}_{0.5}B^{V}_{0.5})O_3$

A^{II}	$B^{III}_{0.5}$	$B^{V}_{0.5}$							
		Ta	Bi	Nb	Sb	Re	Os	W	U	Mo
Ba	Cu							7.88 8.61 (35t)		
	Cr		4.33(35)			H(12)	H(12)		H(17)	
	Co			4.06(35)	5.72 14.00 H(35)	8.086(12)				
	Ni			4.1(35)						
	Fe	4.056(2)(10)		4.06(2)(9)(10)	5.79 14.22 H(35)	8.05(12)				8.08(22)
	Mn	4.076(10)		4.083(10)		8.18(12)				
	Rh			8.17(35)	5.78 14.20 H(35)				H(17)	
	In	8.280(20)		8.279(9)(13)	8.269(28)(35)	8.258(12)	8.224(12)		8.52(17)	
	Sc	8.222(20)(27)		4.121(11)(27)	8.197(28)	8.163(12)	8.152(12)		8.49(17)	
	Lu	8.372(20)		8.364(9)(11)						
	Yb	8.390(20)(27)		8.374(9)(11)(27)						
	Tm	8.406(20)		8.408(9)(11)						
	Er	8.423(20)		8.427(9)(11)		8.354(12)			8.67(17)	
	Ho	8.442(20)		8.434(9)(11)						
	Y	4.205(10)(20)		4.200(10)(11)		8.372(12)			8.69(17)	
	Dy	8.545(20)		8.437(9)(11)						
	Tb			4.229(11)						
	Tl	8.42(28)								
	Gd	8.487 8.513 (20		8.496(9)(11)	8.44(35)	8.431(12)				
	Eu	(20)		8.507(9)(11)						
	Sm	4.24(10)		8.518(9)(10)(11)						
	Nd	4.27(10)(20)		8.540(9)(10)(11)		8.51(12)				
	Pr	4.27(10)		4.27(10)(11)						
	Ce			4.293(11)						

$A^{II}(B^{III}_{0.5}B^{V}_{0.5})O_3$

A^{II}	$B^{III}_{0.5}$	$B^{V}_{0.5}$ = Ta	Nb	Sb	Re	Os	W	U	Mo
Ba	La	8.62(19)(20)(20-o)	8.607 8.690(?t)(11t)(10c)		8.58(12)				
Sr	Ga		3.946(1)	7.84(28t) 7.91	7.843(12)	7.82(12)			
	Cr	3.94(1)	3.9421(13)(35)	7.862(28)(35)	7.82(12)	7.84(12)	7.82(22)		7.82(22)
	Co		3.93(35)	7.88(35)					
	Fe	3.96 3.981(18t)	3.97(2)	7.916(28)(35)					7.89(22)
	Ni			(35t)					
	Mn								7.98(22)
	Rh			5.77 5.55(35-o) 7.99					
	In		4.0569(13)		8.071(12)	8.06(12)		8.33(17)	
	Sc				8.02(12)	8.02(12)			
	Lu	(20)							
	Yb	(20)							
	Tm	(20)							
	Er	(20)							
	Ho	(20)							
	Dy	(20)							
	Gd	(20)							
	Eu	(20)							
	Sm	(20)							
	Nd	(20)							
	La	8.27(19)							

$A^{II}(B^{III}_{0.5}B^{V}_{0.5})O_3$

A^{II}	$B^{III}_{0.5}$	$B^{V}_{0.5}$							
		Ta	Nb	Sb	Re	Os	W	U	Mo
Ca	Cr				5.38 7.67(12-o) 5.47	5.38 7.66(12-o) 5.47	5.47 7.70(22-o) 5.35		5.49 7.70(22-o) 5.36
	Co						5.60 5.43(35-o) 7.73		
	Fe			5.54 5.47(35-o) 7.74					5.53 7.73(22-o) 5.42
	Sc				5.49 7.66(12-o) 5.63				
	Ni						5.55 5.40(35-o) 7.70		
Pb	Fe	4.011(34)	4.017(34)(26)						
	Sc	4.072(25)(34)	4.078(25t)(34) 4.083						
	Yb	4.13(27)	4.15(27)(25)						

$A^{II}(B^{II}_{0.5}B^{VI}_{0.5})O_3$

A^{II}	$B^{II}_{0.5}$	$B^{VI}_{0.5}$ W	Mo	Te	Re	Os	U
Ba	Cr						8.297(17)
	Mg	8.099(14)(15)		8.13(28)	8.082(12)(16)	8.08(12)	8.381(17)
	Ni	8.066(15)(13)	4.0225(13)		8.04 (12)(16)	H(12)	8.336(17)
	Cu						8.18 8.84(17t)
	Co	8.098(15)(13)	4.0429(13)		8.086(12)(16)	H(12)	8.374(17)
	Fe	8.133(15)			8.05 (12)(16)	H(12)	8.312(17)
	Zn	8.116(15)			8.106(12)(16)	8.095(12)	8.397(17)
	Mn				8.18 (12)(16)	H(12)	8.52 (17)
	Cd				8.322(12)(16)	8.325(12)	6.13 8.64(17-o) 6.07
	Ca	8.39(15)(14)	8.355(14)	8.393(28)	8.356(12)(16)	8.362(12)	8.67 (17)
	Sr	8.5 (14)			8.60 8.29(12t)(16)	8.43 8.72(12t)	8.84 (17)
	Ba	8.6 (14)			8.65 8.33(12t)	8.66 8.34(12t)	8.89 (17)
Sr	Cr						8.09 (17)
	Mg	7.9 (14)			7.88 7.94(12t)	7.86 7.92(12t)	8.19 (17)
	Ni	7.86 7.91(15t)(13)(18)	3.9237 3.9474(13t)(18)		7.85 7.92(12t)		8.15 (17)
	Cu	7.66 8.40(35t)					
	Co	7.89 7.98(15t)(13)(18)	3.9367 3.9764(13t)(18)		7.88 7.98(12t)	7.86 7.92(12t)	8.19 (17)
	Fe	7.96 (35)			7.86 7.89(12t)(16)	7.85(12)	8.11 (17)
	Zn	7.92 8.01(15t)(18)			7.89 8.01(12t)		
	Mn	8.01 (35)			8.01(12)		8.28 (17)

$A^{II}(B^{II}_{0.5}B^{VI}_{0.5})O_3$

A^{II}	$B^{II}_{0.5}$	$B^{VI}_{0.5}$ W	Mo	Te	Re	Os	U
Sr	Cd				5.73 8.16 (12-o) 5.81		6.03 8.42 (17-o) 5.91
	Ca	8.2 (14)			5.76 8.21 (12-o) 5.85	8.21 (12)	6.06 8.46 (17-o) 5.93
	Sr	8.2 (14)			8.41 8.13 (12t)	8.32 8.12 (12t)	6.22 8.65 (17-o) 6.01
Ca	Mg	7.7 (14)			5.48 7.77 (12-o) 5.56		
	Ni				5.45 7.67 (12-o) 5.55		
	Co				5.46 7.71 (12-o) 5.58	5.47 7.70 (12-o) 5.59	
	Fe				5.41 7.69 (12-o)(16) 5.53		
	Mn				5.52 7.82 (12-o) 5.55		
	Cd				5.64 7.99 (12-o) 5.77		
	Ca	8.0 (14)			5.67 8.05 (12-o) 5.78	5.73 7.87 (12-o) 5.80	
	Sr	8.1 (14)					
Pb	Mg	4.0 (27)(23)					
	Ca	(27)					

$A^{III}(B^{II}_{0.5}B^{IV}_{0.5})O_3$

A^{III}	$B^{II}_{0.5}$	$B^{IV}_{0.5}$ Ti	Ge	Nb	Ru	Ir
La	Mg	3.932 (1)(27)	3.90 (1)	(20)	(34)	(34)(35-o)
	Ni	3.93 (1)			(34)	(34)(35-o)
	Cu					(35-m)
	Co					(35-o)
	Zn				(34)	
	Mn				(34)	(34)
Nd	Mg	3.90 (1)				

$A^{III}(B^{II}_{0.67}B^{V}_{0.33})O_3$

A^{III}	$B^{II}_{0.67}$	$B^{V}_{0.33}$ Nb	Sb
La	Co	5.58	5.57
		5.58 (35-o)	5.57 (35-o)
		7.89	7.87

$A^{II}(B^{I}_{0.5}B^{VII}_{0.5})O_3$

A^{II}	$B^{I}_{0.5}$	$B^{VII}_{0.5}$ Re	Os	I
Ba	Li	8.118 (12)	8.100 (12)	
	Na	8.296 (12)	8.281 (12)	8.33 (12)(28)
	Ag			8.46 (28)
Sr	Li	7.87 (12)	7.86 (12)	
	Na	8.13 (12)	8.13 (12)	
Ca	Li	7.83 (12)	7.83 (12)	

$A^{II}(B^{I}_{0.25}B^{V}_{0.75})O_3$

A^{II}	$B^{I}_{0.25}$	$B^{V}_{0.75}$
		Ta
Ba	Na	(33)
Sr	Na	(33)

$A^{II}(B^{III}_{0.5}B^{IV}_{0.5})O_{2.75}$

A^{II}	$B^{III}_{0.5}$	$U^{IV}_{0.5}$
Ba	In	8.551 (17)

$A^{II}(B^{II}_{0.5}B^{V}_{0.5})O_{2.75}$

A^{II}	$B^{II}_{0.5}$	$Ta^{V}_{0.5}$	$Mo^{V}_{0.5}$
Ba	Ba	8.69 (19)	
Sr	Sr	8.34 (19)	
Ba	Fe		8.08 (22)

Ferroelectric Compounds

Compound	Curie Temp °C	Reference
$Pb(Co_{0.33}Nb_{0.67})O_3$	- 70	8
$Pb(Co_{0.33}Ta_{0.67})O_3$	-140	8
$Pb(Zn_{0.33}Ta_{0.67})O_3$	140	8
$Pb(Mg_{0.33}Nb_{0.67})O_3$	- 10	8
$Pb(Mg_{0.33}Ta_{0.67})O_3$	- 98	8
$Pb(Ni_{0.33}Nb_{0.67})O_3$	-120	8
$Pb(Ni_{0.33}Ta_{0.67})O_3$	-180	8
$Pb(Fe_{0.5}Nb_{0.5})O_3$	112	26
$Pb(Yb_{0.5}Nb_{0.5})O_3$	280	26

Compound	Curie Temp °C	Reference
$Pb(Fe_{0.5}Ta_{0.5})O_3$	- 30	23
$Pb(Sc_{0.5}Nb_{0.5})O_3$	90	36
$Pb(Sc_{0.5}Ta_{0.5})O_3$	26	36
$Pb(Mg_{0.5}W_{0.5})O_3$	39	23
$Pb(Fe_{0.67}W_{0.33})O_3$	- 90	27

Ferromagnetic Compounds

Compound	Curie Temp °C	Reference
$Ba(Fe_{0.5}Mo_{0.5})O_3$	64	22
$Sr(Fe_{0.5}Mo_{0.5})O_3$	146	22
$Ca(Fe_{0.5}Mo_{0.5})O_3$	104	22
$Sr(Cr_{0.5}Mo_{0.5})O_3$	200	22
$Ca(Cr_{0.5}Mo_{0.5})O_3$	-125	22
$Sr(Cr_{0.5}W_{0.5})O_3$	180	22
$Ca(Cr_{0.5}W_{.05})O_3$	-130	22
$Ba(Fe_{0.5}Re_{0.5})O_3$	43	16
$Sr(Fe_{0.5}Re_{0.5})O_3$	128	16
$Ca(Fe_{0.5}Re_{0.5})O_3$	[illegible]	16
$Sr(Cr_{0.5}Re_{0.5})O_3$	*	12
$Ca(Cr_{0.5}Re_{0.5})O_3$	*	12

*Magnetic at room temperature

Semiconducting Compounds

Compound	Reference
$La(Ni_{0.5}Ru_{0.5})O_3$	34
$La(Mg_{0.5}Ru_{0.5})O_3$	34

* $A(B_x^v B_y^w)O_3$, a series of compounds in which x + y = 1 and v and w are the charges on the ions.

** The numbers for each compound are the cell sizes in angstroms. When a single value of ~4 is given, it indicates that the compound either was of the cubic perovskite type or that it was indexed on a pseudocubic cell because the real cell was not known. When a single value of ~8 is given, the compound is considered to be of the cubic $(NH_4)_3FeF_6$-type and the B ions are ordered. If two values of ~8 are listed, then a "t" is placed after the reference indicating a tetragonal distortion of the ordered cell. Three values (a, b, c) of ~5.5, 8, and 5.5 are listed for orthorhombic distortions and an "o" follows the reference. When two values are given, one of ~6, the other ~7, the compound is considered to have the hexagonal $Ba(Sr_{0.33}Ta_{0.67})O_3$ ordered perovskite-type structure and these values are "a" and "c", respectively. If no cell size is given, the compound was considered to be of the perovskite type by visual examination of the X-ray patterns. An "H" indicates that the compound is of the hexagonal barium-titanate type and does not have a simple perovskite or an ordered-perovskit structure.

† The reference closest to the cell size is the one from which the data was taken. The second reference also contains the data for the compound, but if its X-ray pattern was indexed on a different system, the first letter of the system follows the reference.

REFERENCES

1. Roy, R.: Multiple Ion Substitution in the Perovskite Lattice. Journal of the American Ceramic Society, Vol. 37, No. 12, December 1954, p. 581.

2. Galasso, F., L. Katz, and R. Ward: Substitution in the Octahedrally Coordinated Cation Positions in Compounds of the Perovskite Type. Journal of the American Chemical Society, Vol. 81, 1959, p. 820.

3. Galasso, F., and J. Pyle: Ordering in Compounds of the $A(B'_{0.33}Ta_{0.67})O_3$ Type. Inorganic Chemistry, Vol. 2, 1963, p. 482.

4. Galasso, F., and J. Pyle: $Ba(Ca_{0.33}Ta_{0.67})O_3$, An Ordered Perovskite of the $Ba(Sr_{0.33}Ta_{0.67})O_3$ Type. Journal of Physical Chemistry, Vol. 67, 1963, p. 533.

5. Galasso, F., and J. Pyle: Preparation and Study of Ordering in $A(B'_{0.33}Nb_{0.67})O_3$ Perovskite-Type Compounds. Journal of Physical Chemistry, Vol. 67, 1963, p. 1561.

6. Galasso, F., J. R. Barrante, and L. Katz: Alkaline Earth-Tantalum-Oxygen Phases Including the Crystal Structure of an Ordered Perovskite Compound, $Ba_3SrTa_2O_9$. Journal of the American Chemical Society, 83, 1961, p. 2830.

7. Ismailzade, I. G.: An X-ray Study of the $Pb_3NiNb_2O_9$ - $Pb_3MgNb_2O_9$ System. Soviet Physics, Crystallography, Vol. 5, No. 2. Sept.-Oct. 1960, p. 292.

8. Bokov, V. A., and I. E. Myl'nikova: Ferroelectric Properties of Monocrystals of New Perovskite Compounds. Soviet Physics, Solid State, Vol. 2, No. 11, May 1961, p. 2428.

9. Galasso, F., and W. Darby: Ordering of the Octahedrally Coordinated Cation Position in the Perovskite Structure. Journal of Physical Chemistry, Vol. 66, 1962, p. 131.

10. Filip'ev, V. S., and E. G. Fesenko: Unit Cells of Some Compounds of $A_2B^{I}B^{II}O_6$ Types. Soviet Physics, Crystallography, Vol. 6, No. 5, March-April 1962, p. 616.

11. Brixner, L.: Preparation and Crystallographic Study of Some New Rare Earth Compounds. Journal of Inorganic and Nuclear Chemistry, Vol. 15, 1960, p. 352.

REFERENCES (Contd.)

12. Sleight, A. W., J. Longo and R. Ward: Compounds of Osmium and Rhenium with the Ordered Perovskite Structure. Inorganic Chemistry, Vol. 1, No. 2, May 1962, p. 245.

13. Brixner, L.: Preparation and Structure Determination of Some New Cubic and Tetragonally-Distorted Perovskites. Journal of Physical Chemistry, Vol. 64, 1960, p. 165.

14. Steward, E. G., and H. P. Rooksby: Pseudo-Cubic Alkaline-Earth Tungstates and Molybdates of the R_3MX_6 Type. Acta Crystallographica, Vol. 4, 1951, p. 503.

15. Fresia, F. J., L. Katz and R. Ward: Cation Substitution in Perovskite-like Phases. Journal of the American Chemical Society, Vol. 81, 1959, p. 4783.

16. Longo, J., and R. Ward: Magnetic Compounds of Hexavalent Rhenium with the Perovskite-type Structure. Journal of the American Chemical Society, Vol. 83, 1961, p. 2816.

17. Sleight, A. W., and R. Ward: Compounds of Hexavalent and Pentavalent Uranium with the Ordered Perovskite Structure. Inorganic Chemistry, Vol. 1, No. 4, Nov. 1962, p. 790.

18. Kupriyanov, M. F., and E. G. Fesenko: X-ray Structural Studies of Phase Transitions in Perovskite-type Compounds. Soviet Physics, Crystallography, Vol. 7, No. 3, Nov.-Dec. 1962, p. 358.

19. Brixner, L.: Preparation and Structure of the Strontium and Barium Tantalates $Sr_3TaO_{5.5}$ and $Ba_3TaO_{5.5}$. Journal of the American Chemical Society, Vol. 80, 1958, p. 3214.

20. Prepared at the United Aircraft Corporation Research Laboratories.

21. Wyckoff, R. W. G.: The Structure of Crystals, 2nd Edition, 1931, New York, Reinhold.

22. Patterson, F. K., C. W. Moeller, and R. Ward: Magnetic Oxides of $Mo^{(V)}$ and $W^{(V)}$ with the Ordered Perovskite Structure. Inorganic Chemistry, Vol. 2, No. 1, Feb. 1963.

REFERENCES (Contd.)

23. Smolenskii, G. A., A. I. Agranovskaya, and V. A. Isupov: New Ferroelectrics of Complex Composition. III, Pb_2MgWO_6, $Pb_3Fe_2WO_9$, and Pb_2FeTaO_6, Soviet Physics, Solid State, Vol. 1, No. 1, 1959, p. 907-908.

24. Nomura, S. and T. Kawakubo: Some Properties of Complex Oxides $A(B_{0.5}B'_{0.5})O_3$ of Perovskite Type. Journal of the Physical Society of Japan, 16, 1961, p. 1642.

25. Ismailzade, I. G.: The Results of a Preliminary X-ray Examination of Samples of $Pb(Nb_{0.5}Sc_{0.5})O_3$ and $Pb(Ta_{0.5}Sc_{0.5})O_3$. Soviet Physics, Crystallography, Vol. 4, 1960, p. 389.

26. Smolenskii, G. A., A. I. Agranovskaia, S. N. Popov, V. A. Isupov: New Ferroelectrics of Complex Composition. II, Pb_2FeNbO_6 Pb_2YbNbO_6. Soviet Physics, Technical Physics, Vol. 3, Sept.-Dec. 1958, p. 1981.

27. Agranovskaya, A. I.: Physical-Chemical Investigation of the Formation of Complex Ferroelectrics with the Perovskite Structure. Bulletin of the Acad. of Sciences of the USSR, Physics Series. Vol. 24, 1960, p. 1271-1277.

28. Sleight, A. W. and R. Ward: Compounds of Post-Transition Elements with the Ordered Perovskite Structure. Inorganic Chemistry, Vol. 3, No. 2, Feb. 1964, p. 292.

29. Kupriyanov, M. F. and E. G. Fesenko: An X-ray Study of the Phase Transition in Sr_2FeNbO_6. Soviet Physics, Crystallography, Vol. 6, No. 5, 1961-1962, p. 639.

30. Kupriyanov, M. F. and E. G. Fesenko: An X-ray Study of the Phase Transition in Sr_2FeTaO_6. Soviet Physics, Crystallography, Vol. 7, No. 2, Sept.-Oct., 1962, p. 246.

31. Keller, C.: Ternary and Polynary Oxides of Protactiniums with Perovskite Structure. Journal of Inorganic and Nuclear Chemistry, Vol. 27, 1965, p. 321.

32. Nomura, Shoichiro, and Kawakuba, Tatsuyki: Phase Transition in $Sr(NiW)_{0.5}O_3$-$Ba(NiW)_{0.5}O_3$ System. Journal of Physical Society of Japan, Vol. 17, No. 11, Nov. 1962, p. 1771.

REFERENCES (Contd.)

33. Galasso, F., and J. Pinto: Preparation of $Ba(Na_{0.25}Ta_{0.75})O_3$ and $Sr(Na_{0.25}Ta_{0.75})O_3$ with the Perovskite Structure. Inorganic Chemistry, Vol. 4, Feb. 1965, p. 255.

34. Galasso, F., and W. Darby: Preparation of Single Crystals of Complex Perovskite Ferroelectric and Semiconducting Compounds. Inorganic Chemistry, Vol. 4, No. 1, Jan. 1965, p. 71.

35. Blasse, G.: New Compounds with Perovskite-Like Structures. Journal of Inorganic and Nuclear Chemistry, Vol. 27, (1965), p. 993-1003.

36. Smolenskii, G. A., V. A. Isupov, A. I. Agranovskaya: New Ferroelectrics of Complex Composition of the Type $A_2^{2+}(B_I^{3+}B_{II}^{5+})O_6$ I. Soviet Physics, Solid State, Vol. 1, No. 1, Jan. 1959, p. 150-151.

APPENDIX II

PHASE EQUILIBRIUM STUDIES

The System $Ba(Y_{0.5}Ta_{0.5})O_3$-BaF_2

The binary behavior of this system was confirmed by quenching a sealed platinum tube filled with a mixture 20 weight percent $Ba(Y_{0.5}Ta_{0.5})O_3$, 80 weight percent BaF_2 from 1480°C after a one hour soak period. The quenched material was X-rayed and found to consist only of the components; thus the molten BaF_2 must have been congruently saturated with $Ba(Y_{0.5}Ta_{0.5})O_3$.

The solubility of $Ba(Y_{0.5}Ta_{0.5})O_3$ in BaF_2 was measured in the following way. A 25 ml platinum crucible was filled with BaF_2 by charging and melting in a resistance furnace until the crucible was about 3/4 full. A sintered sample of $Ba(Y_{0.5}Ta_{0.5})O_3$ was placed in the crucible for the final charging. The crucible was then transferred to a vertical tube furnace, and Pt/Pt-10% Rh thermocouple was inserted into the melt. The melt was allowed to soak at constant temperature, and stirred periodically with 1/8 in. O.D. platinum tube. After various times of soak at various temperatures, the platinum tube was inserted about 1/4 in. below the surface of the melt, and a sample withdrawn for spectrochemical analysis.

The chemical analysis for Y and Ta of samples withdrawn at various temperatures are given in Table XI . The data indicate a reasonably constant ratio of about 2.5 moles of Ta per mole of Y. Such a result is inconsistent with the previous observation of congruent saturation of BaF_2 with perovskite, and may be due to the depletion of yttrium at the surface of the melt due to the higher volatility of YF_3. On the assumption that the experimental solubility data for Ta are a valid measure of the solubility of $Ba(Y_{0.5}Ta_{0.5})O_3$ in BaF_2, the solubility curve shown in Fig. 10 was drawn. The excellent agreement between the data obtained by approaching temperatures from above with the data obtained by approaching temperatures from below is an indication that equilibrium had been attained.

The Pseudo-Ternary System BaO-$YTaO_4$-B_2O_3

Preparation and Experimental Techniques

Compositions were prepared from reagent grade barium carbonate, yttrium and tantalum oxides, and anhydrous B_2O_3. For each mixture, the calculated amounts of the components were ground together under acetone, dried, and pressed into pellets.

The pellets then were heated slowly and held for several hours below the melting point of B_2O_3; the temperature was then increased to a final temperature below the solidus, in most cases about 900°C. For compositions along the join BaO-$YTaO_4$, the pellets were heated rapidly to 1450°C and held 6 hours, then normally cooled and X-rayed.

The furnace used in most of the quench runs was a Globar heated vertical tube furnace. Temperature was maintained to within 2 degrees of the desired temperature by a Honeywell Pyr-o-Vane controller. For quenches from temperatures above 1400 C, a cylindrical T-bar heated furnace controlled by a saturable reactor power supply and Leeds and Northrup program controller was used. The quenching apparatus consisted of a length of four-hole aluminum thermocouple tubing: the leads of a Pt/Pt-10% Rh thermocouple passed through two of the holes, and lengths of 20-mil Pt-10% Rh wire passed through the remaining holes. The upper ends of the latter wires were connected across an auto-transformer, and a short length of 10-mil platinum wire was affixed across lower ends and supported the quench envelope. When it was desired to quench the sample, a current was sent through the 10-mil platinum wire, which fused, letting the quench envelope fall into a beaker of water or mercury.

One end of a 5/8-in. length of 3 mm platinum tubing was crimped shut and folded back. The desired prereacted composition was loaded into the tube, and the top similarly crimped: a short length of Pt wire was crimped in place when the top was folded down, and fastened to a small aluminum grommet through which passed the fuse of the quench apparatus. Thus the quench sample was within 0.25 inch of the read-out thermocouple.

In instances where there was considerable liquid formed at the quench temperature, some leakage would frequently occur from the quench packet. For this reason, in the higher temperature runs the packets were evacuated and welded shut in an electron beam welding apparatus.

The samples from the quench runs were ground in an agate mortar, and examined under the petrographic microscope. The indices of refraction of glasses, and of glasses in equilibrium with primary crystals, were measured by the oil immersion technique. X-ray powder camera diffraction photographs also were obtained on quench samples for crystalline phase identification.

The phases present and indices of refraction of glasses for various mixtures at various temperatures as determined by examination of quenched samples are recorded in Table XII.

Mixtures which contained less than about 15 percent B_2O_3 could not be quenched to clear glasses because of rapid devitrification, but always showed the presence of fine quenching crystals, as shown in Fig.32 . A similar phenomena was reported by Levin and McMurdie (Ref. 1) in the system $BaO-B_2O_3$. The presence of quenching crystals in the glass makes the index measurements unreliable. However, these quenching crystals are readily distinguished from primary crystals in the glass as shown in Fig. 3[illegible].

Primary Phases Bounding the Perovskite Field

$YTaO_4$

Ferguson (Ref. 2) synthesized $YTaO_4$ by arc fusion at about 2100°C, and gave the indexed X-ray pattern shown in Table XIII. The X-ray pattern of $YTaO_4$ grown as primary crystals in a B_2O_3 flux at 1015°C (sample 64-331ℓ) and at 1368°C (sample 65-015a), which is also shown in Table XIII, is slightly different from Ferguson's pattern. The flux grown $YTaO_4$ pattern has been indexed on the basis of slightly different cell dimensions, which may indicate some solution of BaO and/or B_2O_3 in the $YTaO_4$ crystals.

$BaTa_2O_6$ - Derived Solid Solutions (α Phase)

Galasso, Katz and Ward (Ref. 3) prepared $BaTa_2O_6$ by reacting $BaCO_3$ and Ta_2O_5 at 1100°C, and showed that it was isomorphous with the tetragonal tungsten bronzes (Ref. 4), having parameter a = 12.60 Å and c = 3.95 Å. They also showed that this compound could be prepared with a considerable oxygen deficiency, thus indicating a broad homogeneity range for the structure. During the course of the present investigation, the homogeneity range of the "bronze" phase in the binary system $BaO-Ta_2O_5$ was determined; it was found to extend from the composition $BaTa_2O_6$ to at least the composition $BaTa_6O_{16}$, which had tetragonal pseudo-cell parameters a = 12.49 Å, c = 3.88 Å. Roth and Waring (Ref. 5) have reported the analogous phases in the system $BaO-Nb_2O_5$ to have a somewhat more narrow homogeneity range, i.e., between $Ba_3Nb_{10}O_{20}$ and $BaNb_6O_{16}$; they have shown this solid solution series to be interrupted by a morphotropic phase transformation.

The X-ray data for compositions along the join $BaO-YTaO_4$ (Table XII, samples 64-322, 323, 324, and 325) indicates that a phase isomorphous with $BaTa_2O_6$ occurs at compositions around 80 weight percent $YTaO_4$. It may be assumed that this composition is simply a member of a solid solution continuum extending from the $BaO-Ta_2O_5$ join out into the ternary diagram $BaO-Y_2O_3-Ta_2O_5$, but as yet no attempt has been made to accurately define the homogeneity region of solid solution in this ternary system.

The "bronze" crystals grown in equilibrium with $Ba(Y_{0.5}Ta_{0.5})O_3$ described on page 11 and shown in Fig. 21, had a chemical composition $BaTa_{1.86}Y_{0.20}B_{0.033}O_6$ and cell dimensions a = 12.59 Å, c = 3.94 Å; thus they were very close in composition to the $BaTa_2O_6$ end member. The indexed diffraction pattern of these crystals is given in Table XIV.

$Ba_5Ta_4O_{15}$ (β Phase)

Galasso and Katz (Ref. 6) prepared $Ba_5Ta_4O_{15}$ and found it to belong to the trigonal system, the axes of the hexagonal unit cell being a = 5.79 Å and c = 11.75 Å. Anion deficiency could be produced by preparing the compound with tetravalent tantalum, thus indicating a considerable homogeneity range. A phase isomorphous with $Ba_5Ta_4O_{15}$ was found to have a primary field in the system $BaO\text{-}YTaO_4\text{-}B_2O_3$. Crystals of this phase were grown as described on pages 7-10 and are shown in Fig. 17. Chemical analyses of the crystals gave a composition about $Ba_5Ta_3B_{1.5}Y_{.17}O_{15}$ indicating that some yttrium and boron can go into the structure. The indexed diffraction pattern of the $Ba_5Ta_4O_{15}$ phase is given in Table XV.

$Ba_3B_2O_6$

Levin and McMurdie (Ref. 1) show $Ba_3B_2O_6$ to be the primary phase in the system $BaO\text{-}B_2O_3$ in mixtures containing about 78 to 87 percent BaO. According to the above authors, $Ba_3B_2O_6$ hydrates and carbonates rapidly when left in air: a sample exposed overnight to a relative humidity above 90% gave the X-ray pattern of $BaCO_3$. In the current experiments X-ray photographs were taken promptly after quenching the samples into mercury, and patterns for samples 65-016a, 016b, 017a, and 028a included the seven or eight reflections that could be attributed to $Ba_3B_2O_6$ as reported by Levin and McMurdie, and no reflections that could be attributed to either $BaCO_3$ or $Ba(OH)_2$. However, in these quenched samples, large amounts of glass were present and powder photographs were faint: the assignment of these reflections to $Ba_3B_2O_6$ must be considered as tentative.

BaO

The evidence for assigning BaO as an equilibrium crystalline phase in two of the quench runs was indirect. Samples of composition 70 weight percent BaO, 20 weight percent $YTaO_4$ quenched from 1380 and 1300°C (sample 65-016a and b respectively) showed X-ray patterns for perovskite and $Ba_3B_2O_6$ only. However, the material had a strong lavender discoloration indicative of reaction of free BaO with the platinum quench packet*, whereas samples close in composition to

*The reaction of BaO with platinum has been reported frequently in the literature, see for example Refs. 1 and 5.

samples 65-016a and b (e.g. samples 65-017a and 65-028a) showed no such discoloration. Lack of direct evidence for BaO, however, renders this assignment tentative also.

Phase Equilibrium Diagram

Figures 34, 35 and 36 show the equilibrium diagrams, constructed from data in Table XII, for portions of the perovskite -B_2O_3, perovskite -BaB_8O_{13}, and perovskite-BaB_2O_4 joins respectively. Where possible, the data for the indices of refraction of glasses in equilibrium with primary crystals have been used in drawing the liquidus curves. All three of the above joins are non-binary, since phases appear which cannot be expressed in terms of the two components. Figure 11 is a projection of the liquidus surface for a portion of the system BaO-$YTaO_4$-B_2O_3 in the neighborhood of the perovskite field, constructed so as to be consistent with all the data of Table XII, using Figs. 34, 35 and 36 as guides to drawing the isotherms. The diagram indicates non-ternary equilibrium.

The data are insufficient to definitely fix the boundary curve between the fields of β and $Ba_3B_2O_6$, which could be drawn either to the left or to the right of the composition 65 weight percent BaO, 20 weight percent $YTaO_4$; the boundary curve was drawn to the left on the basis of a greater intensity of β X-ray reflections than of $Ba_3B_2O_6$ reflections from sample 65-017a.

The composition of eutectics indicated between BaO and perovskite, and between perovskite and $YTaO_4$, and consequently, the position of the boundary curves between the primary fields of BaO and perovskite and between perovskite and $YTaO_4$ were drawn arbitrarily, although with regard for the tracking of isotherms.

The Pseudo-Ternary System BaO-$LuTaO_4$-B_2O_3

The experimental techniques employed in the investigation of the BaO-$LuTaO_4$-B_2O_3 system were the same as those described for the system BaO-$YTaO_4$-B_2O_3. Quench compositions were chosen by analogy with the latter system, on the assumption that similar equilibria would be encountered. The quench run data for this system are presented in Table XVI. The phase diagrams constructed from the quench data is shown in Fig. 12. The data are not as extensive as in the case BaO-$YTaO_4$-B_2O_3 system, and only the $Ba(Lu_{0.5}Ta_{0.5})O_3$-$BaTa_2O_6$ boundary curve and the liquidus isotherms in the neighborhood of this boundary curve were determined, since this information is sufficient to permit selection of satisfactory conditions for the growth of $Ba(Lu_{0.5}Ta_{0.5})O_3$ crystals.

The Pseudo-Ternary System $BaO-LaTaO_4-B_2O_3$

The experimental techniques employed in the investigation of the $BaO-LaTaO_4-B_2O_3$ system were the same as those described for the two previous systems. The quench data are presented in Table XVII. Figure 37 is a map of compositions investigated showing primary crystallization. Note that the perovskite field was not encountered in the location analogous to its location in the $BaO-YTaO_4-B_2O_3$ and $BaO-LuTaO_4-B_2O_3$ systems. Time did not permit further investigation of this system, but it can be assumed that the boundary of the perovskite primary field lies closer to the $Ba(La_{0.5}Ta_{0.5})O_3$ composition. In this case it can be anticipated that the liquidus surface above this field will lie at correspondingly higher temperatures, and/or that the slope of the liquidus surface will be steeper than in the $BaO-YTaO_4-B_2O_3$ and $BaO-LuTaO_4-B_2O_3$ systems.

REFERENCES

1. Levin, E. M. and H. F. McMurdie: J. Research Natl. Bur. Standards, 42, 131 (1949).

2. Ferguson, R. B.: Can. Min., 6, 72 (1957).

3. Galasso, F., L. Katz and R. Ward: J. Am. Chem. Soc., 81, 5898 (1959).

4. Magneli, A. and B. Blomberg: Acta Chem. Scand., 5, 372 (1951).

5. Roth, R. S., and J. L. Waring: J. Research Natl. Bur. Standards, 65A, 337 (1961).

6. Galasso, F. and L. Katz: Acta Cryst., 14, 647 (1960).

TABLE XI

Solubility Data for $Ba(Y_{0.5}Ta_{0.5})O_3$ in BaF_2

Heat Treatment	Spectrochemical Analysis	
	w/o Ta	w/o Y
heat up slowly from room temperature, soak 1.5 hours at 1420°C	1.1	.21
heat up from 1420 to 1520°C, 1.5 hour soak	2.1	.38
cooled from 1520 to 1350°C, soaked 18 hours, then heated to 1610°C, soaked 1 hour	3.9	.78
cooled from 1610°C to room temperature, reheated to 1535°C, 3/4-hour soak	2.3	.38
cooled from 1535 to 1405°C, 1-hour soak	1.0	.19

TABLE XII

Quench Data for Samples in the System $BaO-YTaO_4-B_2O_3$

Sample No.	Composition in Weight %			T °C	Phases Present
	BaO	$YTaO_4$	B_2O_3		
64-322	62.8	37.2	0	1450	P + BaO*
64-323	31.5	68.5	0	1450	P + α
64-324	23.5	76.5	0	1450	P(tr) + α
64-325	18.7	81.3	0	1450	α
64-331i	33.4	36.6	30	1345	gl η = .667
64-331k	33.4	36.6	30	1240	gl η = 1.669
64-331j	33.4	36.6	30	1110	gl η = 1.665
64-331ℓ	33.4	36.6	30	1015	gl η = 1.632 + $YTaO_4$
64-371a	35.9	39.1	25	1345	gl η = 1.750
64-357c	38.2	41.8	20	1390	gl η = 1.770
64-357a	38.2	41.8	20	1310	gl η = 1.770
64-357b	38.2	41.8	20	1235	gl η = 1.743 + α
64-357d	38.2	41.8	20	1160	gl η = 1.740 + α
64-374a	40.7	44.3	15	1420	gl η = 1.795
64-427d	41.8	45.7	12.5	1593	gl η ~ 1.82 + qx
64-427b	41.8	45.7	12.5	1480	gl η ~ 1.82 + qx + P(tr)
64-427f	41.8	45.7	12.5	1432	gl η ~ 1.82 + qx + P
64-427c	41.8	45.7	12.5	1368	gl η + qx + P
64-427a	41.8	45.7	12.5	1315	gl η = 1.787 + P + α(tr)
64-368g	43	47	10	1720	gl η ~ 1.83 + qx + P(tr)
64-368h	43	47	10	1557	gl η ~ 1.83 + qx + P
64-368b	43	47	10	1395	gl η ~ 1.82 + qx + P
64-368a	43	47	10	1305	gl η = 1.787+ P + α
64-368c	43	47	10	1205	gl η = 1.753+ P + α
64-368d	43	47	10	1172	gl + P + α
64-368e	43	47	10	1025	gl + P + α
64-368i	43	47	10	925	gl + P + α + β

TABLE XII (Contd.)

Sample No.	Composition in Weight %			T °C	Phases Present
	BaO	$YTaO_4$	B_2O_3		
64-314b	44	26	30	1150	gl
64-314c	44	26	30	950	gl + α
64-396	45	30	25	1200	gl η = 1.737
64-396a	45	30	25	1100	gl η = 1.725 + α (tr)
64-396b	45	30	25	1035	gl + α
64-396c	45	30	25	908	unidentified solid phases
64-411a	45.5	34.5	20	1300	gl η = 1.762
64-411b	45.5	34.5	20	1215	gl η = 1.745 + α
64-412c	46	39	15	1305	gl η = 1.780
64-412b	46	39	15	1210	gl η = 1.747 + α
64-417e	47	43	10	1470	gl η = 1.797 + P
64-417f	47	43	10	1342	gl η = 1.778 + P
64-417b	47	43	10	1315	gl η = 1.778 + P
64-417c	47	43	10	1300	gl + P + α
64-417d	47	43	10	1253	gl + P + α
64-417a	47	43	10	1145	gl + P + α
65-014a	60.5	19.5	20	1280	gl η = 1.725
65-014c	60.5	19.5	20	1049	gl η = 1.725
65-014b	60.5	19.5	20	1005	gl η = 1.725 + β (tr)
65-002e	57	28	15	1480	gl η = 1.778 + qx
65-002d	57	28	15	1360	gl η = 1.755 + P(tr)
65-002c	57	28	15	1280	gl η = 1.757 + P
65-002b	57	28	15	1193	gl η = 1.743 + P
65-002a	57	28	15	1100	gl η = 1.738 + P
65-001b	54	36	10	1106	gl η = 1.735 + P
65-001a	54	36	10	1083	gl η = 1.735 + P
65-001c	54	36	10	1050	gl η = 1.725 + P
65-001d	54	36	10	1000	gl η = 1.725 + P
65-001j	54	36	10	978	gl(tr) + P + β (tr)
65-001i	54	36	10	945	β + weak unidentified
65-001g	54	36	10	927	β + weak unidentified

TABLE XII (Contd.)

Sample No.	Composition in Weight %			T °C	Phases Present
	BaO	$YTaO_4$	B_2O_3		
65-052a	55	23	22	1055	gl + α (tr)
65-052b	55	23	22	1011	gl + α
65-016b	70	20	10	1380	P + BaO* + $Ba_3B_2O_6$
65-016a	70	20	10	1300	P + BaO* + $Ba_3B_2O_6$
65-028a	63	27	10	1300	gl + P + $Ba_3B_2O_6$ (tr)
65-017a	65	20	15	1005	gl + β + $Ba_3B_2O_6$
65-018a	50	20	30	1010	gl η = 1.685, α + β
65-015a	30	60	10	1368	gl + $YTaO_4$
65-015b	30	60	10	1295	gl + $YTaO_4$ + α
65-039a	35	50	15	1300	gl + $YTaO_4$ + α
65-051a	35	55	10	1358	gl + $YTaO_4$ + α (tr)
65-038a	39	50	11	1297	gl + P(tr) + α
65-116a	57	25	18	1005	gl + α
65-116b	57	25	18	1035	gl, η = 1.725 + α
65-116c	57	25	18	1083	gl, η = 1.73 + α
65-116d	57	25	18	1145	gl η = 1.73
65-092a	55	25	20	991	gl + α
65-092c	55	25	20	1133	gl

TABLE XII (Contd.)

Quaternary Compositions

Sample No.	Composition in Weight %					Phases Present
	BaO	Y_2O_3	Ta_2O_5	B_2O_3	T °C	
64-389	45.25	17.5	27.5	10	1200	gl + P + α
64-394a	45.5	18.4	22.6	13.5	1200	gl + unidentified phases
64-394b	45.5	18.4	22.6	13.5	1100	gl + α + unidentified phases
64-398	45.58	17.88	26.04	10.5	1200	gl + P + unidentified

gl = glass

n = index of refraction

P = $Ba(Y_{0.5}Ta_{0.5})O_3$

α = phase isomorphous with $BaTa_2O_6$

β = phase isomorphous with $Ba_3Ta_4O_{15}$

(tr) = trace

qx = quenching crystals (see text)

*the criterion for assigning BaO as a crystalline phase is explained in the text

TABLE XIII

X-ray Pattern of $YTaO_4$

	Ferguson a = 5.34 Å b = 10.94 Å c = 5.07 Å β = 95.30		UAC a = 5.28 Å b = 10.87 Å c = 5.10 Å β = 95.30	
hkℓ	d	I/I_o	d	I/I_o
020	5.47	10	5.45	35
001			5.08	40
100	4.79	40		
120			3.78	35
021			3.72	35
101			3.45	
$\bar{1}21$	3.14	100	3.15	100
130	3.02	5	3.04	
031,121	2.94	100	2.92	100
040	2.74	40	2.72	40
200,$\bar{1}31$	2.64	40	2.63	40
002	2.52	30	2.537	40
140			2.420	30
220,$\bar{2}11$	2.38	5		
$\bar{1}12$,022	2.30	5		
112,141	2.15	30	2.142	40
032,221			2.068	10
$\bar{2}31$,150	2.02	20		
231,$\bar{2}02$	1.921	30	1.939	40
$\bar{2}12$,240,$\bar{1}51$	1.901	50	1.892	40
042	1.846	60	1.859	50
$\bar{1}42$			1.798	10
202,310,241	1.741	30	1.732	35
$\bar{3}01$,160			1.710	40
$\bar{3}21$,$\bar{2}51$	1.639	60	1.641	50
301,023			1.612	12
$\bar{1}52$,311	1.605	20	1.594	20
330,232			1.578	15
251,$\bar{2}42$	1.570	60		
152,033	1.549	30	1.537	35
071	1.494	50	1.499	45
062			1.477	20
$\bar{2}13$	1.467	20		

TABLE XIV

X-ray Diffraction Pattern for $BaTa_2O_6$ Crystals

Tetragonal cell Space group D_{4h}^5-P4/mbm

a = 12.59 Å b = 3.94 Å

hkℓ	d	I/I_o
310,001	3.94	20
320	3.48	30
211	3.23	40
400	3.15	5
410	3.05	45
221,330	2.96	20
311,420	2.81	100
321	2.62	25
510	2.47	5
411	2.43	<5
520	2.34	5
421	2.30	<5
530	2.17	10
600	2.10	<5
430	1.99	50
402	1.946	<5
202	1.884	10
601,212	1.360	10
550,710,302	1.785	40
312	1.767	15
720	1.731	10
631	1.702	10
402	1.676	30
701	1.630	80

TABLE XV

X-ray Diffraction Pattern for $Ba_5Ta_4O_{15}$ Crystals

Trigonal cell Space group - P $\bar{3}$m1

a = 5.79 Å c = 11.75 Å

hkℓ	d	I/I_o
001	11.76	10
101	4.62	20
102	3.81	20
103	3.09	100
110	2.89	100
104	2.54	20
005	2.34	10
203	2.11	60
204	1.907	20
106	1.827	50
213	1.710	60
300	1.672	40
107	1.595	20
206	1.543	40
220	1.450	40
207	1.396	20
305	1.363	40
313	1.311	40
314	1.257	10
403	1.194	40

TABLE XVI

Quench Data for Samples in the System $BaO-LuTaO_4-B_2O_3$

Sample No.	Composition in Weight % BaO	$LuTaO_4$	B_2O_3	Temp °C	Phases Present
65-142a	38	52	10	1095	gl + P + α
65-142b	38	52	10	1396	gl + P + α
65-142c	38	52	10	998	P + α + unidentified
65-142d	38	52	10	1440	gl + P
65-142e	38	52	10	1040	gl + P + α
65-142f	38	52	10	1020	P + α + unidentified
65-147a	34	46	20	1442	gl, η = 1.765
65-147b	34	46	20	1379	gl, η = 1.765
65-147c	34	46	20	1306	gl, η = 1.753, + α (tr)
65-148a	36	49	15	1442	gl, η = 1.793, + α
65-148b	36	49	15	1379	gl, η = 1.793, + α (tr)
65-148c	36	49	15	1306	gl, η = 1.768, + α
65-152a	49	37	14	1103	gl, η = 1.730, P + α
65-152b	49	37	14	1173	gl, P + α
65-152c	49	37	14	1246	gl, η = 1.750, P + α (tr)
65-152e	49	37	14	1355	gl, η = 1.760, + P
65-152f	49	37	14	1430	gl, η = 1.770
65-153a	55.4	29.6	15	1103	gl + P
65-153b	55.4	29.6	15	1173	gl, η = 1.730, + P
65-153c,	55.4	29.6	15	1138	gl, η = 1.727, + P
65-153c$_2$	55.4	29.6	15	1246	gl, η = 1.735, + P
65-153d	55.4	29.6	15	1055	gl, η = 1.725, + P
65-153e	55.4	29.6	15	1355	gl, η = 1.745, + P
65-153f	55.4	29.6	15	1430	gl, η = 1.750, + P (tr)
65-153g	55.4	29.6	15	1500	gl, η = 1.750
65-189a	50.5	31.5	18	1215	gl, η = 1.740, + α (tr)
65-189b	50.5	31.5	18	1252	gl, η = 1.740

TABLE XVI (Contd.)

Sample No.	Composition in Weight % BaO	$LuTaO_4$	B_2O_3	Temp °C	Phases Present
65-188a	57.5	24.5	.8	1215	gl, η = 1.730
65-188b	57.5	24.5	18	1100	gl, η = 1.727,+ P (tr)
65-195a	59.5	20.5	20	1055	gl, η - 1.723
65-195b	59.5	20.5	20	1000	gl, η = 1.723,+ unidentified (tr)
65-196a	51.5	28.5	20	1055	gl, η = 1.725,+ α
65-196b	51.5	28.5	20	1200	gl, η = 1.727

gl = glass
η = index of refraction
P = $Ba(Lu_{0.5}Ta_{0.5})O_3$
α = phase isomorphous with $BaTa_2O_6$
tr = trace

TABLE XVII

Quench Data for Samples in the System $BaO-LaTaO_4-B_2O_3$

Sample No.	Composition in Weight % BaO	$LaTaO_4$	B_2O_3	Temp °C	Phases Present
65-205a	39.1	48.9	12.0	1345	gl, η = 1.83
65-205b	39.1	48.9	12.0	1258	gl, η = 1.81, + β
65-206a	38.4	48.1	13.5	1345	gl, η = 1.83
65-206b	38.4	48.1	13.5	1258	gl, η = 1.81, + α
65-207a	47.9	37.1	15.0	1250	gl, η = 1.775
65-207b	47.9	37.1	15.0	1150	gl, η = 1.763, + β
65-207c	47.9	37.1	15.0	1075	gl, η = 1.755, + β
65-208a	48.6	34.7	16.7	1250	gl, η = 1.775
65-208b	48.6	34.7	16.7	1150	gl, η = 1.763, + β
65-208d	48.6	34.7	16.7	1075	gl, η = 1.755, + β
65-209a	55.4	28.3	16.3	1250	gl, η = 1.768
65-209b	55.4	28.3	16.3	1145	gl, η = 1.750, + β
65-210a	57.2	24.7	18.1	1050	gl, η = 1.735, + β
65-210b	57.2	24.7	18.1	1075	gl, η = 1.740, + β
65-223a	39.7	50.3	10.0	1300	gl + β + unidentified (tr)
65-223b	39.7	50.3	10.0	1400	gl + β + unidentified (tr)
65-223c	39.7	50.3	10.0	1510	gl + β + unidentified (tr)
65-224a	47.0	40.7	12.3	1300	gl + β + unidentified (tr)
65-224b	47.0	40.7	12.3	1400	gl + β + unidentified (tr)
65-224c	47.0	40.7	12.3	1510	gl + β + unidentified (tr)
65-225a	53.5	33.5	13.0	1300	gl + β + unidentified (tr)
65-225b	53.5	33.5	13.0	1400	gl + β + unidentified (tr)
65-225c	53.5	33.5	13.0	1510	gl + β + unidentified (tr)

gl = glass
η = index of refraction
α = $BaTa_2O_6$ polymorph
β = $Ba_5Ta_4O_{15}$ polymorph
tr = trace

FIG. 32

SAMPLE 65-00 2e, 57 w/o BaO, 28 w/o $YTaO_4$, 15 w/o B_2O_3

QUENCHED FROM 1480 °C
IMMERSED IN OIL OF INDEX 1.75
MAGNIFICATION: 200 X

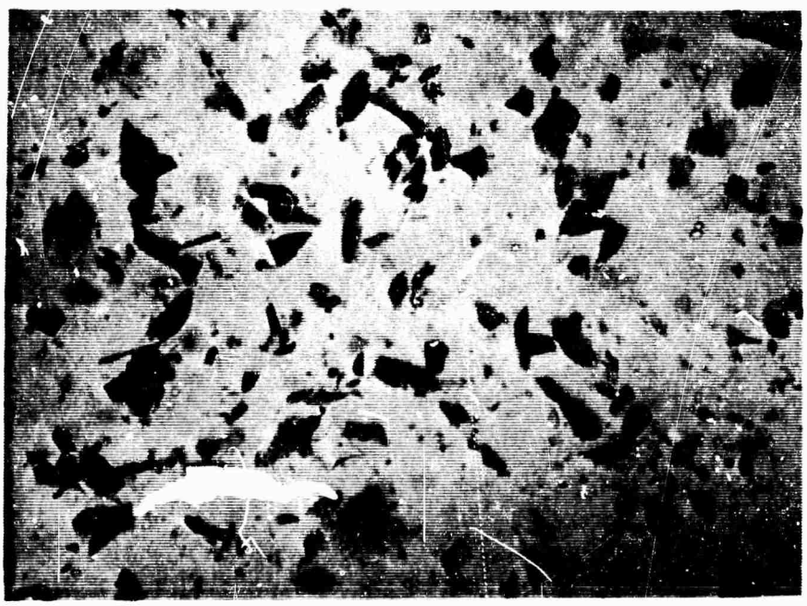

GLASS HAS PARTIALLY DEVITRIFIED, RESULTING IN THE INCLUSION OF VERY SMALL QUENCHING CRYSTALS

SAMPLE 64-427 f, 41.8 w/o BaO, 45.7 w/o $YTaO_4$, 12.5 w/o B_2O_3

QUENCHED FROM 1432 °C
IMMERSED IN OIL OF INDEX 1.75
MAGNIFICATION: 200 X

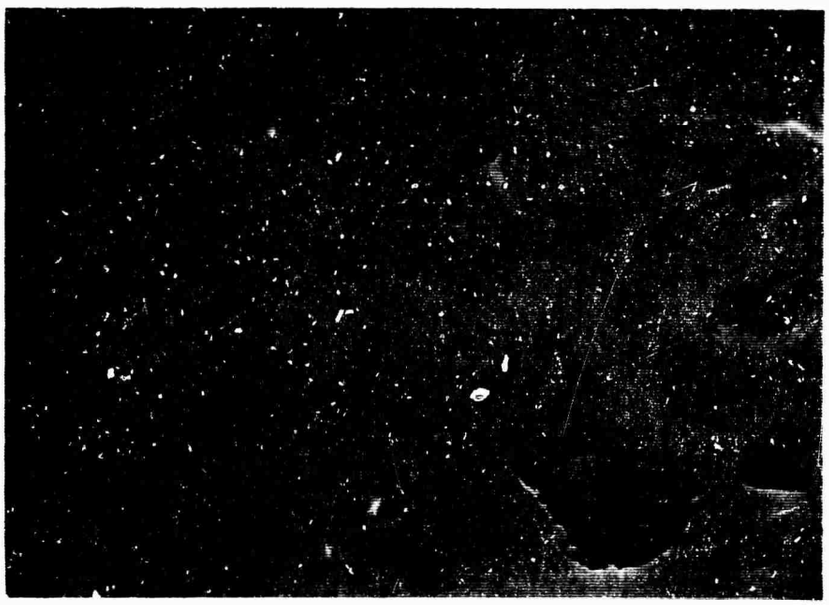

CHIPS OF CLEAN GLASS MAY BE SEEN, AS WELL AS GLASS CONTAINING QUENCHING CRYSTALS, AND GLASS CONTAINING PRIMARY CRYSTALS

D910269-5

FIG. 34

PORTION OF THE JOIN $BaY_{0.5}Ta_{0.5}O_3$ - B_2O_3

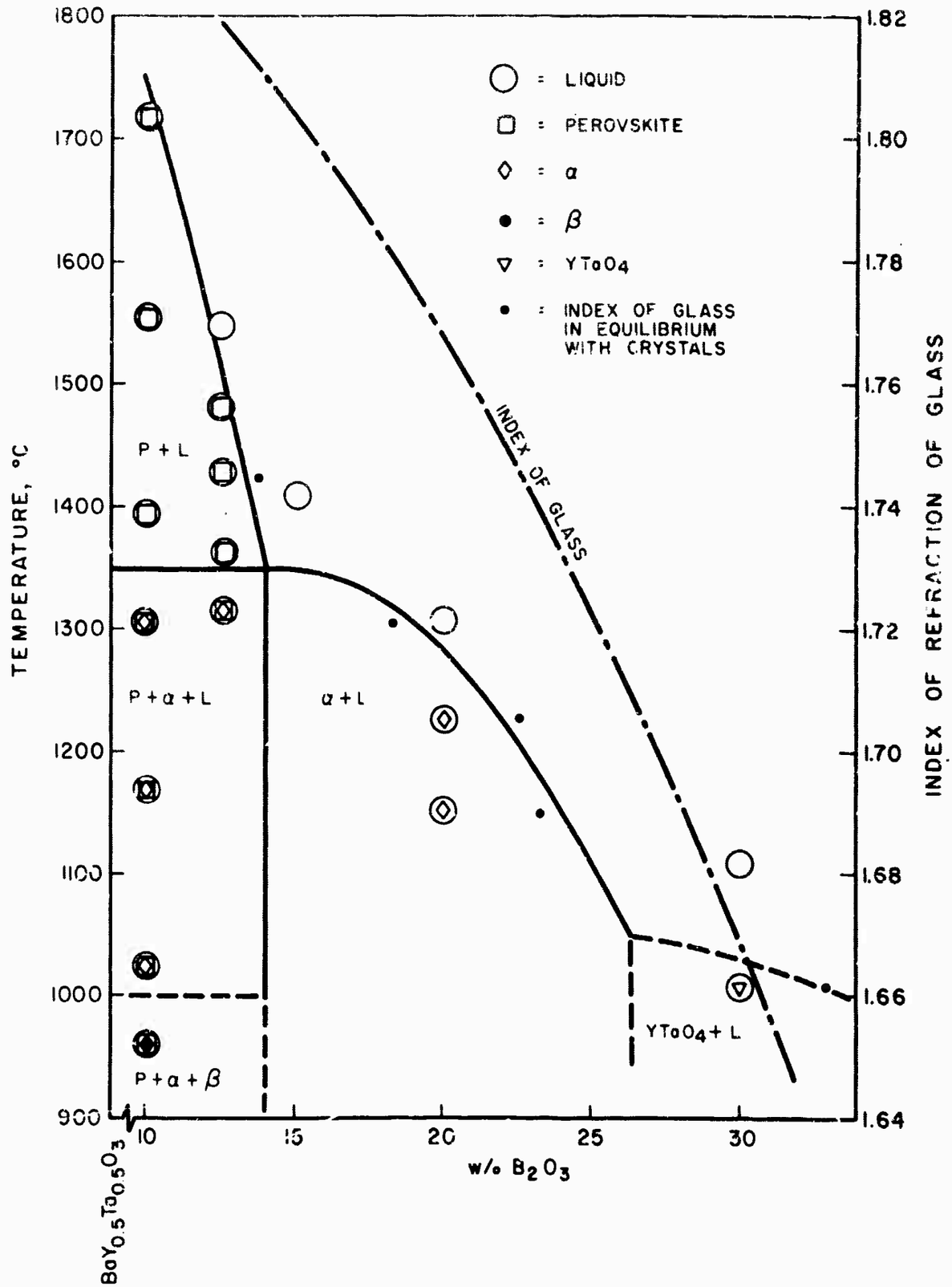

FIG 35

PORTION OF THE JOIN $BaY_{0.5}Ta_{0.5}O_3$ - BaB_8O_{13}

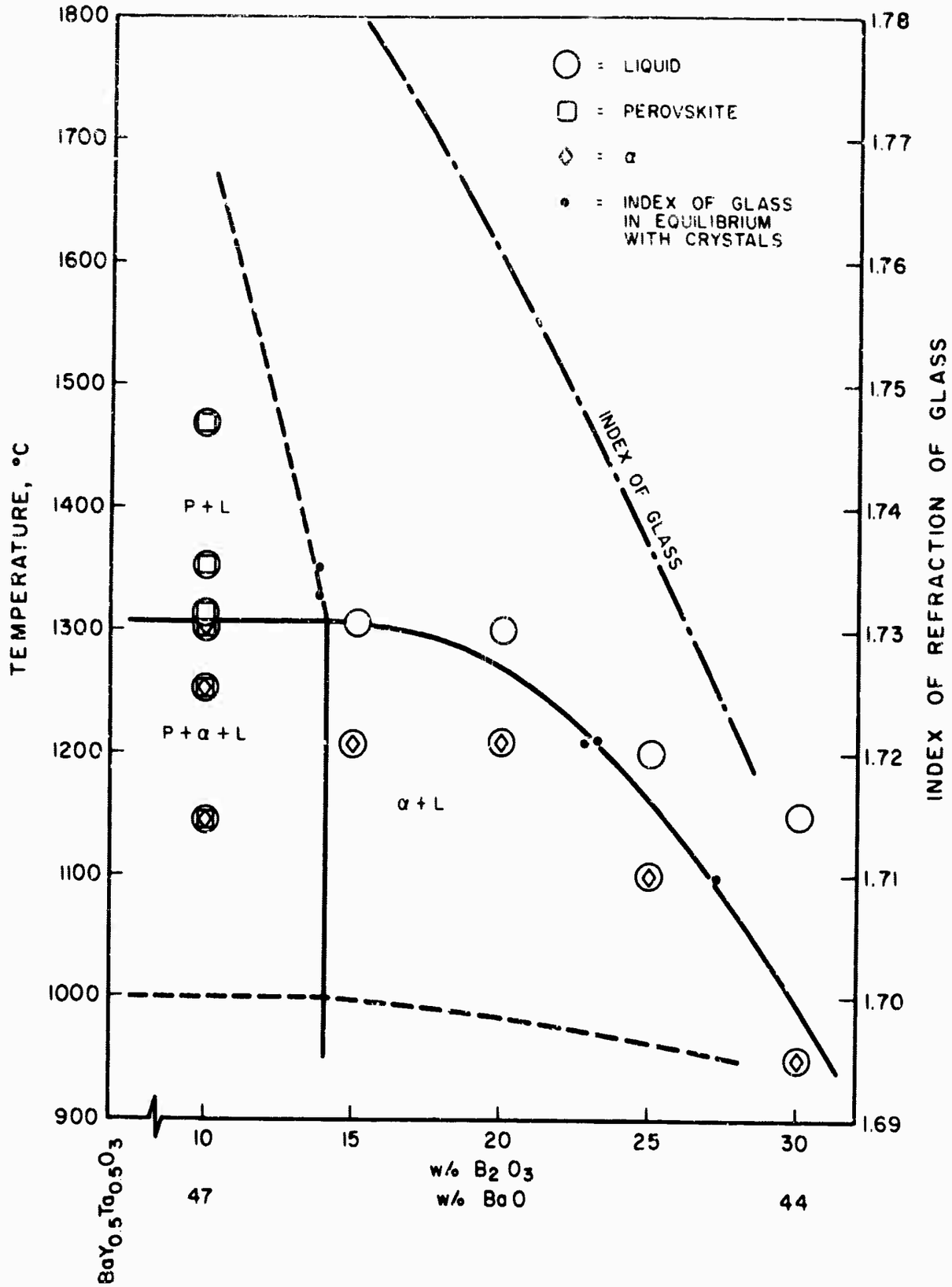

PORTION OF THE JOIN $BaY_{0.5}Ta_{0.5}O_3$ - BaB_2O_4

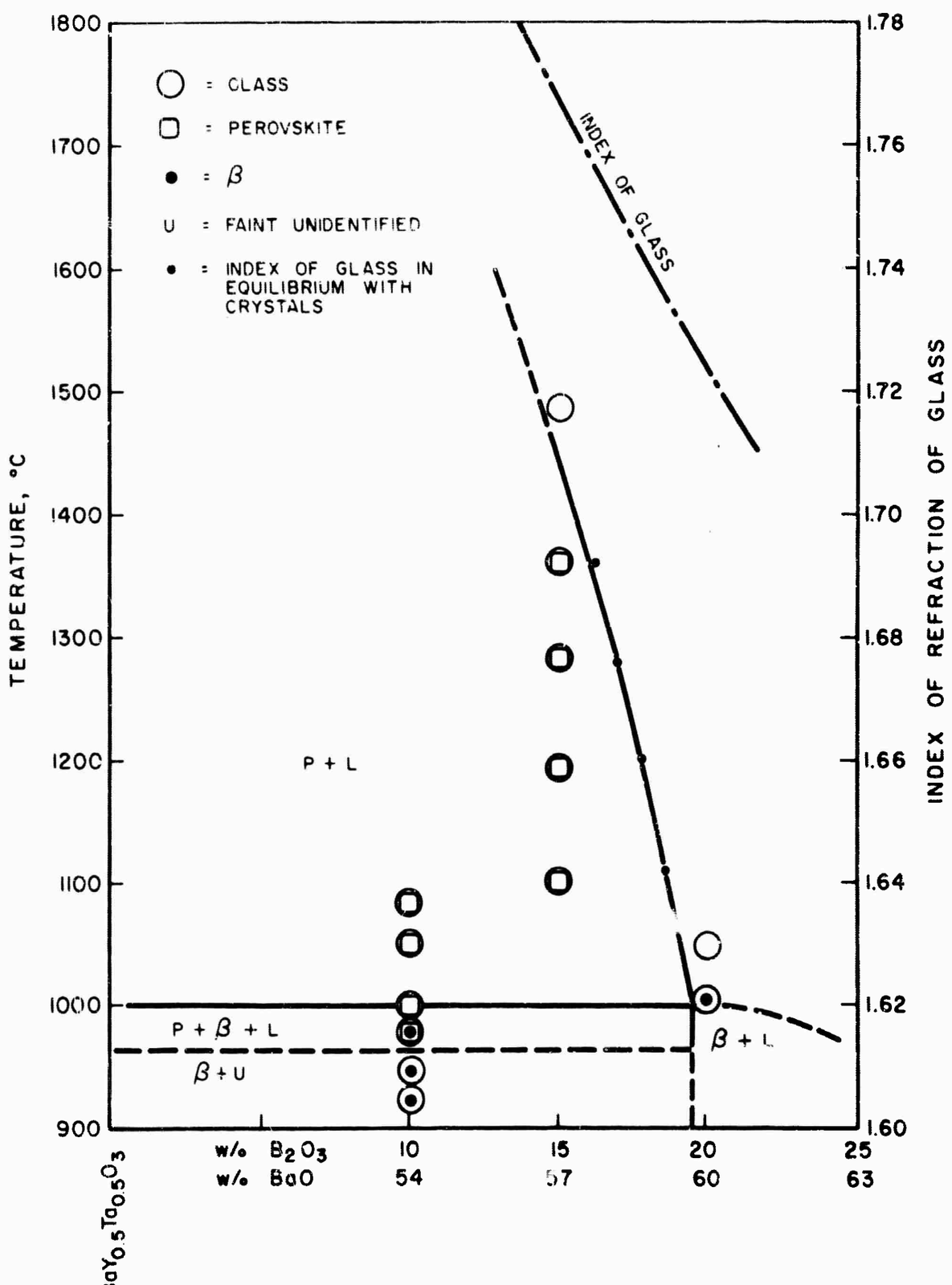

THE SYSTEM BaO-LaTaO4-B2O3

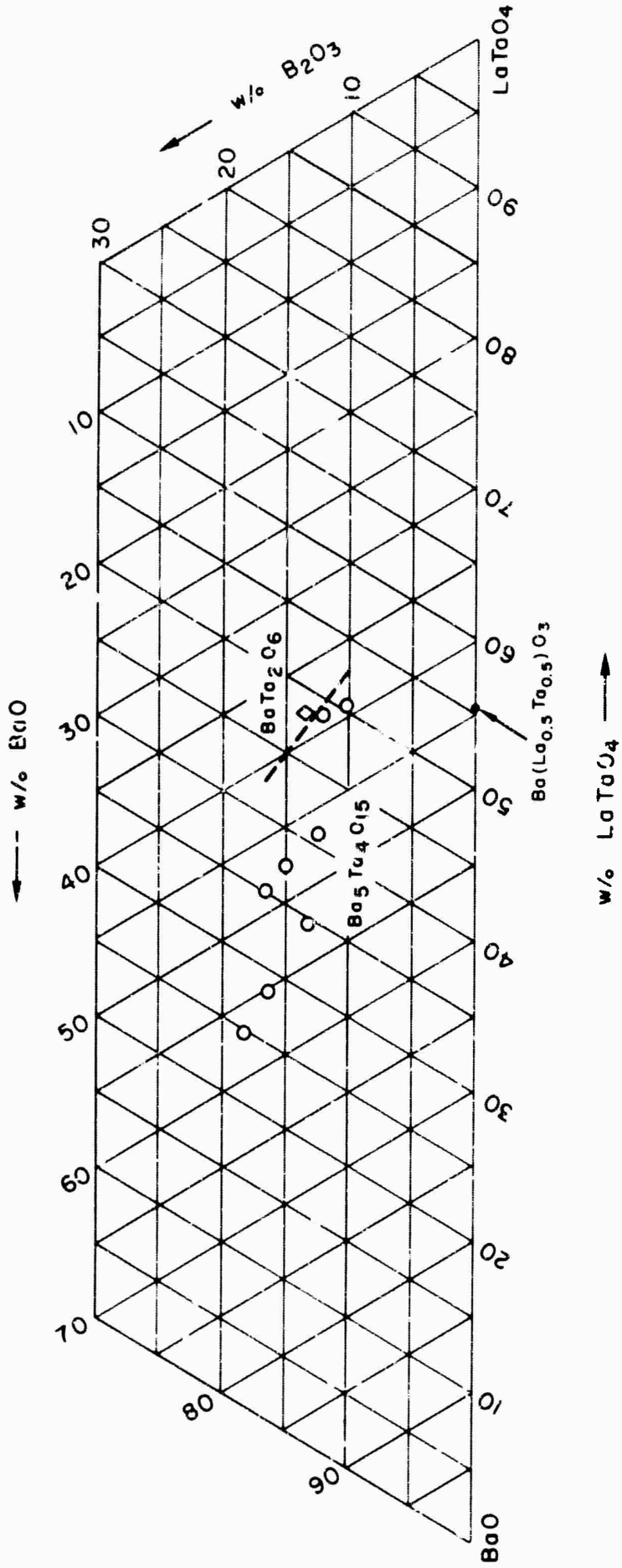

APPENDIX III

B_2O_3 Loss From Melts

Quantitative weight loss data for melts above the perovskite field in the system BaO-$YTaO_4$-B_2O_3 were made necessary in order to permit the actual crystallization paths to be predicted.

An analytical balance was positioned above a furnace: the pan was removed from one arm of the balance, and a platinum wire which passed through holes in the balance case and furnace cover was hung in its place. A 50 ml platinum crucible was affixed to the support wire in such a way as to be freely suspended in the hot zone of the furnace. The crucible had been previously charged with about 194 grams of composition 55 weight percent BaO, 31 weight percent $YTaO_4$ and 14 weight percent B_2O_3. The furnace was heated to 1135°C and maintained at that temperature (±2°C) for approximately 120 hours while weighings were made at various intervals. These data are presented in Fig. 38. Zero time was arbitrarily selected as the time of the first recorded measurement. The weight loss was linear with time over the five day duration of the run, and amounted to 1.1 grams per day.

WEIGHT-LOSS FROM 194 GRAM BATCH OF COMPOSITION 55 BaO, 31 $YTaO_4$, 14 B_2O_3